NASA CONTRACTOR REPORT

NASA CR-2788

NASA CR-2788

STABILITY AND CONTROL OF MANEUVERING HIGH-PERFORMANCE AIRCRAFT

Robert F. Stengel and Paul W. Berry

Prepared by
THE ANALYTIC SCIENCES CORPORATION
Reading, Mass. 01867
for Langley Research Center

NATIONAL AERONAUTICS AND SPACE ADMINISTRATION • WASHINGTON, D. C. APRIL 1977

1. Report No.	2. Government Accession No.	3. Recipient's Catalog No.
NASA CR-2788		

4. Title and Subtitle	5. Report Date
Stability and Control of Maneuvering High-Performance Aircraft	April 1977
	6. Performing Organization Code

7. Author(s)	8. Performing Organization Report No.
Robert F. Stengel and Paul W. Berry	TR-587-1
	10. Work Unit No.

9. Performing Organization Name and Address	11. Contract or Grant No.
The Analytic Sciences Corporation 6 Jacob Way Reading, Massachusetts 01867	NAS1-13618
	13. Type of Report and Period Covered
12. Sponsoring Agency Name and Address	Contractor Report - Final
National Aeronautics and Space Administration Washington, D.C. 20546	14. Sponsoring Agency Code

15. Supplementary Notes

NASA Technical Monitor: Luat T. Nguyen, NASA Langley Research Center. Stephen F. Donnelly, TASC Technical Staff Member, assisted the authors in computer program development.

Final Report

16. Abstract

The stability and control of a high-performance aircraft has been analyzed, and a design methodology for a departure prevention stability augmentation system (DPSAS) has been developed. This work required the derivation of a general linear aircraft model which includes maneuvering flight effects and trim calculation procedures for investigating highly dynamic trajectories. The stability-and-control analysis systematically explored the effects of flight condition and angular motion, as well as the stability of typical air combat trajectories. The effects of configuration variation also were examined. Adaptive departure prevention controllers (based on gain-scheduled optimal regulators) possess the potential for expanding the controllable flight regime of the subject aircraft.

17. Key Words (Suggested by Author(s))	18. Distribution Statement
Aircraft control systems Systems design Stability and Control Atmospheric flight mechanics	Unclassified - Unlimited Subject Category: 08

19. Security Classif. (of this report)	20. Security Classif. (of this page)	21. No. of Pages	22. Price*
Unclassified	Unclassified	204	$7.25

* For sale by the National Technical Information Service Springfield Virginia 22161

TABLE OF CONTENTS

	Page No.
List of Figures	v
List of Tables	vii
List of Symbols	ix
1. INTRODUCTION	1
1.1 Background	1
1.2 Purpose	4
1.3 Summary of Results	4
1.4 Organization of the Report	7
2. DYNAMIC CHARACTERISTICS OF HIGH-PERFORMANCE AIRCRAFT	8
2.1 Overview	8
2.2 Prior Studies of Aircraft at Extreme Flight Conditions	9
2.2.1 Dynamics of the Aircraft	10
2.2.2 Aerodynamics	14
2.2.3 Control	15
2.3 Comparison of Results from Linear and Nonlinear Simulations	18
2.3.1 Elevator Control Input	19
2.3.2 Aileron Control Input	20
2.3.3 Rudder Control Input	20
2.4 Effects of Angular Motion and Flight Condition On Aircraft Stability	26
2.4.1 Altitude and Velocity Effects	27
2.4.2 Aerodynamic Angle Effects	30
2.4.3 Angular Rate Effects	38
2.5 Effects of Angular Motion and Flight Condition On Aircraft Control	44
2.5.1 Velocity and Aerodynamic Angle Effects	45
2.5.2 Angular Rate Effects	49
2.6 Dynamic Variations During Extreme Maneuvering	51
2.6.1 Wind-Up Turn	52
2.6.2 Rolling Reversal	54
2.6.3 Effects of Proportional Tracking	57
2.7 Chapter Summary	59
3. EFFECTS OF CONFIGURATION VARIATIONS ON AIRCRAFT DYNAMICS	62
3.1 Overview	62
3.2 Variations Due to Longitudinal Stability Derivatives	62
3.3 Variations Due to Lateral-Directional Stability Derivatives	68

TABLE OF CONTENTS (Continued)

		Page No.
3.4	Variations Due to Mass and Inertia Effects	74
3.5	Classification of Departures	78
3.5.1	Unforced Departure Modes	78
3.5.2	Forced Departure Modes	82
3.6	Chapter Summary	85
4.	PREVENTION OF DEPARTURE FROM CONTROLLED FLIGHT	86
4.1	Overview	86
4.2	The Linear-Optimal Regulator	89
4.3	DPSAS Control Laws	94
4.3.1	Longitudinal Sweep	97
4.3.2	Lateral-Directional Sweep	103
4.4	Control-Law Adaptation for Varying Flight Conditions	112
4.4.1	Longitudinal Sweep	114
4.4.2	Lateral-Directional Sweep	117
4.4.3	Additional Considerations	119
4.5	Chapter Summary	120
5.	CONCLUSIONS AND RECOMMENDATIONS	122
5.1	Conclusions	122
5.2	Recommendations	124
APPENDIX A	ANALYTICAL APPROACH TO AIRCRAFT DYNAMICS	A-1
APPENDIX B	AIRCRAFT AERODYNAMIC MODEL	B-1
REFERENCES		R-1

LIST OF FIGURES

Figure No.		Page No.
2.3-1	Small Amplitude Elevator Input	20
2.3-2	Small Amplitude Aileron Input	21
2.3-3	Large Amplitude Rudder Input -- Comparison of Initial Response	22
2.3-4	Large Amplitude Rudder Input -- Comparison of Evolved Response With Ad Hoc Reference Point for Linearization	24
2.3-5	Large Amplitude Rudder Input -- Comparison of Evolved Response With Generalized Trim Reference Point for Linearization	25
2.4-1	Altitude and Velocity Effects on Eigenvalues	28
2.4-2	Effects of Aerodynamic Angles on Aircraft Stability	31
2.4-3	Angle-of-Attack Effects on Aircraft Eigenvectors	33
2.4-4	Sideslip Effect on Aircraft Eigenvectors	35
2.4-5	Effects of Body Orientation on Aircraft Stability	36
2.4-6	Variations of Directional Aerodynamic Coefficients with Angle of Attack	37
2.4-7	Yaw-Rate/Pitch-Rate Effects	39
2.4-8	Pitch-Rate Effects on Eigenvectors	40
2.4-9	Stability Boundaries for Sideslip/Roll-Rate Variations (α_0 = 15 deg)	42
2.4-10	Roll-Rate Eigenvector Effects	43
2.5-1	Typical Step Response Forms	45
2.6-1	Eigenvectors of Rolling Reversal	56
3.2-1	Longitudinal Eigenvalue Variations with c.g. Location	66
3.2-2	Longitudinal Eigenvector Variations with c.g. Location	66
3.3-1	Effects of C_{l_β}, C_{n_β}, and C_{l_p} Variations on Lateral-Directional Eigenvalues	69
3.4-1	Effects of Large Rolling Inertia on Aircraft Stability	77
3.5-1	An Example of Lateral-Directional Eigenvalues for Negative Directional Stability	79

LIST OF FIGURES (Continued)

Figure No.		Page No.
3.5-2	An Unforced Departure Due to Negative C_{n_β}	80
3.5-3	An Unforced Departure Due to Negative Dutch Roll Damping	81
3.5-4	Eigenvalues and Eigenvectors for a Flight Condition with Large Sideslip Angle	82
3.5-5	Aileron Input for Negative C_{n_β}	84
4.2-1	Longitudinal Response at the Central Flight Condition	93
4.2-2	Directional Response at the Central Flight Condition	95
4.2-3	Lateral Response at the Central Flight Condition	96
4.3-1	Pitch-Rate Effect on Directional Response	102
4.3-2	Examples of Primary Gain Variation in Lateral-Directional Sweep	105
4.3-3	Examples of Crossfeed Gain Variation in Lateral-Directional Sweep	106
4.3-4	Roll-Rate Effect on Directional Response	109
4.3-5	Roll-Rate/Sideslip Effect on Longitudinal Response	110

LIST OF TABLES

Table No.		Page No.
2.4-1	Dynamic Effects of Steady Angular Rate	39
2.5-1	Velocity Effects on Transfer Function Gain, K_F	46
2.5-2	Aerodynamic Angle Effects on Transfer Function Gains ($V_0 = 94$ m/s)	47
2.5-3	Effects of Angle of Attack on Transfer Function Zeros	48
2.5-4	Pole-Zero Comparison at $\alpha_0 = 15$ deg, $\beta_0 = 10$ deg	48
2.5-5	Effects of Pitch Rate on Transfer Function Gains	50
2.5-6	Effects of Roll Rate on Transfer Function Gain, K_F	50
2.6-1	Wind-Up Turn Working Points	53
2.6-2	Wind-Up Turn Eigenvalues	53
2.6-3	Transfer Function Gain, K_I, Along the Wind-Up Turn	54
2.6-4	Rolling Reversal Working Points	55
2.6-5	Rolling Reversal Eigenvalues	55
2.6-6	Transfer Function Gain, K_I, Along the Rolling Reversal	57
2.6-7	Eigenvalue Changes due to Proportional Tracking -- Symmetric Flight Conditions	58
2.6-8	Eigenvalue Changes Due to Proportional Tracking -- Sideslip and Roll Effects	60
3.2-1	$C_{Z\alpha}$ and C_{m_q} Effects on Eigenvalues	63
3.2-2	Effects of C_{m_q} on Eigenvalues in Asymmetric Flight	64
3.2-3	c.g. Location Effects on Transfer Function Gain, K_F	67
3.2-4	Comparison of Zeros of $\Delta w/\Delta\delta_h$ at Three c.g. Locations	67
3.3-1	Effects of C_{n_β} and C_{l_β} Variations in the Presence of Steady Pitch Rate	70
3.3-2	Effects of C_{n_r} Variations	71
3.3-3	Effects of $C_{n_{\dot\beta}}$ in the Presence of Steady Rolling	73

LIST OF TABLES (Continued)

Table No.		Page No.
3.4-1	Effects of Aircraft Mass on Eigenvalue Location	75
3.4-2	Effect of Rotational Inertia on Eigenvalues	76
4.2-1	Effects of DPSAS at the Central Flight Condition	91
4.2-2	DPSAS Gain Matrix at the Central Flight Condition	92
4.3-1	Closed-Loop Stability in the Longitudinal Sweep	98
4.3-2	DPSAS Gains for the Longitudinal Sweep	100
4.3-3	Closed-Loop Stability in the Lateral-Directional Sweep	104
4.4-1	Gain Correlations for the Longitudinal Sweep	115
4.4-2	Gain Correlations for the Lateral-Directional Sweep	118

LIST OF SYMBOLS

In general, matrices are represented by capital letters and vectors are underscored. The subscript on a vector usually indicates the frame in which the vector is expressed.

VARIABLES	DESCRIPTION
b	Wing span
	Gain scheduling coefficient
C_{1_2}	Partial derivative of the nondimensional coefficient of force or moment 1 with respect to the nondimensional variable 2. (scalar)
$\bar{c}$	Mean aerodynamic chord
c	Gain scheduling coefficient
F	System matrix
$\underline{F}$	Aerodynamic contact force vector
$\underline{f}$	Vector-valued nonlinear function
G	Control input matrix
$\underline{G}$	Thrust moment vector
g	Magnitude of $\underline{g}$ ($g = \|\underline{g}\|$)
$\underline{g}$	Gravitational acceleration vector
H	Altitude (scalar)
	Transfer function matrix
H_1^2	Euler angle transformation from Frame 1 axes to Frame 2 axes
$\underline{h}$	Angular momentum vector

LIST OF SYMBOLS (Continued)

VARIABLES	DESCRIPTION
I	Rotational inertia matrix
I	Identity matrix
	Product or moment of inertia (with appropriate subscripts)
J	Cost functional
J	State derivative premultiplying matrix
K	Gain (matrix)
	Axis transformation matrix for complete state vector
k	Gain (scalar)
L	Aerodynamic moment about the x-axis (scalar)
	Angular rate transformation matrix
M	Aerodynamic moment about the y-axis (scalar)
	Modal matrix composed of eigenvectors
$\underline{M}$	Aerodynamic contact moment vector
m	Mass of the vehicle
	Gain scheduling independent variable
N	Aerodynamic moment about the z-axis (scalar)
n_z	Load factor
P	Riccati matrix
p	Pole of a system
	Rotational rate about the body x-axis
Q	Weighting matrix
q	Rotational rate about the body y-axis

LIST OF SYMBOLS (Continued)

VARIABLES	DESCRIPTION
q_∞	Free stream dynamic pressure ($\frac{1}{2}\rho V^2$)
R	Weighting matrix
r	Rotational rate about the body z-axis
S	Reference area (usually wing area)
s	Laplace transform variable
T	Thrust force magnitude ($T=\|\underline{T}\|$)
$\underline{T}$	Thrust force vector
t	Time
$\underline{u}$	Control vector
u	Body x-axis velocity component
	Element of control vector
V	Inertial velocity magnitude ($V=\|\underline{V}\|$)
v	Velocity vector of body observed from inertial axes
v	Body y-axis velocity component
w	Body z-axis velocity component
X	Aerodynamic force along the x-axis (scalar)
$\underline{x}$	State vector
$\Delta\bar{x}$	Distance between actual c.g. location and point used for aerodynamic moment measurements
$\underline{x}_I$	Inertial position vector
x	Position along the x-axis
	Element of state vector

LIST OF SYMBOLS (Continued)

VARIABLES	DESCRIPTION
Y	Aerodynamic force along the y-axis
$\underline{y}$	Normal mode state vector
	Output vector
y	Position along the y-axis
Z	Aerodynamic force along the z-axis
$\underline{z}$	Eigenvector
z	Position along the z-axis
	Zero of a transfer function

VARIABLES (Greek)	DESCRIPTION
α	Wind-body pitch Fuler angle (Angle of Attack)
β	Negative of wind-body yaw Euler angle (Sideslip angle)
Γ	Controllability test matrix
γ	Inertial-velocity axis pitch Euler angle (Flight path angle)
δ_a	Aileron deflection
δ_f	Flap/slat deflection
δ_h	Horizontal tail deflection
δ_r	Rudder deflection
δ_{SB}	Speed brake deflection
δ_T	Thrust command
ζ	Damping ratio
θ	Inertial-body pitch Euler angle
λ	Eigenvalue
$\Delta\mu$	Euler angle perturbation vector expressed in an orthogonal frame

LIST OF SYMBOLS (Continued)

VARIABLES (Greek)	DESCRIPTION
μ	Relative density
$\underline{\nu}$	Orientation or velocity magnitude and orientation vector
ξ	Inertial-velocity axis yaw Euler angle (Heading angle)
ρ	Air density
	Correlation coefficient
σ	Real part of eigenvalue
ϕ	Inertial-body roll Euler angle
ψ	Inertial-body yaw Euler angle
$\underline{\omega}_1^2$	Rotational rate vector of Reference Frame 2 with respect to Reference Frame 1 and expressed in Frame 1 coordinates. ($\underline{\omega}_1^2 = H_2^1 \underline{\omega}_2^1$ so $\underline{\omega}_2^1$ is left-handed. Thus, Frame 1 and Frame 2 are <u>not</u> interchangeable.)
ω	Frequency (Imaginary part of eigenvalue)
ω_n	Natural frequency

VARIABLES (Subscripts or Superscripts)	DESCRIPTION
B	Body axes
DR	Pertaining to Dutch roll mode
dyn	Stability axis derivative
F	Final value
I	Inertial axes
	Initial value
l	Aerodynamic moment about the x-axis
m	Aerodynamic moment about the y-axis

LIST OF SYMBOLS (Continued)

VARIABLES (Subscripts or Superscripts)	DESCRIPTION
n	Aerodynamic moment about the z-axis
roll	Pertaining to roll mode
W	Wind axes
X	Aerodynamic force along the x-axis
x	Component along the x-axis
Y	Aerodynamic force along the y-axis
y	Component along the y-axis
Z	Aerodynamic force along the z-axis
z	Component along the z-axis

PUNCTUATION

$(\dot{})$	Time derivative - occurs after any transformation unless explicitly indicated otherwise
$(\tilde{})$	Matrix equivalent to vector cross product. Specifically, if $\underline{x}$ is the three-dimensional vector $\underline{x} = \begin{bmatrix} x \\ y \\ z \end{bmatrix}$ then $\tilde{x} = \begin{bmatrix} 0 & -z & y \\ z & 0 & -x \\ -y & x & 0 \end{bmatrix}$ the cross product of $\underline{x}$ and another vector ($\underline{F}$, for example) is equal to the product of the matrix $\tilde{x}$ and the vector $\underline{F}$. $\underline{x} \times \underline{F} = \tilde{x}F$
$(\ )^T$	Transpose of a vector or matrix

LIST OF SYMBOLS (Continued)

PUNCTUATION (Continued)	DESCRIPTION
$(\hat{})$	Scheduled or estimated value
$(\bar{})$	Mean value
$( )^{-1}$	Inverse of a matrix
$( )_0$	Reference or nominal value of a variable
$\Delta( )$	Perturbation about the nominal value of a variable

ACRONYM	DEFINITION
ARI	Aileron-rudder-interconnect
ARDP	Acceleration response departure parameter
c.g.	Center of gravity
DPSAS	Departure-prevention stability augmentation system
IAS	Indicated air speed
LCDP	Lateral control departure parameter

STABILITY AND CONTROL OF MANEUVERING HIGH-PERFORMANCE AIRCRAFT

Robert F. Stengel and Paul W. Berry
The Analytic Sciences Corporation

1. INTRODUCTION

1.1 BACKGROUND

As aircraft become capable of flying higher, faster, and with more maneuverability, prevention of inadvertent departure from controlled flight takes on added significance. To some extent, the airframe can be designed to provide inherent protection against loss of control, as in the addition of nose strakes to regulate high angle-of-attack (α) vortices; however, performance objectives are likely to dominate the choice of such features as wing planform and chord section, nose shape, aircraft density ratio, and tail area. It is likely, therefore, that the freedom to configure the aircraft for intrinsic departure prevention will be restricted and that the flight control system will be called upon to provide additional protection.

Flight at high α invariably complicates the control problem. Dynamic coupling between longitudinal and lateral-directional motions becomes apparent, aerodynamic trends vary considerably, and control surface effects diminish or become adverse. Coupling and nonlinearities can cause a self-sustained oscillation ("wing rock") at high α, degrading precision tracking tasks without necessarily causing loss of control. Abrupt maneuvering, external disturbances, control system failure, or pilot error can produce a "departure" (pitch, yaw, or roll divergence), possibly leading to high acceleration and to a fully developed spin. The recovery from spin or gyration is, at best, an emergency procedure which is not always successful. Clearly, it is preferable to

prevent the departure before it occurs rather than to be forced to take emergency measures.

Although departure and spin are related topics, there are at least as many dissimilarities between the phenomena as there are similarities. Departure is a transient event, while spin is a quasi-steady condition. Departure connotes instability with respect to the initial flight condition, while spin can be thought of as a bounded, periodic (and therefore stable) motion about a near-equilibrium flight path. Departure can occur in level flight, but spinning equilibrium ultimately results in vertical motion of the aircraft's center of gravity.

Departure and spin both are beset by the difficulties inherent in describing fully coupled dynamic systems of high order and in describing static and rotary aerodynamics at complex flight conditions. However, as suggested by the preceding comparison, the approximations and assumptions which hold for one are not necessarily appropriate for the other. In particular, it appears that linearized dynamic models may have a practical utility in preventing departure which does not readily carry over to spin recovery. The reason is that a closed-loop control law which continuously acts to prevent departure restricts angular excursions to small values; hence, their dynamic effects can be described by linear models. A spin recovery strategy necessarily must operate with large angular changes which result in significant nonlinear effects.

The key to developing a linear model which is satisfactory for the study and control of departure is in the recognition that the nominal flight path, used as a reference for the variational (linearized) motions, need not

represent a steady, unaccelerated flight condition. A flight path in dynamic equilibrium is equally satisfactory as long as it is understood that variational motions are referenced to the continuously changing nominal flight path. The intermediate step of linearizing the aircraft model with non-zero but constant sideslip angle (β_0), angular rate (p_0, q_0, r_0), and load factor (n_{z_0}) provides the coupling between longitudinal and lateral-directional motions which is so important in the study of departure.

It is essential to recognize that the combined effects of non-zero mean motions lead to significant coupling which otherwise might be missed in a linear dynamic model. It has been demonstrated that large mean values of roll rate and sideslip angle separately produce significant coupling of the short period and Dutch roll modes. It is less well known that the combined effects of these two variables produce coupling which is qualitatively different from that induced by a single variable. This variability in stability effect is similar to the seeming unpredictability of the departure modes of some aircraft, in which the aircraft is known to have more than one departure mode for supposedly similar flight conditions. This also suggests that departure modes are more predictable than might have been assumed.

The complexity of the coupled dynamics and the possibility for misinterpreted control cues at high α indicate a need for departure preventing control systems in highly maneuverable aircraft. New developments are required in characterizing the evolution of motions during extreme maneuvering and in the computation of control solutions.

1.2 PURPOSE

The purpose of this investigation is to identify general rules for the design of departure-preventing control systems. In achieving this objective, the analytic foundations for linear-time-invariant modeling of aircraft dynamics are extended to include extreme maneuvering conditions. Using tools of linear systems analysis, the stability and control characteristics of a high-performance aircraft are examined over a wide range of flight conditions, and specific effects of configurational modification are developed. The study culminates in the development and evaluation of control laws for a Departure-Prevention Stability Augmentation System (DPSAS) using linear-optimal control theory.

1.3 SUMMARY OF RESULTS

The major tasks of this project were defined at the outset as:

- Dynamic Model Development
- Characterization of Departure Modes
- Controllability Effects on Aircraft Departure
- Control Laws for Departure Prevention

These tasks can be summarized briefly as follows: Dynamic Model Development provided a range of nonlinear and linear dynamic models for use in the analysis of departure and the design of DPSAS control laws. Characterization of Departure Modes addressed the unaugmented stability of high-performance aircraft. Controllability Effects on Aircraft Departure considered the direct (open-loop) effects of control forces on aircraft departure. Control Laws for Departure Prevention resulted in the design and simulation of linear-optimal

regulator control laws which stabilize the reference aircraft during extreme maneuvering and which adapt to changing flight condition.

Although aircraft equations of motion are developed in several texts, no derivation which retains all coupling terms in the linearized equations of motion was found. Therefore, the present investigation began with the development of nonlinear equations in four axis systems (inertial or earth-relative, velocity, wind, and body). This was followed by derivation of the associated linear equations of motion, as well as equilibrium equations which define a generalized trim condition. The validity of these equations was established by direct comparisons of the time responses of the linear and nonlinear equations.

A small, supersonic fighter aircraft was chosen as a baseline for study. A comprehensive model of subsonic nonlinear aerodynamic coefficients was available for this aircraft and was used to generate aircraft local stability derivatives as flight condition was varied. These stability derivatives formed a large part of the linear-time-invariant dynamic model, which was analyzed by eigenvalue/eigenvector, transfer function, and time response methods. Thus, the significant aspects of aerodynamic nonlinearity and inertial coupling, i.e., the local sensitivities to initial condition, disturbance, and control perturbations, were retained in the aircraft model.

Using the reference aircraft as a starting point, the analysis proceeded along two separate lines. The first approach was to assess the effects of maneuvers and flight condition on the reference aircraft, recomputing the linear model for each variation in nominal angle, angular rate,

altitude, and velocity. In order to distinguish between aerodynamic and purely inertial effects, a limited number of cases were evaluated with varying flight condition and fixed aerodynamic derivatives. The second approach was to vary individual coefficients of the linear model so that specific configurational effects could be analyzed. The quantitative results presented here strictly apply only to the specific configurations studied; hence, care should be exercised in generalizing these results to other configurations.

The linear-optimal regulator was applied to the DPSAS design problem, and the present results demonstrate the substantial benefits offered by the linear-optimal controllers. A design procedure which also identifies gain-scheduling relationships is presented; it has the following features:

- Complete longitudinal/lateral-directional coupling is accounted for in the design process.
- All significant feedback gains, cross-feeds, and control interconnects are identified.
- The control structure is guaranteed to stabilize the aircraft, assuming that aircraft parameters are known and motions are measured precisely.
- Tradeoffs between control authority, control power, and aircraft motions are incorporated in the design process.
- The DPSAS adapts to varying flight condition.

The extension of this design procedure to a full command augmentation system is direct, as the control design algorithms are easily restructured to consider handling qualities requirements, control-actuator rate limits, noisy feedback measurements, and digital implementation.

In the process of conducting this investigation, a flexible computer program (ALPHA) for the analysis of high angle-of-attack stability and control was developed. Program ALPHA generates linear dynamic models and trim conditions from nonlinear aerodynamic and inertial data; presents results for body-axis, stability-axis, and reduced-order models; computes eigenvalues, eigenvectors, transfer functions, departure parameters, and linear-optimal control gains; calculates time histories for various initial conditions, control inputs, and disturbances; and incorporates a logical (executive) structure which facilitates parameter sweeps, initial condition variations, and model modifications during a single computer run.

1.4 ORGANIZATION OF THE REPORT

This report presents dynamic equations, stability and control characteristics of high-performance aircraft, and control laws for departure prevention. Prior results related to extreme maneuvering of aircraft are reviewed in Chapter 2, which then presents a validation of the linear model and describes the effects of extreme maneuvering on the dynamics of the reference aircraft. Configurational effects on maneuvering dynamics are discussed in Chapter 3. Control laws for a Departure-Prevention Stability Augmentation System (DPSAS) are derived in Chapter 4, and the report is concluded by Chapter 5. Appendix A is directed to the development of nonlinear equations of motion, linear equations, generalized trim conditions, and tools for linear systems analysis. The model for the reference aircraft is summarized in Appendix B.

2. DYNAMIC CHARACTERISTICS OF HIGH-PERFORMANCE AIRCRAFT

2.1 OVERVIEW

The problems associated with extreme maneuvering have two common characteristics: loss of control and large angles and/or angular rates, i.e., angles and rates generally beyond the range of normal, "1-g" flight operations. Extreme maneuvering difficulties fall in the following categories, which contain some overlap:

- Decreased inherent stability
- Degraded handling qualities
- Longitudinal/lateral-directional coupling
- Stall
- Wing rock
- Departure
- Post-stall gyrations
- Incipient spin
- Fully evolved spin

The ordering of this list suggests that the severity of these phenomena increases with angle of attack and is aggravated by angular rates and sideslip angle.

Appendix A presents a formal development of fully coupled linear-time-invariant models for aircraft motion. These models are suitable for investigating perturbation motions which are referenced to large angles and large angular rates. After reviewing prior investigations of aircraft dynamics in Section 2.2, the remainder of the chapter concerns the application of linear systems analysis to the stability and control of a high-performance aircraft

(which is described in Appendix B). Section 2.3 compares the time responses of linear and nonlinear dynamic models. Section 2.4 is directed at aircraft stability, and Section 2.5 treats aircraft control. Variations in the aircraft's dynamic characteristics during extreme maneuvering are addressed in Section 2.6, which also introduces rudimentary effects of the pilot's control actions while executing a tracking task. The chapter is summarized in Section 2.7.

2.2 PRIOR STUDIES OF AIRCRAFT AT EXTREME FLIGHT CONDITIONS

Although published studies of aircraft dynamics shortly followed the Wright brothers' flight (Ref. 1), and the concept of stability derivatives was published in 1913 (Ref. 2), the dynamics of aircraft which are executing extreme maneuvers received little attention until the late 1940's. (Investigation of the related problem of aircraft spinning had begun a decade earlier.) There are several reasons for this, but the most significant reason is that extreme maneuvers had not presented sufficient problems to merit detailed engineering study. The advent of fighter aircraft with higher speeds, higher roll rates, higher density, lower inherent damping, and higher cost accentuated the importance of understanding extreme maneuvering dynamics. Furthermore, the improved analytical tools and techniques spawned by World War II became available for application to flight dynamic problems.

In addition to the extensive flight testing which high-performance aircraft received, three fundamentally different avenues have been followed in the investigation of maneuvering flight. The first approach is the study of rigid-body dynamics of the aircraft, the second is the study of aerodynamics, and the third is the study of control. The

first two areas have a cause-and-effect relationship -- aerodynamic forces modify the momentum and energy of the airplane -- and there is "feedback," in the sense that the changing velocity and attitude of the vehicle contribute to changes in the aerodynamic forces. Although dynamic problems result from the interaction of dynamics and aerodynamics, one can distinguish between these two areas in reviewing past work. The third area considers methods of augmenting the natural aircraft stability, of limiting excursions from the normal flight regime, of providing adequate response, and of recovering from fully evolved spins.

2.2.1 Dynamics of the Aircraft

The objective of study is the solution of nonlinear and linear equations of motion, e.g., those derived in Appendix A. Options for analysis can be classified as explicit, in which a direct solution of motion equations is sought, or implicit, in which the evolution of motions is inferred from characteristics of the system. The solution of these equations describes the aircraft's response to initial conditions and disturbances, and it provides a basis for identifying control policies. The stability of the solution describes its tendency to return to a nominal value. Given an initial disturbance, the stable aircraft's solution returns to the nominal solution (or its error is, at least, bounded); the unstable aircraft's solution diverges. These analytical methods can be summarized as follows:

Explicit Analysis - Stability, Response, and Control

- Analog integration of differential equations
- Numerical integration of differential equations
- Closed-form solution of differential equations
- Equilibrium solution of algebraic equations

Implicit Analysis - Stability

- Generalized energy balance (Liapunov method)
- Absolute stability bounds (Popov criterion, circle criterion, etc.)
- Stability bounds of "classical" differential equations (Mathieu's equation, etc.)
- Eigenvalue analysis (Routh-Hurwitz criterion, root locus, etc.)
- Quasi-linear Eigenvalue analysis

Implicit Analysis - Response and Control

- Eigenvector analysis
- Time-domain methods (Impulse or indicial response, auto- and cross-correlation functions, etc.)
- Transform methods (Frequency response, transfer functions, spectral density, etc.)

Applications of some of these techniques to the maneuvering flight problem are documented in the literature. Much of the work related to handling qualities, stability, coupling, and departure is based upon linear-time-invariant models and uses eigenvalue and transfer function analysis. Work of this type is reported in Refs. 3 to 10. In addition, parameters of linear-time-invariant models ($Cn_{\beta,dyn}$, LCDP, etc.) have been correlated with flight test or piloted simulation data using little or no direct analysis of the equations of motion (Refs. 11 to 14). Quasi-linearization of a significant sideslip nonlinearity is applied to the wing rock problem in Ref. 15, and closed-form solutions for a class of large maneuvers are presented in Ref. 16. Since the early 1960's, a large number of investigations have used analog and numerical integration in the

study of departure, stall, post-stall gyrations and spin (Refs. 17 to 27). Equilibrium solutions of nonlinear equations of motion have been used to determine spin conditions and are discussed in Refs. 24 and 28 to 30.

A number of linear-time-invariant departure parameters have been identified, as reported in Refs. 5, 13, and 14. These parameters relate to transfer function numerators and denominators and are expressed in terms of stability and control derivatives (C_{n_β}, C_{l_β}, $C_{n_{\delta_a}}$, $C_{l_{\delta_a}}$, $C_{n_{\delta_r}}$, $C_{l_{\delta_r}}$), angle of attack (α_0), moments of inertia (I_x, I_z), directional stability augmentation gain (k_1), and aileron-rudder-interconnect (ARI) gain (k_2):

Directional Stability Parameter

$$C_{n_{\beta,dyn}} = C_{n_\beta} \cos \alpha_0 - \frac{I_z}{I_x} C_{l_\beta} \sin \alpha_0 \qquad (2.2\text{-}1)$$

Lateral Control Departure Parameter

$$LCDP = C_{n_\beta} - C_{l_\beta} \frac{C_{n_{\delta_a}}}{C_{l_{\delta_a}}} \qquad (2.2\text{-}2)$$

Augmented Lateral Control Departure Parameter

$$LCDP_A = C_{n_\beta} - C_{l_\beta} \frac{C_{n_{\delta_a}}}{C_{l_{\delta_a}}} + k_1 \left(\frac{C_{n_{\delta_a}}}{C_{l_{\delta_a}}} C_{l_{\delta_r}} - C_{n_{\delta_r}} \right) \qquad (2.2\text{-}3)$$

ARI Lateral Control Departure Parameter

$$LCDP_{ARI} = C_{n_\beta} - C_{l_\beta} \left(\frac{C_{n_{\delta_a}} + k_2 C_{n_{\delta_r}}}{C_{l_{\delta_a}} + k_2 C_{l_{\delta_r}}} \right) \qquad (2.2\text{-}4)$$

Acceleration Response Departure Parameter ("β plus δ Stability Indicator")

$$ARDP_{\beta} = \alpha_0 - \tan^{-1}\left(\frac{C_{n_\beta} I_x}{C_{l_\beta} I_z}\right) \qquad (2.2\text{-}5)$$

$$ARDP_{\delta} = \alpha_0 - \tan^{-1}\left(\frac{C_{n_\delta}}{C_{l_\delta}} \frac{I_x}{I_z}\right) \qquad (2.2\text{-}6)$$

The first four criteria indicate resistance to departure when their magnitudes are greater than zero, while the last requires $ARDP_{\beta}$ to be greater than zero and greater than $ARDP_{\delta}$. The first criterion relates to the open-loop static stability of the Dutch roll mode; $C_{n_{\beta,dyn}} > 0$ is an approximate requirement for stability. The LCDP's are approximations to the closed-loop static stability of the Dutch roll mode when lateral control is used to maintain constant roll rate; when they are greater than zero, the Dutch roll mode is statically stable, but when they are less than zero, the Dutch roll mode is statically unstable. The "β plus δ" criterion is an attempt to combine stability and control considerations in a single departure indicator.

There are a number of inadequacies in the above parameters, although they provide insight for future developments. They are approximations to the exact transfer function coefficients and do not indicate actual pole-zero locations; they neglect damping terms entirely; and they do not account for longitudinal/lateral-directional coupling induced by large sideslip angle (β) and angular rates (p,q,r) -- in fact, the longitudinal dynamics are ignored completely. References 8, 9, 31, and 32 introduce coupling effects due to β, illustrating the importance of some of the neglected terms, and Ref. 33 treats the dynamics of steady turning flight.

2.2.2 Aerodynamics

Equally important developments have been made in the area of aerodynamics. Measurements of forces and moments and visualization of flow phenomena have indicated the large variations in aerodynamic conditions to be expected at high angles of attack (α) and sideslip (β), and there is an increasing body of data related to the effects of large angular rates (Refs. 34 to 46). While these several references cover a variety of topics, they provide an introduction to the kinds of aerodynamic problems which can be expected when aircraft fly at high angles and high rates.

The two dominant phenomena which complicate the collection of valid data and the flight of actual aircraft are vortices and separated flow. The vortex is a by-product of aerodynamic lift, and each surface or body which generates lift has a corresponding vortex that trails downstream from the lifting source. This swirling airflow affects pressure distributions on the downstream surfaces of the aircraft, and it can combine with vortices generated on other parts of the aircraft to produce a very complex flow field. At low angles of attack or sideslip, the vortices from nose, wing, and tail usually form a unified flow field, which varies smoothly as the aircraft's attitude with respect to the wind changes. As the incidence increases, this smooth variation may break down, causing the flow to become less unified.

The difficulties in predicting the actual forces and moments on full-scale aircraft from wind-tunnel data are greatest for large-angle flight conditions, not only because tunnel correction factors can become significant but because separation effects depend on the Reynolds number of the flow (and, therefore, on the size of the aircraft). High-performance aircraft are most likely to perform

extreme maneuvers at subsonic velocity, in which case Mach number effects may not be significant; however, scaling of the flow to provide representative Reynolds number is required, if model test data is to be applied to the full-scale aircraft.

Stability problems associated with large aerodynamic angles may arise from either the nose, wing, or tail, depending on aircraft configuration. Consequently, it is impossible to identify a single aerodynamic solution to problems of departure (other than to make all aircraft use the same configuration). Aerodynamic solutions include wing-root leading-edge extensions, nose strakes, redesign of the nose cross-section and profile, maneuvering (leading-edge) flaps, and adjustment of horizontal tail anhedral.

The aerodynamic forces and moments discussed above are static, in that they arise from fixed values of α and β. These terms establish the static stability and trim points of the aircraft. Forces and moments which result from angular rates (p,q,r) and accelerations ($\dot{u},\dot{v},\dot{w},\dot{p},\dot{q},\dot{r}$) are dynamic and thus contribute to damping and transient response. There is indication that assumptions which conventionally are made for low-angle flight conditions, e.g., that the $\dot{\beta}$ and yaw-rate effects are simply additive, break down at high angles. Unfortunately, dynamic forces and moments are difficult to measure in practice, and relatively few facilities are equipped to measure dynamic forces, much less to separate $\dot{\beta}$ and r effects.

2.2.3 Control

The third subject for study is control of flight motions during rapid maneuvering, and it is clear that the emphasis of recent studies has shifted away from spin

recovery to departure and spin prevention. At best, spin recovery is an emergency procedure, and it is not always successful. Safety is important, but it is not the only issue: an aircraft which is prone to spin is less likely to complete its mission successfully. It is preferable, therefore, to prevent the spin before it occurs.

Nevertheless, if a spin occurs, it is important to understand what control actions can be used to recover. The most favored technique for recovery is to command constant, anti-spin control settings (Ref. 47). The proper control settings depend on the type of spin (flat, steep, oscillatory, or erratic) and on the aircraft configuration--particularly the tail damping, aircraft density, and mass distribution. In many cases. the available anti-spin control moment is less than the restoring moments which maintain spin equilibrium, i.e., the spin cannot be broken with constant control settings. The idea of "resonating" the aircraft out of the spin by applying oscillatory controls was proposed as early as 1931 (Ref. 48) and as recently as 1974 (Ref. 49). While this task may be difficult for the pilot to execute, simple logic for pulsing the controls automatically can be designed.

The concept of automatic control systems which prevent stall, departure, and spin has gained momentum, and it is now recognized that departure prevention can be built into the stability augmentation system (SAS), which virtually all modern high-performance aircraft contain. The basic approaches to departure prevention taken to date can be classified as limiters (or inhibitors), stability augmenters, control interconnects, or some combination of these three. A dual-mode spin-prevention system is developed in Ref. 50. This system applies constant antispin controls

when α and r exceed separate threshold values, then switches to a rate-damping mode once the spin is neutralized. Reference 51 presents a departure-prevention system which inhibits α, increases directional stiffness (by stability augmentation), and restricts the aircraft to roll about its flight path. A stall-inhibitor system for a variable-sweep aircraft is described in Ref. 52. This system incorporates an α limiter, α-dependent command- and stability-augmentation gains, increased directional stiffness and damping, and aileron-rudder interconnect. A similar philosophy is adopted in Ref. 53, where speed stability also is augmented to account for α-limiting effects in the landing approach. Departure prevention considerations are evident in the designs for two additional high-performance aircraft (Refs. 54 and 55), and the effects of stability augmentation and roll/yaw interconnect are demonstrated in Ref. 56.

While a common thread runs through the designs reported in Refs. 50 to 56, these reports suggest the need for a unifying control theory to aid the design of future departure prevention systems. These studies have made extensive use of experience, nonlinear simulation, and flight testing to arrive at successful designs, but the underlying concepts of stability, response, and control remain to be identified.

Summary - This section has presented a brief survey of prior developments related to maneuvering flight, distinguishing between investigations of dynamics, aerodynamics, and control of the aircraft. It is shown that the range of problems, from degraded handling qualities to fully evolved spin, can not be completely solved by focusing on only one area. New developments are required in characterizing the evolution of motions; in the measurement and understanding of forces and moments at extreme flight conditions; and in

the computation of control solutions. In following sections of this report, the problems of dynamics and control are addressed in detail.

2.3 COMPARISON OF RESULTS FROM LINEAR AND NONLINEAR SIMULATIONS

The use of linear models in highly dynamic situations has been restricted, in the past, by a lack of linear models which include complete dynamic effects and by the lack of a general method of finding the proper nominal flight condition. The linear models developed in Appendix A include all the effects of a dynamic nominal flight condition. To verify these models and to develop methods of using them, this section presents a comparison of linear and nonlinear results. The nonlinear results are in the form of test trajectories generated by a nonlinear aircraft simulation using aerodynamic and mass data for the reference aircraft.

During the early part of this investigation, large differences between the linear and nonlinear results appeared along highly dynamic flight trajectories. These were traced to the use of an incorrect nominal state vector. From these observations, the concept of generalized trim (Section A.3.2) was developed, and a method of finding generalized trim points was derived. (Section A.3.2 describes the generalized trim calculation computer program.)

The generalized trim condition is one in which the derivatives of the velocity and angular rate states are as close to zero as possible. Dimensionality considerations, as discussed in Section A.3.2, lead to the conclusion that the generalized trim problem involves six of the aircraft

state equations, the corresponding six states, and six control parameters (in this case, four control settings and two Euler angles). The problem becomes a search for those values of nominal body-axis velocities and angular rates that null the selected nominal state rates.

The following subsections examine specific results of the comparison of linear and nonlinear trajectories to support these points.

2.3.1 Elevator Control Input

Elevator deflection produces a change in pitch moment, causing an immediate change in the aircraft angle of attack. This causes the aircraft to climb or dive. In combination with the throttle, elevator position establishes the aircraft flight speed, angle of attack, and flight path angle. The tests presented here involve small-amplitude elevator inputs when the aircraft is in straight-and-level flight at slow speed and high angle of attack. Figure 2.3-1 illustrates the time history of the most important longitudinal motion variables for eight seconds following the control application. All lateral variables are approximately zero for the nonlinear model and exactly zero for the linear model.

Comparison of the linear and nonlinear curves indicates excellent agreement. It is important to note that the nonlinear aircraft response verifies that the lateral and longitudinal modes are truly uncoupled in this flight condition. The nominal flight condition is a steady-trim flight condition and satisfies the generalized trim condition.

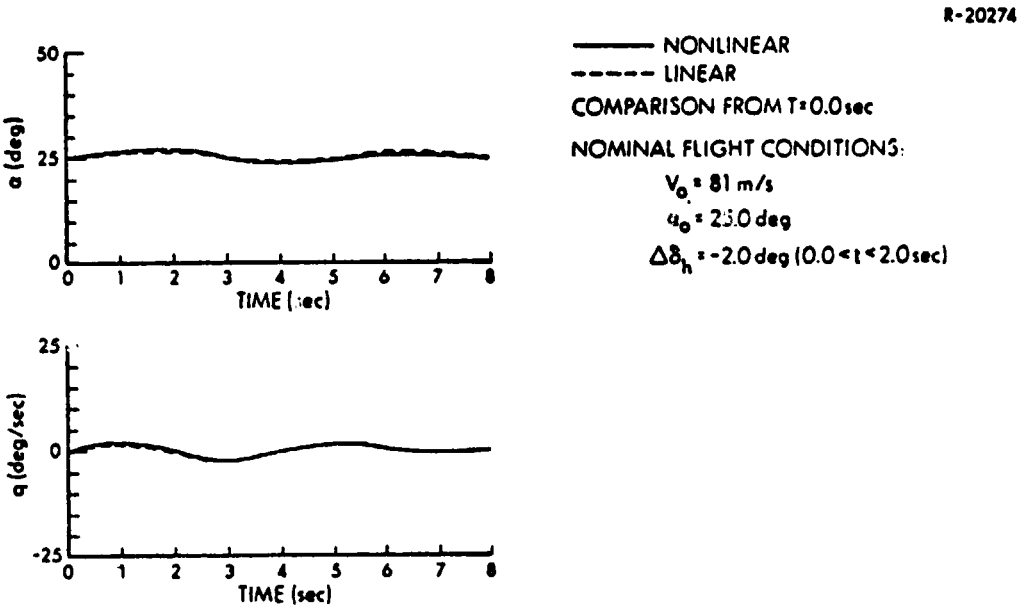

Figure 2.3-1 Small Amplitude Elevator Input

2.3.2 Aileron Control Input

The ailerons primarily provide roll moment, and the trajectories shown in Fig. 2.3-2 illustrate the aircraft response to a small amplitude aileron doublet. The linearized trajectory, whose nominal flight condition is again straight-and-level flight, differs only slightly from the true nonlinear response, and the linear and nonlinear trajectories exhibit lateral-longitudinal separation.

2.3.3 Rudder Control Input

Large-input, large-response trajectories resulting from rudder deflection are examined in this subsection, with the goal of testing the trajectory matching capabilities of a linear simulation for a highly dynamic flight condition. The nonlinear test trajectory lasts eight seconds after the

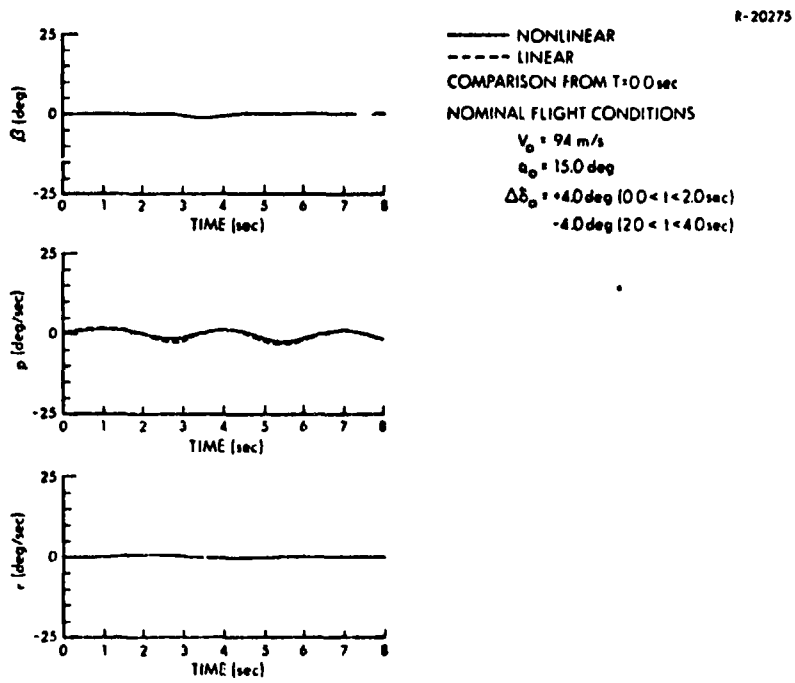

Figure 2.3-2 Small Amplitude Aileron Input

control is applied; linear trajectories starting at the initial time and at four seconds into the trajectory are tested.

Figure 2.3-3 compares the nonlinear trajectory to a linear trajectory starting at the time of control application. The nominal trajectory for linearization is the original static trim flight condition of straight-and-level flight. The trajectory match is acceptable for about two seconds, and the angle-of-attack plot illustrates the cause of the deviation. Because it exhibits lateral-longitudinal separation, the linear trajectory does not capture the change in angle of attack that the nonlinear trajectory contains. This change in angle of attack has a large effect on the subsequent dynamics which the linear model fails to duplicate.

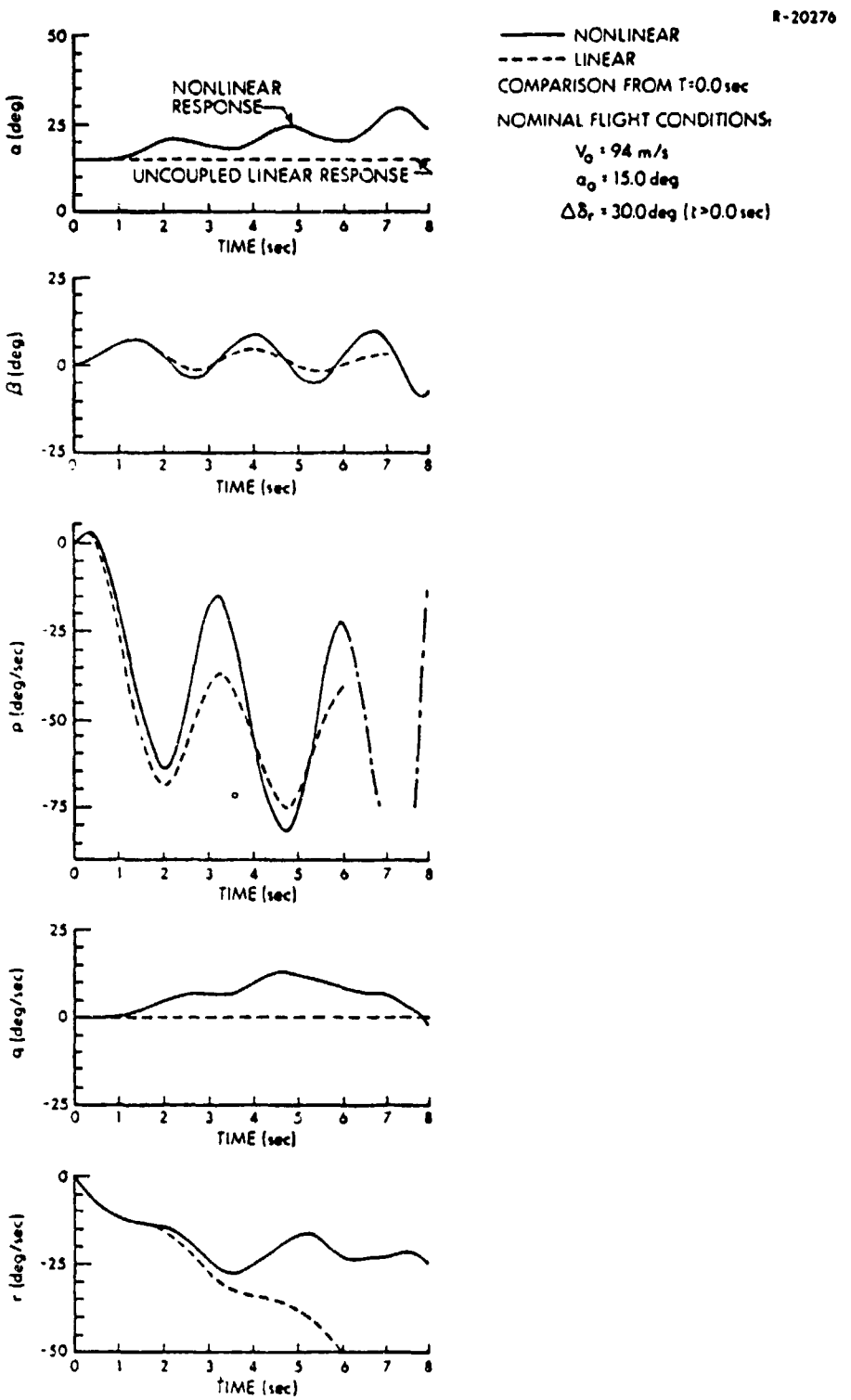

Figure 2.3-3 Large Amplitude Rudder Input -- Comparison of Initial Response

By examining the trajectory beginning four seconds after the control is applied, methods of linearization for highly dynamic trajectories can be derived. Figure 2.3-4 illustrates an early attempt. Here, the point of linearization is approximate, i.e., it does not satisfy the generalized trim condition discussed below and in Appendix A. The resulting linear trajectory diverges from the nonlinear trajectory fairly quickly, and the slopes do not match at the initial point for some states. Furthermore, the frequency of the resulting motion is considerably different from that of the nonlinear motion. Due to its dependence on ad hoc estimation of the nominal flight condition, the results of this approach are highly variable in quality.

One of the most striking errors in the linear trajectories shown in Fig. 2.3-4 is that the slopes of the states do not match at the beginning of the linear trajectory. This observation, which implies that the nominal state rates are not zero, led to the development of the generalized trim concept. In this context, this concept indicates that to provide an accurate representation of a nonlinear system by a linearized one, it is necessary to choose a point of linearization that exhibits zero nominal state rates.

Applying this generalized trim procedure to the point four seconds after control application produces the results shown in Fig. 2.3-5. Compared to the previous figure, the generalized trim procedure produces clearly superior results. There are no initial slope errors evident, the match is excellent for two seconds, and it is reasonably close for much longer. Additionally, the frequency of the linearized motions is close to that of the nonlinear

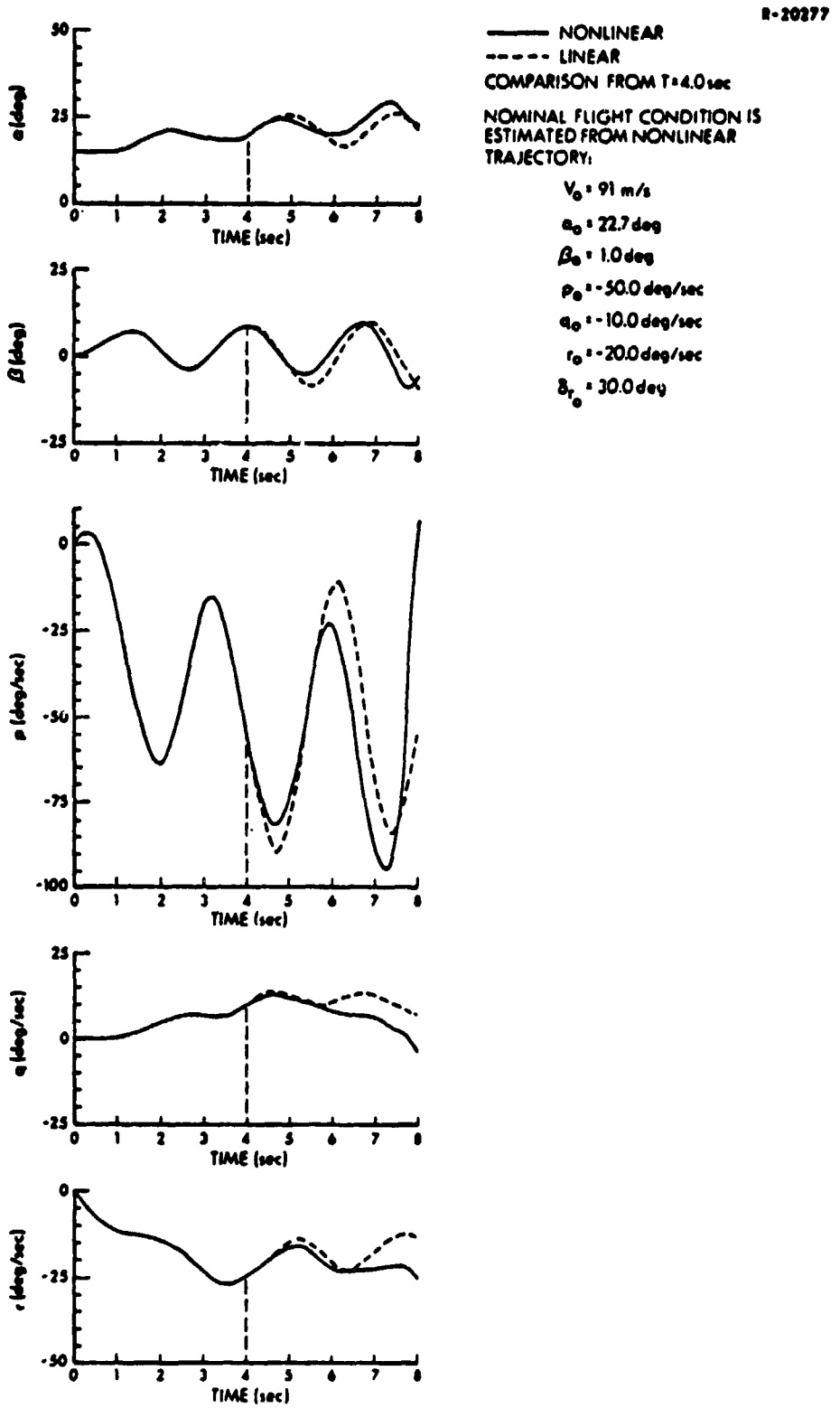

Figure 2.3-4 Large Amplitude Rudder Input -- Comparison of Evolved Response With Ad Hoc Reference Point for Linearization

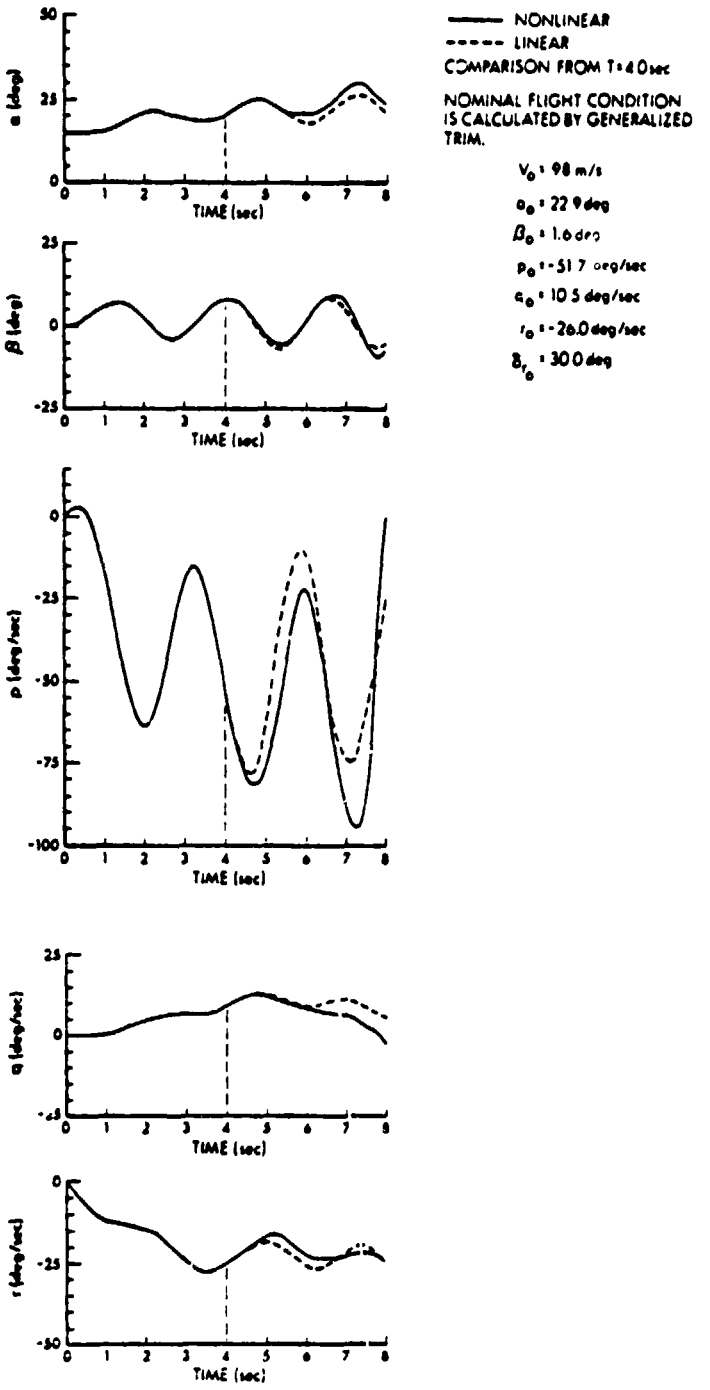

igure 2.3-5 Large Amplitude Rudder Input -- Comparison of Evolved Response With Generalized Trim Reference Point for Linearization

trajectory. This, along with the amplitude match, supports the use of a properly linearized model for the analysis of a nonlinear vehicle along a highly dynamic trajectory. The significance of this result is put in proper perspective when it is realized that the vehicle has performed a 360-deg roll between t = 0 and t = 7.2 sec, and the pitch angle goes from 15 deg to -45 deg from t = 0 to t = 5 sec.

It should be noted that the nominal flight condition for linearization was found by an analytic method that does not require the solution of a nonlinear trajectory from which to estimate nominal values. The generalized trim procedure is a useful method for calculating nominal flight conditions even along highly dynamic trajectories.

Summary - These comparisons presented here establish that nominal flight conditions which satisfy the generalized trim condition produce good trajectory matches and that the corresponding linear models should provide accurate information about the nonlinear system dynamics.

2.4 EFFECTS OF ANGULAR MOTION AND FLIGHT CONDITION ON AIRCRAFT STABILITY

The effects of altitude and velocity variations, angle-of-attack and sideslip angle variations, and steady angular rates on aircraft stability are examined in this section using the linearized dynamic models and eigenvalue/eigenvector analysis technique presented in Appendix A. The purpose of this analysis is to show the effects of individual flight variables, as well as the combined effects of flight variables which normally are zero in "1-g" straight-and-level flight. For this study, the aircraft is trimmed initially for "1-g" flight at an angle of attack of 15 deg

and at an altitude of 6100 m. As flight variables change, the load factor may change accordingly; however, the primary objective of this chapter is to isolate the individual effects of each specific flight variable being examined, so all other variables are held at their initial values.

2.4.1 Altitude and Velocity Effects

Altitude affects the air density and, therefore, the dynamic pressure. This causes the aerodynamic forces and moments to be reduced, relative to the inertial effects, as altitude increases, as shown in Fig. 2.4-1. Higher altitude causes both the natural frequencies and damping ratios of the Dutch roll and short period modes to decrease. The roll mode also slows down as altitude increases.

Changes in velocity affect the dynamic pressure, as well as the angular rate normalization terms ($b/2V$ and $\bar{c}/2V$) and the velocity-angular rate cross-product terms. These changes cause significant increases in Dutch roll and short period frequencies as velocity increases (Fig. 2.4-1a). The damping ratio of the short period mode is affected only slightly by velocity changes over the range shown in Fig. 2.4-1b. The Dutch roll damping decreases as velocity decreases, so that the Dutch roll is unstable at the lowest velocities presented here. The reference aircraft's roll mode (Fig. 2.4-1c) is changed only slightly as velocity varies, contrary to the result obtained from the approximate lateral-longitudinal equations discussed below.

Figure 2.4-1 indicates only small increase in spiral mode speed and phugoid frequency and damping at lower altitudes. Low velocity results in low phugoid

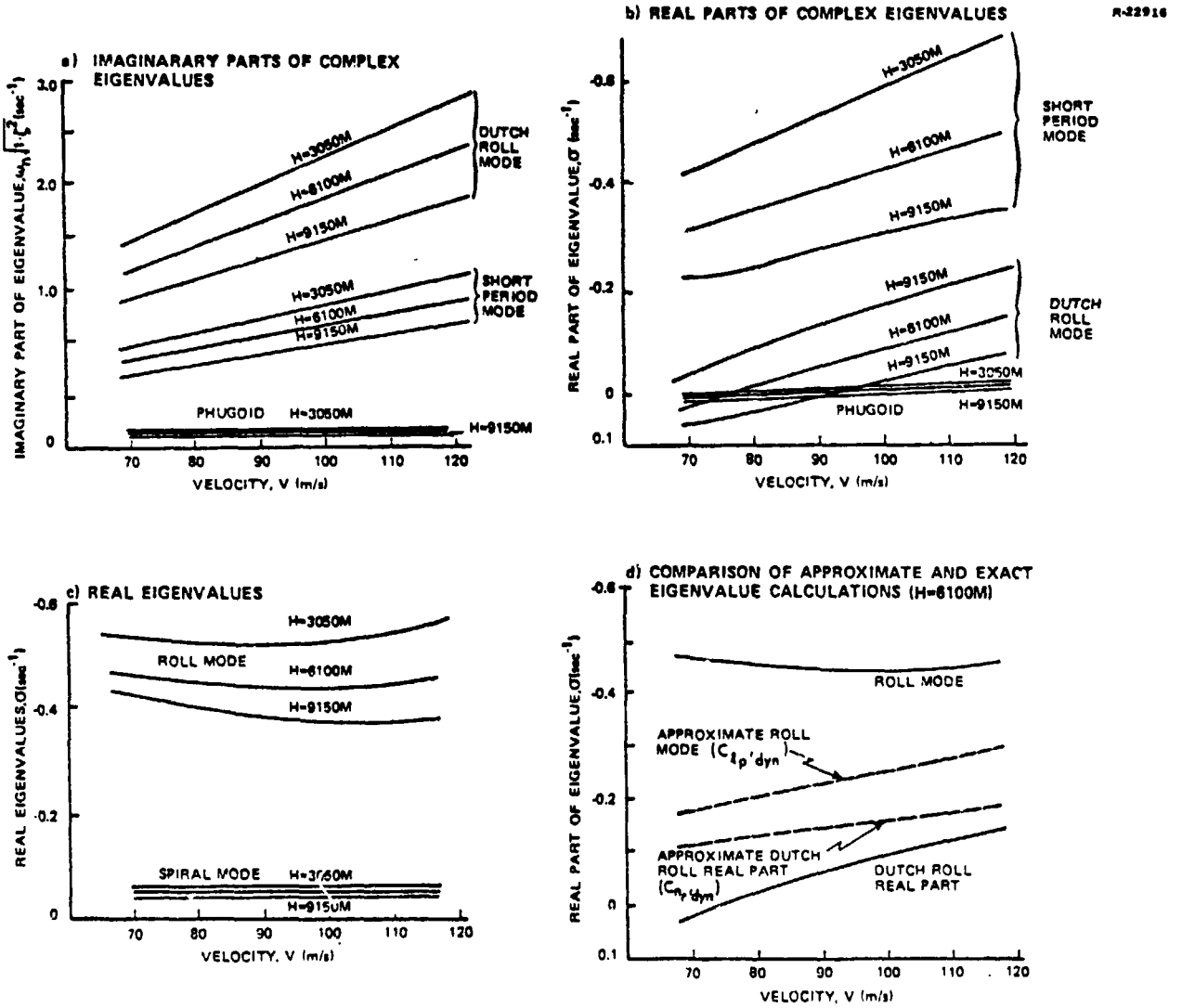

Figure 2.4-1 Altitude and Velocity Effects on Eigenvalues

damping, so much so that the mode is unstable over a significant portion of the velocity range examined in Fig. 2.4-1.

As noted above, the lack of roll mode variation with velocity is contrary to results obtained with accepted approximations. The expected linear change in roll mode with velocity is deduced from approximate lateral-directional equations, which can be derived by neglecting the roll angle equation (and, therefore, the spiral mode), by assuming that the Dutch roll mode consists of wind-axis yawing motion, and by assuming that the roll mode consists of wind-axis roll. The approximations that result from these approximate lateral-directional equations are

$$\lambda_{roll} \cong \frac{1}{4I_x} \rho_0 V_0 S b^2 C_{l_{p,dyn}} \tag{2.4-1}$$

$$\zeta\omega_{n,DR} \cong -\frac{1}{8I_z} \rho_0 V_0 S b^2 C_{n_{r,dyn}} \tag{2.4-2}$$

$$\omega^2_{n,DR} \cong \frac{1}{2I_z} \rho_0 V_0^2 S b C_{n_{\beta,dyn}} \tag{2.4-3}$$

where λ_{roll} is the roll mode eigenvalue, $C_{n_{\beta,dyn}}$ is defined as in Eq. (2.2-1) and

$$C_{l_{p,dyn}} = \cos \alpha_0^2 C_{l_p} + \cos \alpha_0 \sin \alpha_0 C_{l_r} + \left(I_x/I_z\right)\left(\sin \alpha_0 \cos \alpha_0 C_{n_p} + \sin^2 \alpha_0 C_{n_r}\right) \tag{2.4-4}$$

$$C_{n_{r,dyn}} = \cos^2 \alpha_0 C_{n_r} - \sin \alpha_0 \cos \alpha_0 C_{n_p} + \left(I_z/I_x\right)\left(-\sin \alpha_0 \cos \alpha_0 C_{l_r} + \sin^2 \alpha_0 C_{l_p}\right) \tag{2.4-5}$$

Equations (2.4-1) and (2.4-2) predict values for λ_{roll} and $\zeta\omega_{n,DR}$ as shown by the dotted lines in Fig. 2.4-1d for the 6100-m case. The actual values, taken from Figs. 2.4-1b and c, are shown by solid lines on the same figure. The approximate equations do a poor job of predicting mode speed because the subject aircraft is fuselage-heavy (high I_Z/I_X ratio); hence, the Dutch roll contains more rolling response than is assumed when deriving the approximate equations. As can be seen from Fig. 2.4-1d, this leads to a damping interchange such that the roll mode is faster than expected and the Dutch roll mode is more poorly damped than predicted.

This examination leads to the following conclusions for the reference aircraft:

- Higher altitudes result in lower damping and frequency of the Dutch roll and short period modes, as well as increased roll mode time constant.
- Lower velocities result in a decrease in short period frequency at constant damping ratio, as well as decreased Dutch roll frequency and damping.
- The approximate lateral-directional equations do not predict roll mode or Dutch roll damping accurately for the subject aircraft. The complete equations should be used for an accurate determination of these parameters.

2.4.2 Aerodynamic Angle Effects

The aerodynamic angles, α and β, specify the orientation of the vehicle relative to the velocity vector, and, to a large extent, they define the flow field around the vehicle. For this reason, the aerodynamic angles are prime determinants of the aerodynamic forces and moments. Consequently,

significant differences in the speeds and shapes of the normal modes occur as α_0 and β_0 are varied.

Figure 2.4-2 illustrates the boundaries between stability and instability which result from these variations. These boundaries define the α_0 and β_0 for which the real part of one or more eigenvalues migrates from negative (stable) to positive (unstable) sign (see Section A.4.1). The phugoid mode is a slow mode and is unstable at low α_0. The Dutch roll mode, a fast mode, becomes unstable at high α_0. The dashed line in Fig. 2.4-2 is an important boundary, indicating the transition of a relatively slowly divergent phugoid oscillation into two real roots, one of which is highly unstable. This transition line occurs at high β_0 -- about 10 to 15 deg.

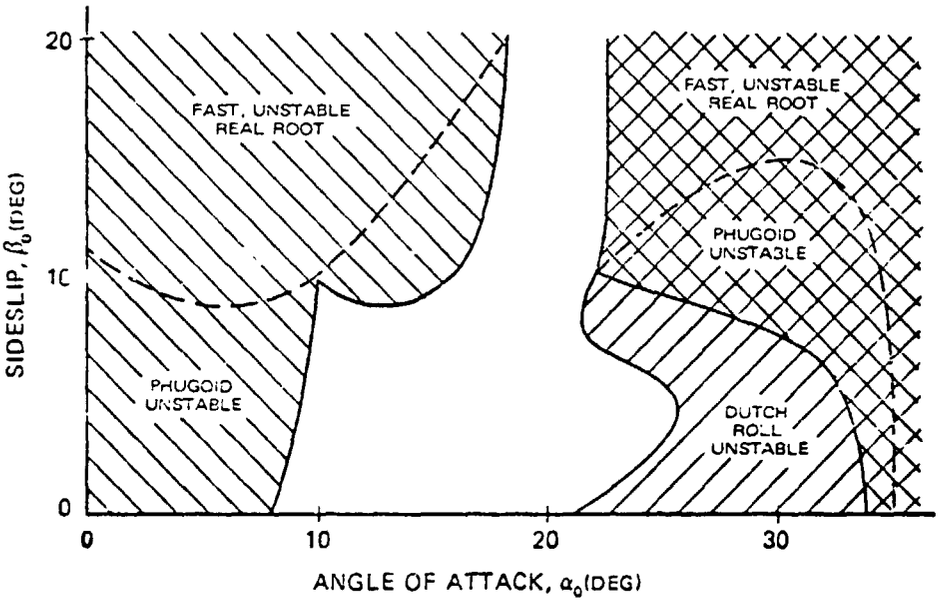

Figure 2.4-2 Effects of Aerodynamic Angles on Aircraft Stability

The shape of the Dutch roll stability boundary indicates that moderate values of nominal sideslip angle (two to five deg) stabilize the mode. This is due to lateral-longitudinal coupling; a close examination of the

Dutch roll/short period eigenvalues indicates that, up to about five deg of sideslip, Dutch roll damping increases as short period damping decreases.

The eigenvectors of the linearized model provide information about the normal mode shapes which indicate the involvement of each state in each mode. Figure 2.4-3 illustrates some specific eigenvalue/eigenvector variations with angle of attack. Real eigenvectors, such as those associated with the roll mode, are characterized only by the relative magnitudes of each state, as the phase angles are either 0 or 180 deg. A time history of this mode would show a constant ratio between the various state amplitudes. These amplitudes would evidence exponential decays with equal time constants, given by the negative inverse of the eigenvalue. Complex eigenvectors, such as those of the Dutch roll, are characterized by the relative magnitudes of the involved states and by the phase angle between them. A time history of this oscillatory mode is generated by the projections of the eigenvectors on the real axis as the entire eigenvector set rotates with angular rate given by the imaginary part of the eigenvalue. The magnitudes decay exponentially with the time constant given by the negative inverse of the eigenvalue's real part.

Despite the large changes in eigenvalues with angle of attack, Fig. 2.4-3 shows little corresponding change in eigenvector shape. The only major changes involve the proportions of angular rates in the fast modes, and these changes are due to mode speed variations, as described above for the roll mode. The short period mode contains increased pitch rate at large α_0 for this reason; in the Dutch roll eigenvector, the roll rate-to-sideslip ratio increases and decreases with the Dutch roll frequency. Overall, the Dutch

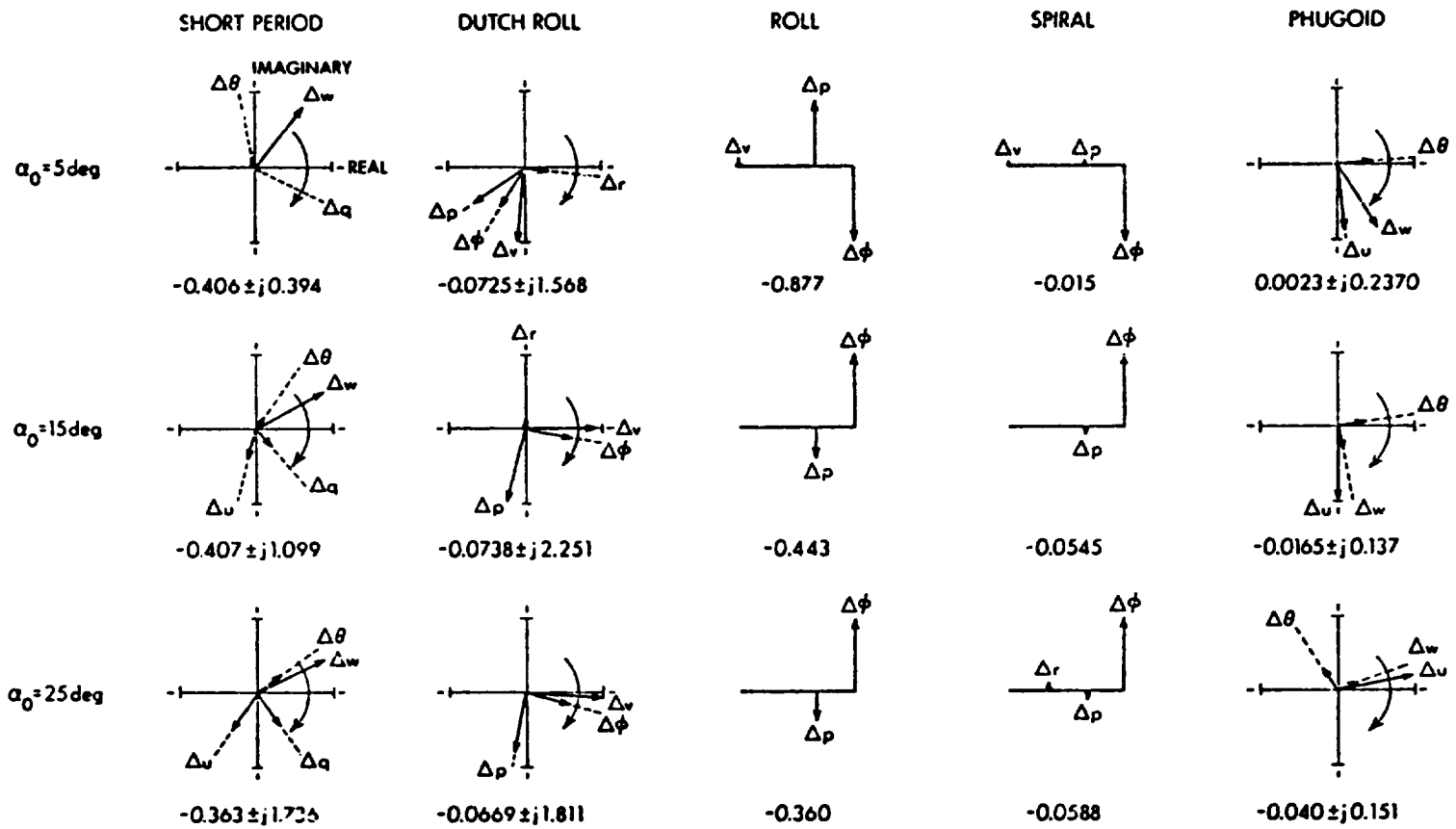

Figure 2.4-3 Angle-of-Attack Effects on Aircraft Eigenvectors

roll mode of this aircraft involves a great deal of rolling motion, underlining the low rolling inertia typical of modern fighters.

The short period eigenvector shows that this oscillation typically involves angle-of-attack perturbations at constant velocity, as axial and normal velocity perturbations are approximately 180 deg out of phase with each other and are related in magnitude by tan α_0. The short period mode is faster at high angle of attack, and it includes more pitch rate than at low angle of attack.

The changes in specific eigenvalues and eigenvectors with sideslip angle are illustrated in Fig. 2.4-4. Lateral-longitudinal coupling is quite prominent for the asymmetric flight conditions portrayed in this figure. Modes of comparable speed couple most readily. Roll angle response is found in the phugoid mode, and pitch angle becomes a component of the spiral mode, so that both modes involve slow roll-pitch motion. Angle of attack appears in the Dutch roll eigenvector, and a roll-sideslip combination becomes important in the short period mode, so that both modes involve an angle of attack-sideslip oscillation. In both cases, Δw and Δv (or, equivalently, $\Delta\alpha$ and $\Delta\beta$) are almost 180 deg out of phase. Note that the changes in the speeds of these modes are small and gradual as the sideslip angle is varied.

To demonstrate some of the causes of aerodynamic angle effects observed above, the aerodynamic coefficients are held constant (at the values for α_0 = 15 deg and β_0 = 0 deg), and the body orientation with respect to the velocity vector is varied over the same range of aerodynamic angles used in Fig. 2.4-2. The results, shown in Fig. 2.4-5, differ significantly from those shown in Fig. 2.4-2. There is only a slight sideslip effect. The Dutch roll mode, rather than

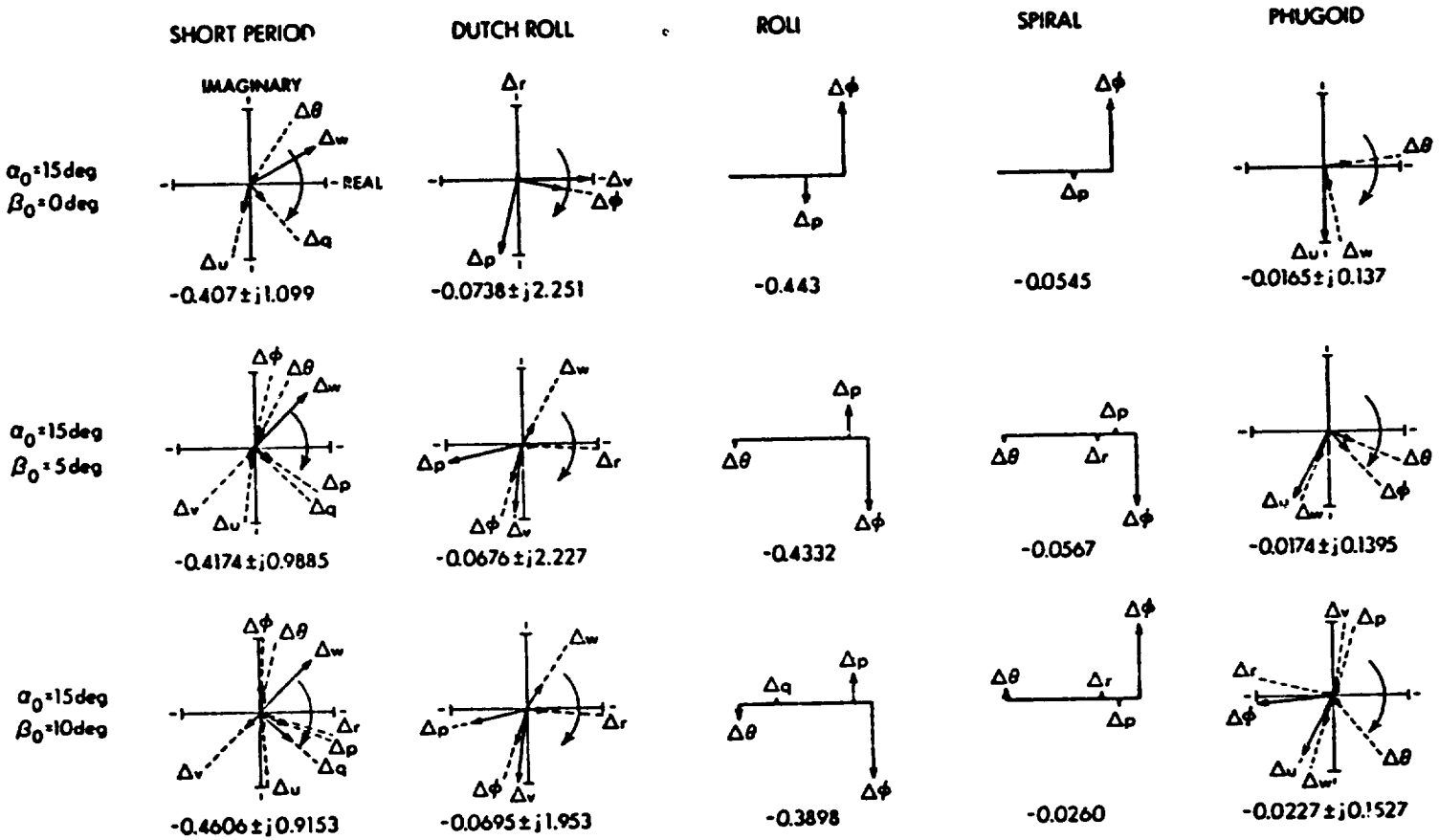

Figure 2.4-4 Sideslip Effect on Aircraft Eigenvectors

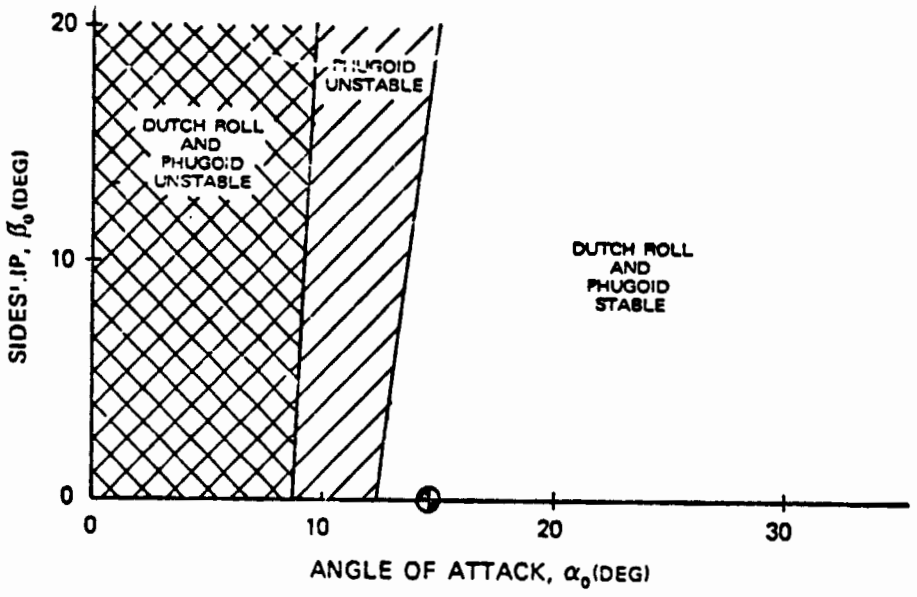

Figure 2.4-5 Effects of Body Orientation on Aircraft Stability

becoming unstable at high α_0, is destabilized by lower α_0. The phugoid stability boundary near α_0 = 12 deg is roughly similar to that found in Fig. 2.4-2, indicating that the lack of phugoid stability in this area is not due to aerodynamic variations.

Figure 2.4-6 assists in the evaluation of the high angle-of-attack Dutch roll instability. This figure compares the Dutch roll eigenvalue to the departure parameter $C_{n_{\beta,dyn}}$ (see Section 2.2) and to C_{n_r} and $C_{n_{r,dyn}}$, the last of which is defined in Eq. (2.4-5).

The results of Fig. 2.4-6 indicate that, at least in this case, $C_{n_{\beta,dyn}}$ is a good indicator of the Dutch roll mode's imaginary part. Neither C_{n_r} nor $C_{n_{r,dyn}}$ provide a particularly useful indication of Dutch roll stability. This example indicates that $C_{n_{\beta,dyn}}$ has only limited value as a departure parameter. For this aircraft, Dutch roll

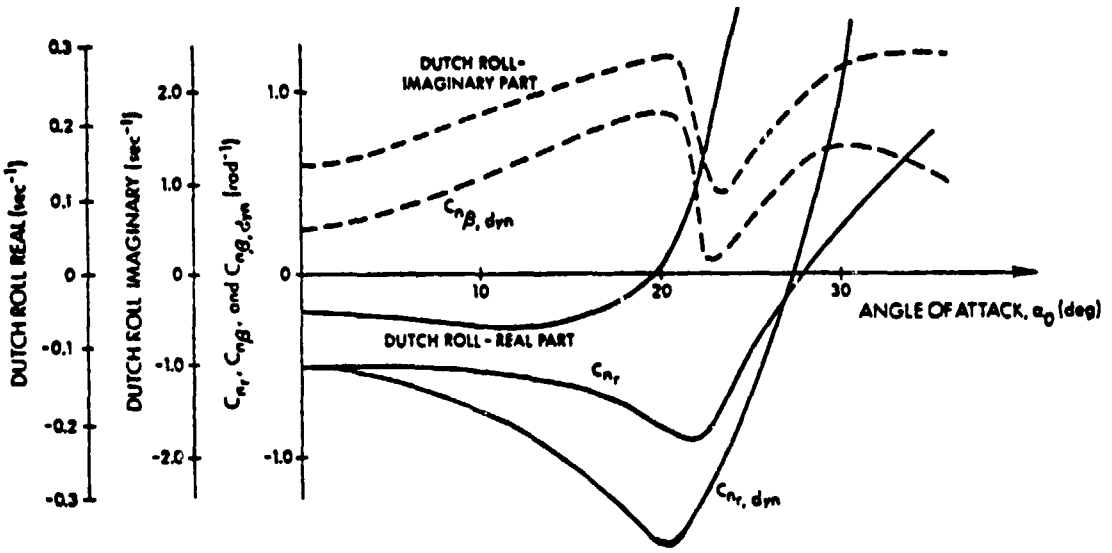

Figure 2.4-6 Variations of Directional Aerodynamic Coefficients with Angle of Attack

instability is due to negative damping, and $C_{n_{\beta,dyn}}$ is inadequate as a predictor of departure.

The following conclusions concerning aerodynamic angle effects on stability of the reference aircraft can be made:

- The Dutch roll mode becomes unstable due to negative damping at high α_0. This is caused by changes in the aerodynamics as α_0 increases.
- Mean angle of attack variations have significant effect on the eigenvalues, but mode shape (eigenvector) changes are small relative to other effects.
- Mean sideslip angle introduces lateral-longitudinal coupling; therefore it has a large effect on the mode shapes (eigenvectors), without causing large changes in the eigenvalues. This lateral-longitudinal coupling primarily occurs between modes of similar speed and can lead to a transfer of damping, as in the situation where small sideslip angles

stabilize the Dutch roll mode at the expense of short period damping.

- The parameter $C_{n_{\beta,dyn}}$ gives a good indication of Dutch roll frequency, but it is not useful as a departure parameter for the subject aircraft.

2.4.3 Angular Rate Effects

Non-zero nominal angular rates have two effects on the linearized aircraft dynamics. The first, an aerodynamic effect, results in a change in the nominal forces and moments due to the steady angular rates. The second is dynamic, and it is due to the cross product of angular rate with velocity (in the force equations) and with angular momentum (in the moment equations). The specific terms involved (for $I_{xz} = 0$) are given in Table 2.4-1. A close examination reveals that mean pitch angular rate, q_0, enters both the lateral and longitudinal equations but does not affect lateral-longitudinal coupling terms. Mean roll and yaw rates, p_0 and r_0, enter as lateral-longitudinal coupling terms. Steady roll-rate capability of most high-performance aircraft is much higher than pitch- or yaw-rate capability, so roll-rate effects are especially important.

Stability boundaries as functions of pitch rate and yaw rate are illustrated in Fig. 2.4-7. The destabilizing influence of q_0 is the major effect, and it has an especially severe effect on the Dutch roll mode. Yaw rate has a mild stabilizing effect on the Dutch roll and spiral modes. This is due partially to lateral-longitudinal coupling, because short period and phugoid damping decrease as Dutch roll damping increases.

TABLE 2.4-1

DYNAMIC EFFECTS OF STEADY ANGULAR RATE

Angular Rate	Multiplied By	Enters Term
p_0	$(I_z-I_x)/I_y$	$\partial\dot{q}/\partial r$
p_0	-1	$\partial\dot{w}/\partial v$
p_0	1	$\partial\dot{v}/\partial w$
p_0	$(I_x-I_y)/I_z$	$\partial\dot{r}/\partial q$
q_0	-1	$\partial\dot{u}/\partial w$
q_0	1	$\partial\dot{w}/\partial u$
q_0	$(I_x-I_y)/I_z$	$\partial\dot{r}/\partial p$
q_0	$(I_y-I_z)/I_x$	$\partial\dot{p}/\partial r$
r_0	1	$\partial\dot{u}/\partial v$
r_0	$(I_z-I_x)/I_y$	$\partial\dot{q}/\partial p$
r_0	-1	$\partial\dot{v}/\partial u$
r_0	$(I_y-I_z)/I_x$	$\partial\dot{p}/\partial q$

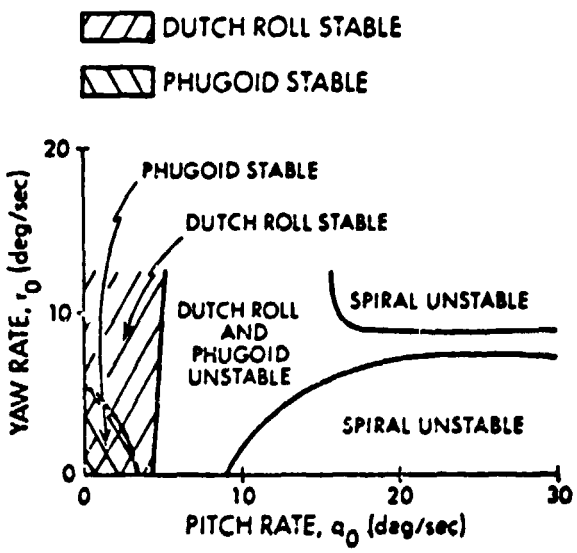

Figure 2.4-7 Yaw-Rate/Pitch-Rate Effects (α_0=15 deg)

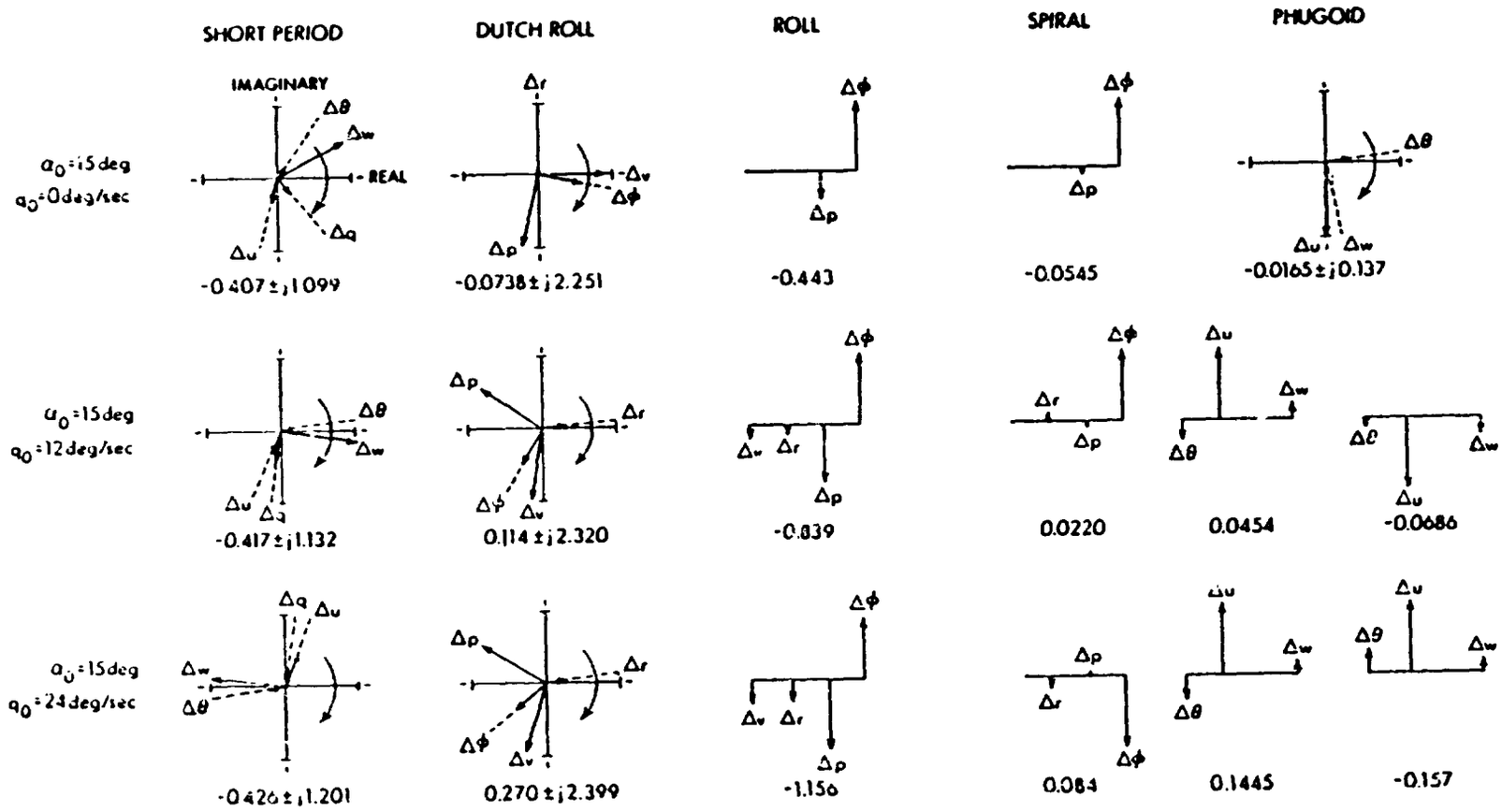

Figure 2.4.8 Pitch-Rate Effects on Eigenvectors

The eigenvector changes that accompany increases in q_0 are shown in Fig. 2.4-8. Steady pitch rate does not introduce lateral-longitudinal coupling, but some changes in mode shapes appear in the roll mode and in the separation of the complex phugoid mode into two real roots. Both frequencies and damping ratios of the Dutch roll and short period modes change, but changes in the mode shape are minor.

Steady roll rate is important because fighter aircraft are capable of high p_0, and air combat maneuvers often include such motions. For the aircraft to roll with constant aerodynamic angles, the roll rate must occur about the wind x-axis (which is the same as the stability x-axis for constant nominal aerodynamic angles). Sideslip variations also are considered, since piloting error can easily result in non-zero β_0 during a rolling maneuver. Both positive and negative p_0 are considered, to account for roll "into" or "out of" the sideslip.

The stability boundaries that result from combined roll rate and sideslip are shown in Fig. 2.4-9. These boundaries indicate that p_0 has only a small effect on the fast modes, primarily the Dutch roll mode. The combination of p_0 and small values of β_0 of opposite sign serves to destabilize the Dutch roll mode. Roll rate destabilizes the phugoid mode in general, but there is a combination of β_0 and p_0 that maintains phugoid stability. High β_0 results in a fast divergence for all values of p_0 tested.

Eigenvector variations due to steady rolling are illustrated in Fig. 2.4-10. Eigenvalue changes are significant, considering the angular rates involved. The mode shapes also change, so that lateral-longitudinal coupling is important. Large roll-rate/sideslip perturbations in

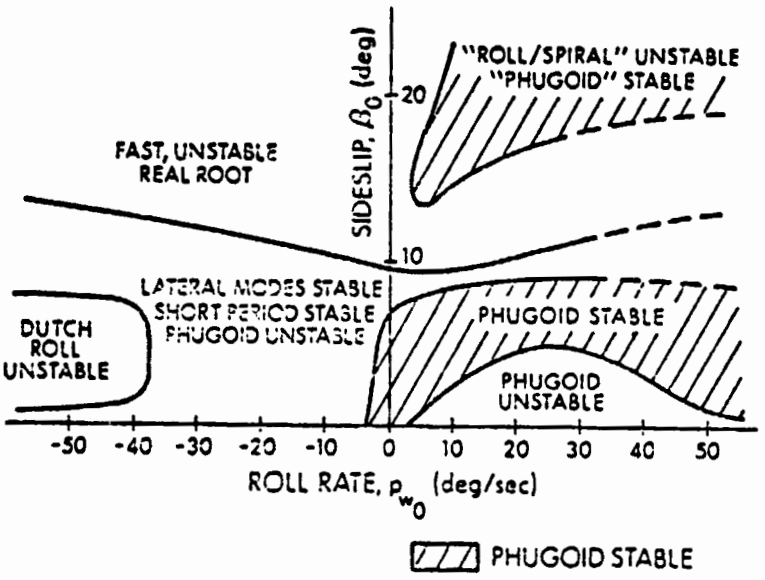

Figure 2.4-9 Stability Boundaries for Sideslip/ Roll-Rate Variations ($\alpha_0 = 15$ deg)

the short period mode and large angle of attack perturbations in Dutch roll mode are examples of this coupling.

Conclusions about steady angular rate effects are as follows:

- Mean yaw rate and roll rate cause lateral-longitudinal coupling and therefore change the mode shapes significantly. Roll rate is by far the more significant because of the large values it can exhibit.
- Mean pitch rate changes the speeds of the normal modes without affecting their shapes significantly. Even low values of q_0 (about 5 deg/sec) can cause the Dutch roll mode to be unstable.

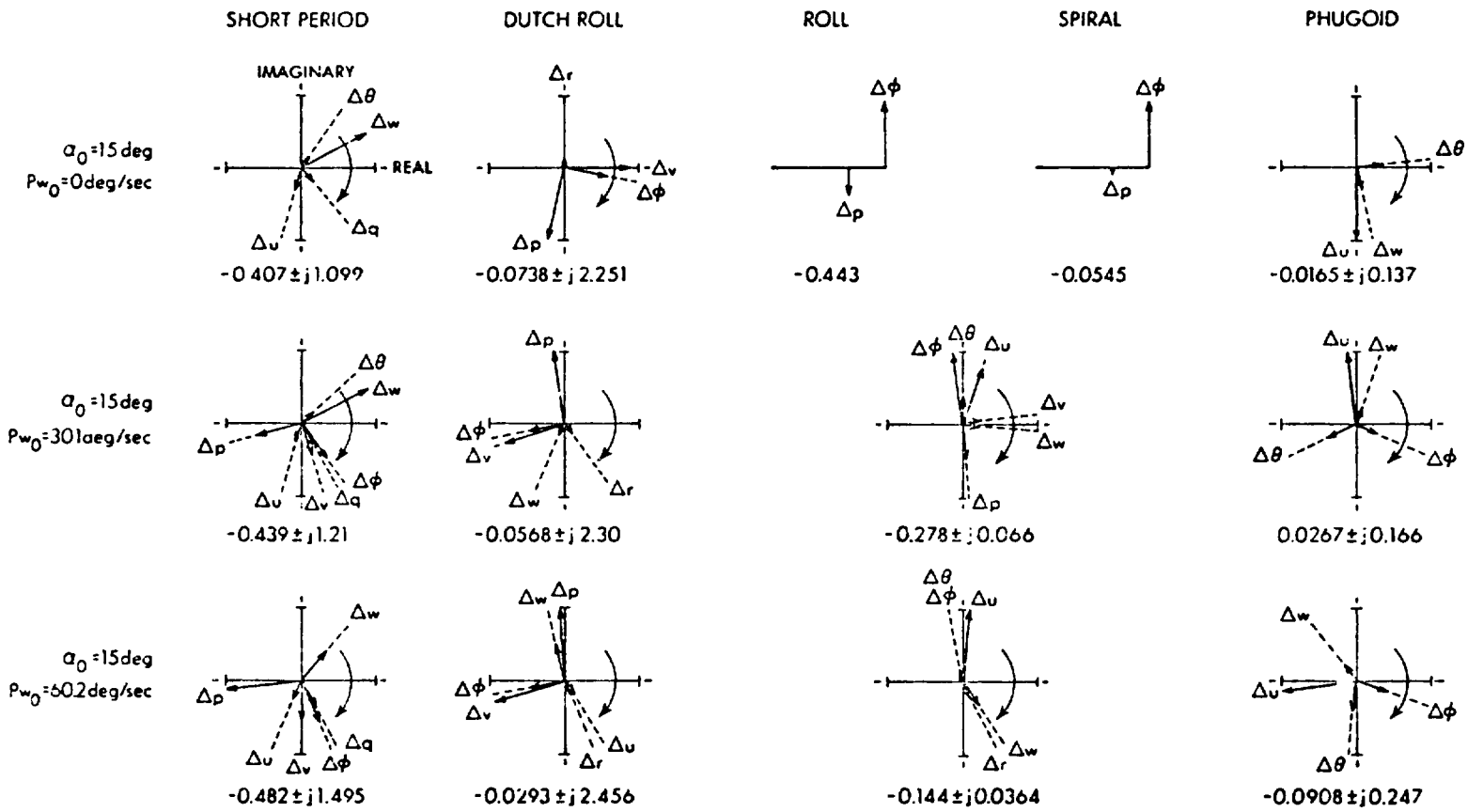

Figure 2.4-10 Roll-Rate Eigenvector Effects

2.5 EFFECTS OF ANGULAR MOTION AND FLIGHT CONDITION ON AIRCRAFT CONTROL

The transfer function provides a primary measure of the quality of aircraft control, as it is the Laplace transform of the ratio between a specific output and a specific input (Appendix A). The transfer function gain, K_F, is the stady-state value of the transfer function after all transients damp out, assuming that all transients are stable. The transfer function gain, K_I, is (for most aircraft), the initial state rate response to a transfer function's control step. The poles of the transfer function are the eigenvalues of the unforced system, as described in Appendix A.

The zeros affect the magnitudes of excitation of the normal modes, which are related to the distance between the zeros and the appropriate eigenvalues in the s plane. In the limiting case, a zero and pole in the same location cancel, and the corresponding mode does not appear in that response. Zeros located in the right half-plane are called nonminimum-phase zeros (due to their effects on the phase-shift of sinusoidal inputs), and they have major impact on the aircraft's transient response and on controller design. For example, an undesirable reversal in the initial response is caused by such zeros, as illustrated in Fig. 2.5-1.

The nonminimum-phase type of response is undesirable because it makes closed-loop control difficult. The pilot can be misled by this type of response, as the magnitude and sign of the motion are uncertain. Addition of a high-gain feedback loop around a transfer function that exhibits nonminimum-phase properties can result in instability of the

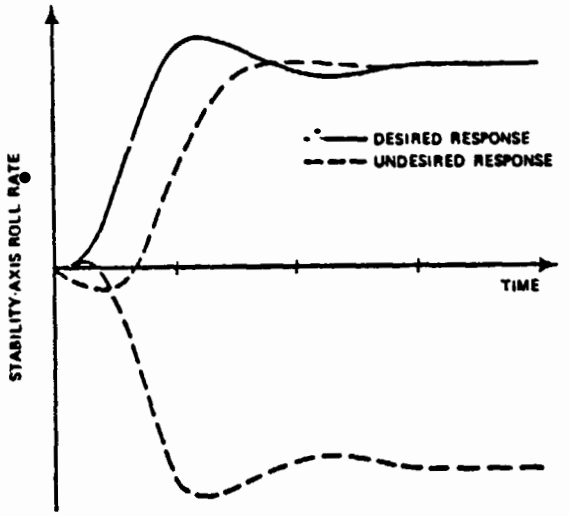

Figure 2.5-1 Typical Step Response Forms

closed-loop system (Ref. 9). Finally, this type of response can make it impossible to implement some simple forms of adaptive control, as they can suffer from instability for an analogous reason (Ref. 57).

2.5.1 Velocity and Aerodynamic Angle Effects

As has been observed previously (Section 2.4.1), velocity changes the dynamic pressure, which affects the control effectiveness. Table 2.5-1 illustrates some typical values of the transfer function gain, K_F, at different speeds, and the variation is as expected. Altitude also affects dynamic pressure in that increasing altitude decreases atmospheric density; hence, dynamic pressure decreases.

TABLE 2.5-1
VELOCITY EFFECTS ON TRANSFER FUNCTION GAIN, K_F

Velocity	$\Delta w/\Delta\delta_h$	$\Delta p/\Delta\delta_a$	$\Delta r/\Delta\delta_a$
70 m/s	-3.88	-0.50	-4.04
94 m/s	-5.17	-0.66	-5.39
117 m/s	-6.47	-0.83	-6.74

Aerodynamic angle variations can cause large changes in the system eigenvalues and can be expected to have significant effects on the numerator of the transfer function as well. Table 2.5-2 illustrates variations in K_I and K_F as α_0 and β_0 vary. (See Section A.4.3 for the definition of K_I.) The invariability of K_I with sideslip indicates that the control effectiveness does not depend on sideslip. This is a function of the aerodynamic data used here (Appendix B), as the data does not model the effects of β_0 on control effectiveness. The steady-state gain, K_F, shows a large dependence on sideslip because this gain depends on the pole and zero locations, which themselves vary with β_0.

The sign changes in K_F (at small α_0) as β_0 varies are due to changes in the number of unstable poles and nonminimum-phase zeros. From Eq. (2.5-6), it can be seen that such a change results in a K_F sign change if the sign of K_I remains the same.

One of the major effects of angle-of-attack variations (best seen in the K_I gain of the $\Delta p/\Delta\delta_a$ transfer

TABLE 2.5-2

AERODYNAMIC ANGLE EFFECTS ON TRANSFER FUNCTION GAINS (V_0=94 m/s)

		K_F							K_I		
α(deg)	β(deg)	$\Delta w/\Delta\delta_h$	$\Delta v/\Delta\delta_a$	$\Delta r/\Delta\delta_a$	$\Delta p/\Delta\delta_a$	$\Delta v/\Delta\delta_r$	$\Delta r/\Delta\delta_r$	$\Delta p/\Delta\delta_r$	$\Delta w/\Delta\delta_h$	$\Delta p/\Delta\delta_a$	$\Delta r/\Delta\delta_r$
5.0	0.0	-1.04	2.46	18.39	-4.91	-0.95	-7.11	1.90	-0.10	2.98	-0.53
5.0	10.0	0.33	-3.86	-32.02	8.64	0.37	3.04	-0.82	-0.10	2.98	-0.53
15.0	0.0	-1.58	0.41	2.47	-0.66	-0.89	-5.39	1.44	-0.14	1.71	-0.57
15.0	10.0	-2.37	1.43	9.88	-2.64	-1.71	-11.85	3.17	-0.14	1.71	-0.57
25.0	0.0	-0.84	0.03	0.49	-0 13	-0.27	-4.29	1.15	-0.11	-0.001	-0.44
25.0	10.0	-1.50	0.01	0.42	-0.11	-0.05	-3.83	1.02	-0.11	-0.001	-0.44

function)is the loss of aileron roll control at high α_0. This loss of aileron roll effectiveness, combined with the continued effectiveness of the rudder for roll and yaw control, leads to the conclusion that this aircraft is rolled more effectively with the rudder at high angles of attack.

An examination of the transfer function zeros (Table 2.5-3) indicates that nonminimum-phase zeros are quite prevalent, although often accompanied by right-half-plane poles, i.e., they often occur in unstable systems. Right-half-plane zeros are important in control system design because closed-loop poles of a system with a simple loop closure migrate from the open-loop poles to the zeros as the loop gain is increased. Therefore, in a system with right-half-plane zeros, too high a gain may result in an unstable closed-loop system.

When β_0 is not zero, there is mode coupling, and a control input excites all modes. This is indicated by Table 2.5-4, which presents the poles and zeros of three transfer functions at a flight condition where β_0 is non-

TABLE 2.5-3

EFFECTS OF ANGLE OF ATTACK ON TRANSFER FUNCTION ZEROS

Transfer Function	α_0(deg)	Zeros
$\Delta w/\Delta\delta_h$	5	0.0084 ±j 0.0824 -25.89*
	15	-0.0025 ±j 0.1167 -21.07
	25	-0.0281 ±j 0.1500 -25.56
$\Delta v/\Delta\delta_a$	5	-0.168 -1.465 86.43
	15	-0.137 -0.512 1325.0
	25	-0.164 0.178 133.7*
$\Delta r/\Delta\delta_a$	5	0.350 ±j 2.914 -1.06
	15	2.06 ±j 9.63 -0.385
	25	0.036 ±j 1.725 -0.237*
$\Delta p/\Delta\delta_a$	5	-0.141 ±j 1.399 0.0270
	15	-0.152 ±j 1.295 0.0278
	25	-13.67 22.49 0.0300*
$\Delta v/\Delta\delta_r$	5	0.0198 -0.840 -40.97
	15	0.0956 -0.393 -45.74
	25	0.0795 -0.188 -41.70*
$\Delta r/\Delta\delta_r$	5	0.036 ±j 0.686 -0.916
	15	-0.025 ±j 1.720 -0.391
	25	0.023 ±j 1.694 -0.238*
$\Delta p/\Delta\delta_r$	5	0.027 -1.80 1.79
	15	0.028 -2.98 3.54
	25	0.030 -2.66 3.05*

*Accompanied by right-half-plane poles

TABLE 2.5-4

POLE-ZERO COMPARISON AT $\alpha_0 = 15$ DEG, $\beta_0 = 10$ DEG

Poles				
Short Period	Dutch Roll	Roll	Spiral	Phugoid
-0.461 ±j 0.915	-0.0695 ±j 1.953	-0.390	-0.026	-0.0227 ±j 0.183
Zeros of $\Delta w/\Delta\delta_h$				
-20.75	-0.0928 ±j 2.032	-0.435	-0.033	-0.0009 ±j 0.114
Zeros of $\Delta r/\Delta\delta_r$				
-0.593 ±j 1.001	0.153 ±j 1.301	-0.391		-0.0219 ±j 0.147
Zeros of $\Delta p/\Delta\delta_a$				
-0.449 ±j 1.161	-0.121 ±j 1.272		0.028	-0.0204 ±j 0.143

zero. Note that the lateral mode poles are not canceled in $\Delta w/\Delta\delta_h$ and that the longitudinal mode poles are not canceled in the $\Delta r/\Delta\delta_r$ and $\Delta p/\Delta\delta_a$ transfer functions.

The effects of velocity and aerodynamic angles on control of the example aircraft can be summarized as follows:

- Lower velocities lead to decreased control effectiveness, as demonstrated by transfer function gains.
- Non-zero β_0 does not affect K_I, but does change the poles and zeros so that all modes are excited.
- Mean angle of attack leads to significant changes in control effectiveness, so much so that the rudder is more efficient than the aileron for producing roll at high angles of attack.
- Nonminimum-phase zeros are prevalent in the aircraft transfer functions at increased angle of attack.

2.5.2 Angular Rate Effects

Although no explicit effects of nominal angular rates on the control effectiveness are included in the specific aerodynamic data used here, angular rates cause significant changes in the transfer functions due to pole and zero shifts. This is apparent in Table 2.5-5, which shows changes in transfer function gains due to nominal pitch rate. The initial value of the transfer function, K_I, does not vary with q_0 because K_I depends only on the control effectiveness. The steady-state gain, K_F, does vary with q_0 because of the pole and zero variations. As above, sign variations in K_F indicate the appearance of unequal numbers of nonminimum-phase zeros and right half-plane poles.

TABLE 2.5-5

EFFECTS OF PITCH RATE ON TRANSFER FUNCTION GAINS (α_o=15deg)

	K_F							K_I		
q(deg/sec)	$\Delta w/\Delta\delta_h$	$\Delta v/\Delta\delta_a$	$\Delta r/\Delta\delta_a$	$\Delta p/\Delta\delta_a$	$\Delta v/\Delta\delta_r$	$\Delta r/\Delta\delta_r$	$\Delta p/\Delta\delta_r$	$\Delta w/\Delta\delta_h$	$\Delta r/\Delta\delta_r$	$\Delta p/\Delta\delta_a$
0	-1.58	0.41	2.47	-0.66	-0.89	-5.39	1.44	-0.14	-0.58	1.71
12	-5.67	-0.02	-2.61	2.44	0.04	5.68	-5.32	-0.14	-0.57	1.71
24	-2.51	0.17	-0.39	0.72	-0.37	0.84	1.56	-0.14	-0.57	1.71

Mean wind-axis roll rate, like β_0, has no effect on control power but does change the mode shapes significantly. The steady-state transfer function gain varies with p_0 as shown in Table 2.5-6. This variation is fairly smooth, compared to the effects of q_0, and the only sign changes are in the roll-rate transfer functions. Because non-zero roll rate creates lateral-longitudinal coupling, any control displacement excites all of the normal modes.

TABLE 2.5-6

EFFECTS OF ROLL RATE ON TRANSFER FUNCTION GAIN, K_F (α_o=15 deg)

T-0244

p_{W_o} (deg/sec)	$\Delta w/\Delta\delta_h$	$\Delta v/\Delta\delta_a$	$\Delta r/\Delta\delta_a$	$\Delta p/\Delta\delta_a$	$\Delta v/\Delta\delta_r$	$\Delta r/\Delta\delta_r$	$\Delta p/\Delta\delta_r$
0	-1.58	0.41	2.47	-0.66	-0.89	-5.39	1.44
15	-1.64	0.24	0.69	-0.11	-0.52	-1.49	0.23
30	-1.40	0.22	0.32	0.06	-0.51	-0.73	-0.13
45	-1.25	0.22	0.18	0.10	-0.62	-0.51	-0.29
60	-1.23	0.22	0.10	0.04	-1.34	-0.62	-0.27

Conclusions about angular rate effects on the controllability of the subject aircraft are as follows:

- Non-zero nominal angular rates do not change control effectiveness, but do change mode shapes and/or speeds, as well as zero locations.

- Nominal q_0 has a large effect on K_F, primarily due to the creation of non-minimum-phase zeros and unstable modes.

- Nominal p_0 primarily changes mode shapes rather than pole locations, and it causes any control deflection to excite all response modes.

2.6 DYNAMIC VARIATIONS DURING EXTREME MANEUVERING

Aircraft may be especially prone to departure from controlled flight during air combat maneuvering because such maneuvers are executed using the highest possible aircraft performance, and pilot workload during maneuvering flight is high. Although it is possible to fly most combat maneuvers in a smooth, coordinated manner, even small errors can cause difficulty due to instability, unfamiliar coupled mode shapes, or changes in control effectiveness.

Many air combat maneuvers include periods of high angle-of-attack flight, in order to produce a large normal force for climbing or turning. High angular rates also are typical of many air combat maneuvers. High normal acceleration may be accompanied by large q_0, and large p_0 may be generated to rapidly orient the lift force in a desired direction.

Referring to the earlier sections in this chapter, the difficulties involved in extreme maneuvering become clear. High angles of attack and pitch rate destabilize the normal modes of motion and reduce the available control power, while high roll rate causes lateral-longitudinal coupling and produces mode shapes unfamiliar to the pilot.

The first two of the following sections examine the changes in aircraft stability and control along two typical air combat trajectories. The third section approaches the same problem from a different viewpoint, examining the effects of an elementary target-tracking pilot model on aircraft stability.

2.6.1 Wind-Up Turn

In a wind-up turn, the aircraft is rolled and high load factor is commanded, resulting in a high pitch rate. As airspeed bleeds off (which may occur even at maximum thrust), angle of attack is increased, and the aircraft stability decreases. Five points taken from a typical wind-up turn time history are described in Table 2.6-1, and the corresponding eigenvalues are given in Table 2.6-2. Of special interest is the Dutch roll damping, which decreases so that the Dutch roll mode becomes unstable as the wind-up turn progresses. These are not symmetric flight conditions, so it is expected that the Dutch roll eigenvector also contains angle-of-attack perturbations.

In addition to lateral-longitudinal coupling and the general reduction in damping, the control effectiveness also decreases, as illustrated by the initial value of the transfer function, shown in Table 2.6-3. It is necessary for the pilot to use rudder as the roll control at high angles of attack, and this can cause sideslip perturbations, which can lead to further problems.

These representative points from a wind-up turn demonstrate the deterioration of the stability and control of the example aircraft as it executes one form of air combat maneuver.

TABLE 2.6-1

WIND-UP TURN WORKING POINTS

Working Point	Description	Flight Condition	
1	Roll and Turn t = 0 sec	V_0 = 217 m/s p_0 = 5 deg/sec ϕ_0 = 45 deg	α_0 = 5 deg r_0 = 5 deg/sec θ_0 = 5 deg
2	Rapid Turn t = 13 sec	V_0 = 217 m/s q_0 = 10 deg/sec ϕ_0 = 85 deg	α_0 = 11 deg r_0 = 5 deg/sec θ_0 = -15 deg
3	Turning t = 30 sec	V_0 = 177 m/s q_0 = 10 deg/sec ϕ_0 = 70 deg	α_0 = 15 deg r_0 = 5 deg/sec θ_0 = -20 deg
4	Turning t = 52 sec	V_0 = 134 m/s p_0 = 10 deg/sec r_0 = 10 deg/sec ϕ_0 = 70 deg	α_0 = 22 deg q_0 = 15 deg/sec θ_0 = -20 deg
5	Turning t = 75 sec	V_0 = 116 m/s p_0 = 12.5 deg/sec ϕ_0 = 60 deg	α_0 = 27 deg q_0 = 12.5 deg/sec θ_0 = -25 deg

TABLE 2.6-2

WIND-UP TURN EIGENVALUES

Working Point	Short Period	Dutch Roll	Roll	Spiral	Phugoid
1	-0.935±j1 76	-0.383±j3.43	-1 61	0.064	-0.051±j0.126
2	-0.952±j2.19	-0.302±j4.37	-1.04	-0.043	0.002±j0.191
3	-0.777±j1.74	-0.181±j4.04	-0.826	-0.074	-0 012±j0.209
4	-0.456±j2.66	0.0766±j3 26	-0 758	-0.096	-0.035±j0.327
5	-0.438±j2.16	0.213±j2.55	-0 543	-0.154	-0.057±j0.214

TABLE 2.6-3

TRANSFER FUNCTION GAIN, K_I, ALONG THE WIND-UP TURN

Working Point	$\Delta w/\Delta\delta_h$	$\Delta p/\Delta\delta_a$	$\Delta p/\Delta\delta_r$	$\Delta r/\Delta\delta_a$	$\Delta r/\Delta\delta_r$	$\Delta v/\Delta\delta_a$	$\Delta v/\Delta\delta_r$
1	-0.42	15.80	3.80	0.321	-2.87	-0.018	0.127
2	-0.49	12.12	3.45	0.095	-2.91	-0.011	0.131
3	-0.49	5.91	2.14	-0.035	-2.03	-0.002	0 090
4	-0.31	1.32	1.08	0.037	-1.06	0•002	0.048
5	-0.17	-0.001	0.24	0.067	-0.36	0.002	0.029

2.6.2 Rolling Reversal

A rolling reversal combines a rapid pull-up with a rapid rolling maneuver, resulting in a "corkscrew-like" path through space. The combination of a high-acceleration pull-up and rapid rolling is expected to produce unstable modes with considerable lateral-longitudinal coupling. Table 2.6-4 describes the rolling reversal working points examined here. The corresponding eigenvalues, shown in Table 2.6-5, illustrate the changes in aircraft stability as the rolling reversal progresses. Due to the high q_0 involved in this maneuver, the Dutch roll mode is unstable throughout most of the maneuver.

The initial and final working points of the rolling reversal are symmetric flight conditions so there is no lateral-longitudinal coupling during these phases of the flight. This is demonstrated by the eigenvectors of the fast modes at the first working point, which are shown in Fig. 2.6-1. The intermediate working points all occur during the aircraft's roll and involve significant lateral-longitudinal coupling. The eigenvectors of the fast modes at Working Point 3, shown in Fig. 2.6-1, demonstrate this. There is significant

TABLE 2.6-4

ROLLING REVERSAL WORKING POINTS

Working Point	Description	Flight Condition	
1	Hi-G Pull-up t = 0 sec	V_0 = 217 m/s q_0 = 15 deg/sec θ_0 = 30 deg	α_0 = 25 deg
2	Roll t = 4 sec	V_0 = 168 m/s p_0 = -10 deg/sec ϕ_0 = -90 deg	α_0 = 26 deg q_0 = 15 deg/sec θ_0 = 50 deg
3	Roll t = 10 sec	V_0 = 101 m/s p_0 = -15 deg/sec r_0 = -5 deg/sec θ_0 = -30 deg	α_0 = 26 deg q_0 = 15 deg/sec ϕ_0 = -180 deg
4	Roll and Pull-up t = 15 sec	V_0 = 117 m/s p_0 = 10 deg/sec r_0 = 5 deg/sec θ_0 = -55 deg	α_0 = 23 deg q_0 = 15 deg/sec ϕ_0 = 45 deg
5	Final Pull-up t = 22 sec	V_0 = 152 m/s p_0 = 0 deg/sec ϕ_0 = 0 deg	α_0 = 20 deg q_0 = 10 deg/sec θ_0 = -10 deg

TABLE 2.6-5

ROLLING REVERSAL EIGENVALUES

Working Point	Short Period	Dutch Roll	Roll	Spiral	Phugoid
1	-0.873±j4.07	0.191±j4.54	-0.910	0.139	-0.178 -0.056
2	-0.691±j3.15	0.180±j3.55	-0.716	-0.169	0.0124±j0.406
3	-0.403±j1.91	0.107±j2.10	-0.409	-0.224	0.122 ± j0.124
4	-0.394±j2.34	0.131±j2.70	-0.711	-0.093	-0.153 ± j0.124
5	-0.593±j1.78	-0.010±j3.83	-0.818	-0.082	-0.073 ± j0.095

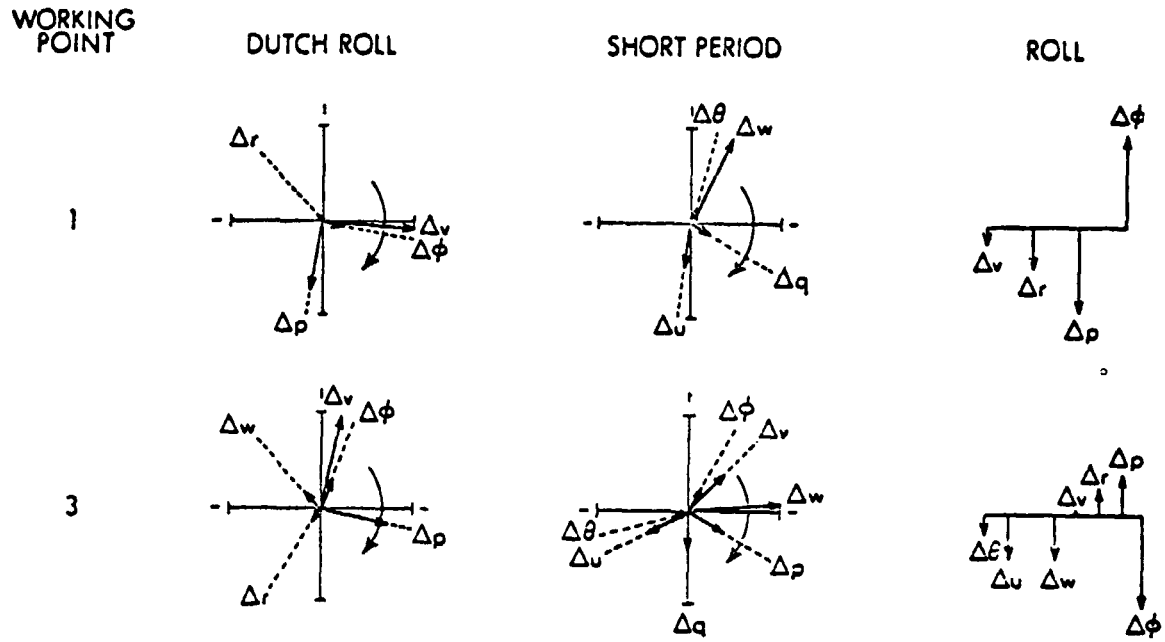

Figure 2.6-1 Eigenvectors of Rolling Reversal

angle-of-attack (or Δw) motion in the Dutch roll mode and large roll-sideslip perturbation in the short period mode. Even the roll mode contains a significant angle-of-attack excursion.

The aircraft control effectiveness follows trends similar to the aircraft stability, i.e., the control effectiveness is degraded throughout the first half of the maneuver, but it improves during the second half, as illustrated in Table 2.6-6. The pilot must use the rudder as a roll control during the middle portion of this maneuver. This difficulty is complicated by high angular rates, lateral-longitudinal coupling, and extreme attitudes.

An aircraft executing a rolling reversal exhibits unstable modes, lateral-longitudinal coupling, and reduced control effectiveness as the maneuver progresses. all of which make the pilot's task more difficult.

TABLE 2.6-6

TRANSFER FUNCTION GAIN, K_I, ALONG THE ROLLING REVERSAL

Working Point	$\Delta w/\Delta\delta_h$	$\Delta p/\Delta\delta_a$	$\Delta p/\Delta\delta_r$	$\Delta r/\Delta\delta_a$	$\Delta r/\Delta\delta_r$	$\Delta v/\Delta\delta_a$	$\Delta v/\Delta\delta_r$
1	-0.62	1.87	1.53	0.204	-2.25	0.004	0.109
2	-0.36	0.597	0.781	0.142	-1.29	0.003	0.063
3	-0.012	-0.001	0.282	0.053	-0.465	0.001	0.023
4	-0.23	0.683	0.722	0.044	-0.771	0.001	0.036
5	-0.42	2.91	1.73	-0.031	-1.513	0.002	0.066

2.6.3 Effects of Proportional Tracking

Rudimentary piloting effects can be examined by assuming that the pilot attempts to control the aircraft's attitude. This can be modeled by a proportional feedback of angular deviation (pitch or roll angle) to the appropriate control surface (elevator or aileron). Pilot lags or time delays are neglected. As an example, pitch attitude control is chosen, and the feedback gains are set so that the effective pitch moment due to pitch angle, M_θ, is a multiple of the pitch moment due to angle of attack, M_α. Since this is achieved by elevator feedback, there are changes to the coefficients X_θ and Z_θ as well. The multiplying factor is denoted by "i" in the following tables, and the feedback gain that produces equal M_θ and M_α (i = 1) for the reference flight condition is 0.64 deg elevator per deg of pitch angle. This simple model also disregards pitch-rate feedback, which the pilot also might normally provide.

For symmetric flight conditions, this loop closure does not affect the lateral eigenvalues; the longitudinal eigenvalue variations are shown in Table 2.6-7. The short-period mode is both increased in frequency and decreased in

TABLE 2.6-7

EIGENVALUE CHANGES DUE TO PROPORTIONAL TRACKING -- SYMMETRIC FLIGHT CONDITIONS

V_0 = 94 m/s α_0 = 15 deg q_0 = 0 deg/sec		
i	Short Period	Phugoid (Pitch Angle/Speed)
0	-0.407±j1.099	-0.017±j0.137
1	-0.342±j1.552	-0.082±j0.068
2	-0.319±j1.906	-0.157 -0.0522
4	-0.302±j2.47	-0.218 -0.0260

V_0 = 94 m/s α_0 = 15 deg q_0 = 12 deg/sec		
i	Short Period	Phugoid (Pitch Angle/Speed)
0	-0.417±j1.13	0.045 -0.069
1	-0.351±j1.57	-0.096 -0.058
2	-0.327±j1.92	-0.140 -0.063
4	-0.307±j2.48	-0.178 -0.064

damping by the addition of a pitch attitude-to-elevator feedback. For straight-and-level flight, attitud control increases the phugoid damping while decreasing th tural frequency, resulting in the conversion of the phugoid mode into two real modes -- a pitching mode and a speed mode. In steady pitching motion, pitch-attitude control results in increased stability for the pitch angle mode with relatively little effect on the speed mode.

Coupled flight conditions lead to significant effects on the lateral modes due to the longitudinal loop closure. In Ref. 9, a pitch attitude-to-elevator loop

closure resulted in an unstable lateral mode when the subject aircraft was in a steady sideslip. As shown in Table 2.6-8 for the example aircraft used in this report, pitch angle-to-elevator feedback generally has a beneficial influence on the lateral eigenvalues when this aircraft is rolling at zero sideslip. However, the presence of a non-zero nominal sideslip angle results in a mildly diverging speed mode for moderate-to-large feedback gains. There is an indication that large attitude feedback gains destabilize the Dutch roll mode (for a non-rolling aircraft) or the short period mode (when the aircraft is rolling and slipping).

Regarding the pitch attitude-to-elevator feedback as a simple pilot model, this examination confirms the earlier result that pilot control of the longitudinal motion of an aircraft could result in the destabilization of the aircraft when the vehicle is in a steady sideslip. This would be due to the pilot disregarding the lateral-longitudinal coupling present in asymmetric flight conditions.

This simple attitude feedback underlines the necessity for considering lateral-longitudinal crossfeeds when designing a stability augmentation system for a high-performance aicraft. To achieve acceptable performance, it may be necessary to design a system that recognizes the aircraft flight condition and adjusts its gains to suit the situation.

2.7 CHAPTER SUMMARY

This chapter has presented a study of the dynamic charac eristics of a high-performance aircraft, with special emphasis on the effects of extreme flight conditions on

TABLE 2.6-8

EIGENVALUE CHANGES DUE TO PROPORTIONAL TRACKING --
SIDESLIP AND ROLL EFFECTS

V_0 = 94 m/s α_0 = 15 deg β_0 = 0 deg p_{w_0} = 0 deg/sec					
i	Short Period	Dutch Roll	Roll	Spiral	Phugoid
0	-0.407±j1.099	0.0738±j2.25	-0.442	-0.0545	-0.017±j0.137
1	-0.342±j1.552	0.0738±j2.25	-0.442	-0.0545	-0.082±j0.068
2	-0.319±j1.906	0.0738±j2.25	-0.442	-0.0545	-0.157 -0.0522
4	-0.302±j2.47	0.0738±j2.25	-0.442	-0.0545	-0.218 -0.0260

V_0 = 94 m/s α_0 = 15 deg β_0 = 10 deg p_{w_0} = 0 deg/sec					
i	Short Period	Dutch Roll	Roll	Spiral	Phugoid
0	-0.353±j1.368	-0.134±j2.11	-0.434	-0.0315	-0.024±j0.146
1	-0.303±j1.76	-0.153±j2.11	-0.431	-0.081	-0.032±j0.124
2	-0.298±j2.15	-0.143±j2.03	-0.430	-0.021	-0.287 0.133
4	-0.327±j2.63	-0.101±j2.08	-0.428	-0.152	-0.0247±j0.108

V_0 = 94 m/s α_0 = 15 deg β_0 = 10 deg p_{w_0} = -39 deg/sec					
i	Short Period	Dutch Roll	Roll	Spiral	Phugoid
0	-0.511±j1.32	-0.057±j2.28	-0.246±j0.199		0.071±j0.207
1	-0.349±j1.58	-0.116±j2.34	-0.157±j0.413		-0.193 -0.050
2	-0.201±j1.77	-0.202±j2.44	-0.215±j0.480		-0.249 -0.0035
4	-0.038±j1.93	-0.306±j2.80	-0.270±j0.518		-0.275 0.0155

V_0 = 94 m/s α_0 = 15 deg β_0 = 0 deg p_{w_0} = -39 deg/sec					
i	Short Period	Dutch Roll	Roll	Spiral	Phugoid
0	-0.464±j1.29	-0.032±j2.34	-0.293±j0.144		0.043±j0.189
1	-0.400±j1.56	-0.044±j2.37	-0.167±j0.500		-0.207 -0.062
2	-0.334±j1.82	-0.073±j2.42	-0.208±j0.600		-0.229 -0.035
4	-0.169±j2.10	-0.201±j2.67	-0.246±j0.666		-0.238 -0.0228

aircraft stability and control. The chapter first examines previous studies of the dynamics, aerodynamics, and control in this flight environment. The difficulty of measuring angular rate and translational acceleration effects leads to limited availability of this aerodynamic data, which has a significant impact on the simulation and analysis of dynamic departures. The survey of stability and control indicates a need for additional developments in these areas.

3. EFFECTS OF CONFIGURATION VARIATIONS ON AIRCRAFT DYNAMICS

3.1 OVERVIEW

Variations of aircraft configuration lead to changes in the aircraft's eigenvalues, eigenvectors, and control effectiveness. Section 3.2 presents the effects of changes in the most important longitudinal stability derivatives on the mode shapes and speeds. Similar effects caused by changes in lateral stability derivatives are detailed in Section 3.3. The effects of aircraft mass and rotational inertia variations are given in Section 3.4. Section 3.5 presents a general discussion of possible departure modes and illustrates some of the possible departure time histories. Section 3.6 is a summary of the chapter.

3.2 VARIATIONS DUE TO LONGITUDINAL STABILITY DERIVATIVES

The longitudinal stability derivatives determine the aerodynamic force and moment contributions to the longitudinal perturbation equations, and these stability derivatives can vary considerably from aircraft to aircraft. This section surveys the changes in normal mode shapes and speeds for different ranges of the most important longitudinal stability derivatives.

Three aerodynamic derivatives dominate the short period motion of the aircraft: C_{m_q}, C_{m_α}, and C_{Z_α}. The significance of these terms can be seen in reduced-order approximations to the damping ratio, ζ, and natural frequency, ω_n, of this mode:

$$\zeta \cong - \frac{1}{8I_y\omega_n} \rho_0 V_0 S\bar{c}^2 \left[C_{m_q} + \frac{2I_y}{\bar{c}^2 m} C_{Z_\alpha} \right] \qquad (3.2\text{-}1)$$

$$\omega_n \cong \left[- \frac{1}{2I_y} \rho_0 V_0^2 S\bar{c} \left(C_{m_\alpha} - \frac{1}{4m} \rho_0 S\bar{c}\, C_{m_q} C_{Z_\alpha} \right) \right]^{\frac{1}{2}} \qquad (3.2\text{-}2)$$

Over the range of likely values of the coefficients, the $C_{m_q}C_{Z_\alpha}$ product usually is considerably smaller than C_{m_α}, so it can be expected that C_{m_q} and C_{Z_α} primarily affect short period damping, while C_{m_α} changes only the short period natural frequency.

The specific effects of varying C_{Z_α} and C_{m_q} are illustrated in Table 3.2-1. The primary short period eigenvalue changes occur in the damping, as expected. The phugoid mode does change somewhat, as an increase in the lift-curve slope (C_{Z_α} more negative) increases the phugoid natural frequency at essentially constant damping ratio. An increase in the magnitude of pitch damping (C_{m_q}) decreases phugoid frequency and damping significantly.

TABLE 3.2-1

C_{Z_α} AND C_{m_q} EFFECTS ON EIGENVALUES

(V_0 = 94 m/s, α_0 = 15 deg)

$C_{Z_\alpha}(\text{rad}^{-1})$	Short Period	Phugoid
-2.0	-0.345±j1.096	-0.0146±j0.128
-3.2	-0.396±j1.099	-0.0162±j0.135
-5.0	-0.471±j1.099	-0.0181±j0.145

$C_{m_q}(\text{rad}^{-1})$	Short Period	Phugoid
-34.4	-0.642±j1.058	-0.013±j0.130
-17.2	-0.399±j1.099	-0.017±j0.137
-5.73	-0.236±j1.098	-0.020±j0.143

Variations in the longitudinal stability derivatives affect the lateral modes only when the aircraft is in asymmetric flight. In that case, mode coupling occurs--Table 3.2-2 illustrates the changes in the Dutch roll and short period modes for asymmetric flight as C_{m_q} varies. The transfer of damping from the short period mode to the Dutch roll mode for non-zero β_0 has been observed in Section 2.4. In the case of reduced C_{m_q}, this transfer is essentially unchanged, indicating that short period damping due to CZ_α (see Eq. (3.2-1)) is transferred whereas damping due to C_{m_q} is not. This is supported by the observation that Dutch roll eigenvectors for non-zero β_0 (Fig. 2.4-4) include much more angle-of-attack motion than pitch rate.

TABLE 3.2-2

EFFECTS OF C_{m_q} ON EIGENVALUES IN ASYMMETRIC FLIGHT

α_0 = 15 deg β_0 = 0 deg p_{w_0} = 0 deg/sec		
	Short Period	Dutch Roll
C_{m_q} = -17.8 (rad^{-1})	-0.407±j1.099	-0.074±j2.251
C_{m_q} = -5.73 (rad^{-1})	-0.236±j1.098	-0.074±j2.251

α_0 = 15 deg β_0 = 5 deg p_{w_0} = 0 deg/sec		
	Short Period	Dutch Roll
C_{m_q} = -17.8 (rad^{-1})	-0.382±j1.201	-0.0946±j2.024
C_{m_q} = -5.73 (rad^{-1})	-0.205±j1.205	-0.0956±j2.024

α_0 = 15 deg β_0 = 0 deg p_{w_0} = -39 6 deg/sec		
	Short Period	Dutch Roll
C_{m_q} = -17.8 (rad^{-1})	-0.464±j1.294	-0.0319±j2.342
C_{m_q} = -5.73 (rad^{-1})	-0.291±j1.295	-0.0343±j2.337

None of the stability derivatives discussed has any effect on the control effectiveness, which determines the transfer function gain, K_I; therefore, the initial response to control inputs does not vary with Cz_α and C_{m_q}. However, stability derivative variations do affect the transient response through changes in poles and zeros.

Variations in the aircraft's center of gravity cause variations in aerodynamic moment coefficients. The center of gravity (c.g.) is the rotational center of the aircraft. For fixed aerodynamic center of pressure, c.g. variation leads to static margin variation; hence, the moment relationships are altered.

The static margin is the distance between the c.g. location and the aerodynamic center, and it is usually expressed as a fraction of the mean aerodynamic chord, $\bar{c}$. Figure 3.2-1 details the changes in the longitudinal eigenvalues as the static margin is varied from 0.33 through its usual reference location of 0.17 to -0.15. This results in a C_{m_α} variation from -1.17 to 0.554 rad^{-1}, as well as changes in C_{m_q} from -21.1 rad^{-1} to -11.2 rad^{-1}.

The eigenvectors (Fig. 3.2-2) change considerably as the c.g. moves aft. While the short period and phugoid modes still are recognizable at a static margin of 0.06 (C_{m_α} = -0.17 rad^{-1}), a transition region is entered as the c.g. moves further aft. At a static margin of 0.01 (C_{m_α} = -0.02 rad^{-1}), a new ("third") oscillatory mode which displays significant perturbations in all longitudinal states is evident. Two real convergences comprise the other longitudinal modes -- one fast attitude mode occurring at constant velocity and flight path angle and one slow velocity mode that involves significant flight path angle variations.

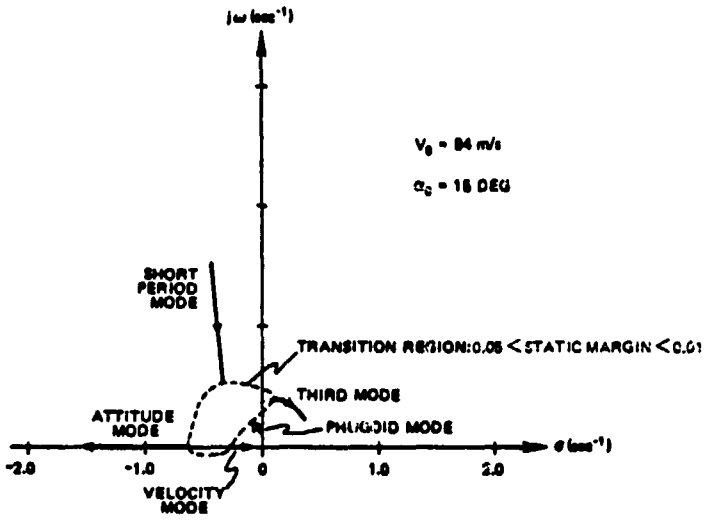

Figure 3.2-1 Longitudinal Eigenvalue Variations with c.g. Location

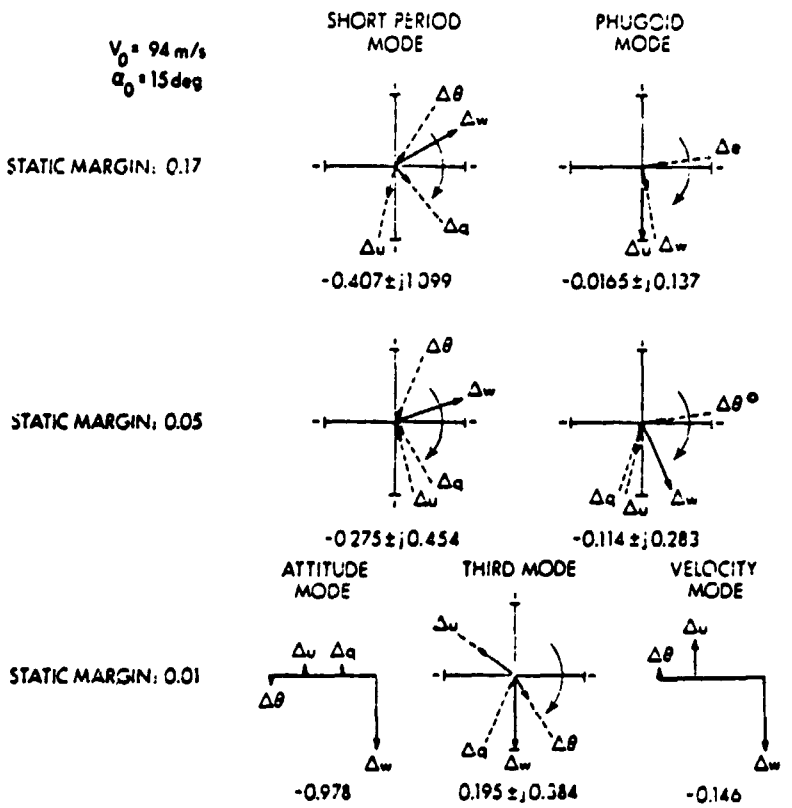

Figure 3.2-2 Longitudinal Eigenvector Variations with c.g. Location

Control effectiveness changes only slightly with c.g. location, but the transfer function gain, K_F, does vary as shown in Table 3.2-3. The zeros of the $\Delta w/\Delta\delta_h$ transfer function are given in Table 3.2-4. Both of these tables indicate the well-behaved nature of the numerator of the elevator-to-angle of attack transfer function.

TABLE 3.2-3

C.G. LOCATION EFFECTS ON TRANSFER FUNCTION GAIN, K_F

(V_0 = 94 m/s, α_0 = 15 deg)

Static Margin	$\Delta w/\Delta\delta_h$	$\Delta p/\Delta\delta_a$	$\Delta r/\Delta\delta_r$
0.17	-5.17	-0.66	-5.39
0.05	-5.76	-0.57	-5.51
-0.03	-6.15	-0.51	-5.59

TABLE 3.2-4

COMPARISON OF ZEROS OF $\Delta w/\Delta\delta_h$ AT THREE C.G. LOCATIONS

Static Margin	$Z_{1,2}$	Z_3
0.17	-0.0025±j0.1167	-21.07
0.05	-0.0038±j0.1238	-20.998
-0.03	-0.0047±j0.1283	-20.950

This section examines the effects of longitudinal stability derivatives, and the following conclusions are made:

- Reductions in pitch damping (C_{m_q}) and lift-curve slope (C_{Z_α}) reduce the short period damping without changing the frequency.

- Lateral-longitudinal coupling produced by sideslip transfers damping due to C_{Z_α} to the Dutch roll mode from the short period mode, but damping due to C_{m_q} remains in the longitudinal plane.

- The c.g. location affects C_{m_α} directly, and a rearward c.g. location results in the creation of a new unstable oscillatory mode that exhibits significant perturbations in all longitudinal variables. In addition, two stable real modes are created -- a fast attitude mode and a slow velocity mode.

- The numerator of the elevator-to-angle of attack transfer function is well behaved at rearward c g. locations.

3.3 VARIATIONS DUE TO LATERAL-DIRECTIONAL STABILITY DERIVATIVES

In this section, variations in C_{l_β}, C_{n_r}, C_{l_p}, and C_{n_r} are studied to determine their effects on the lateral-directional modes. Experimental information on the value of $C_{n_{\dot\beta}}$ is limited, so an investigation of possible effects of $C_{n_{\dot\beta}}$ on eigenvalues is included in this section.

The effects of C_{n_β}, C_{l_β}, and C_{l_p} variations are shown in Fig. 3.3-1. Increases in magnitude of C_{n_β} and C_{l_β} cause an increase in the frequency of the Dutch roll mode. Additionally, both parameters cause some change in damping, with larger C_{n_β} increasing the damping ratio and larger C_{l_β} magnitude decreasing the Dutch roll damping ratio. Larger C_{l_β} magnitude causes the spiral mode to be more stable.

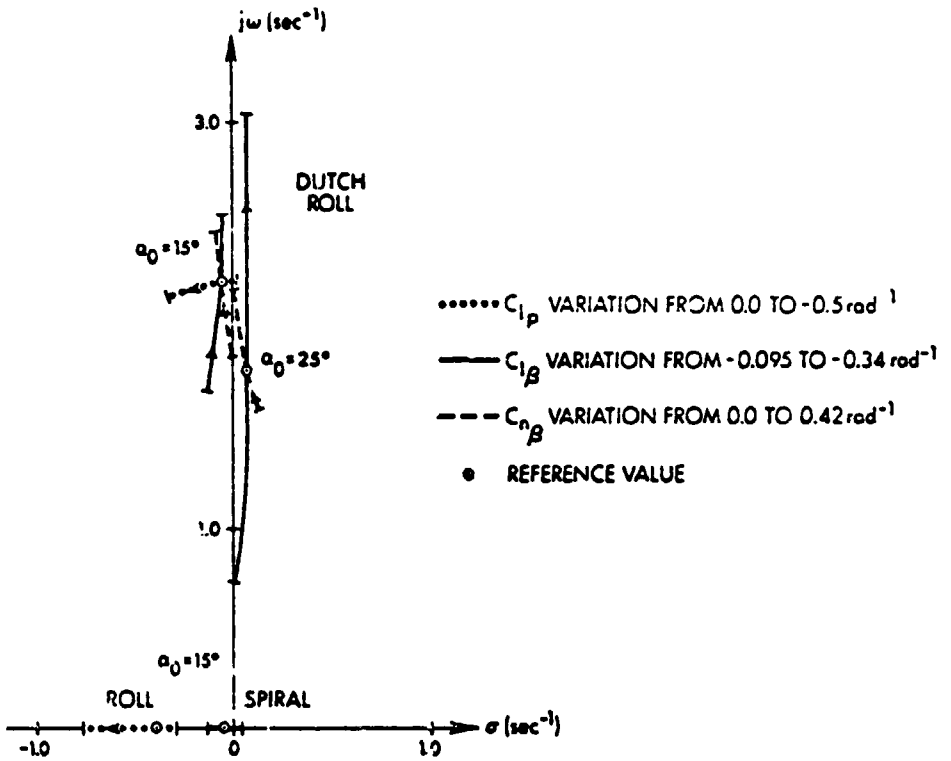

Figure 3.3-1 Effects of C_{l_β}, C_{n_β}, and C_{l_p} Variations on Lateral-Directional Eigenvalues

Figure 3.3-1 indicates that at α_0 of 15 deg the effects of C_{l_p} appear in the Dutch roll damping ratio and in the roll convergence mode. The presence of these effects is predicted by the approximate lateral-directional equations, Eqs. (2.4-1) to (2.4-5), but the approximate equations give an inaccurate indication of the size of these effects. Equations (2.4-1) and (2.4-4) predict much larger variation in the roll mode eigenvalue due to C_{l_p} variation than is indicated in Fig. 3.4-1. Conversely, Eqs. (2.4-2) and (2.4-5) predict a much smaller variation in Dutch roll damping ratio than occurs in the complete model of the subject aircraft.

The lack of accuracy of the approximate equations results from the fact that the subject aircraft does not conform to the assumptions upon which the approximate equations are based. The subject aircraft exhibits much more roll motion in Dutch roll mode (as shown by the eigenvectors in Fig. 2.4-3) because it rolls easily (due to low I_x/I_z ratio) and because its roll-yaw and roll-sideslip cross derivatives (C_{l_r}, C_{n_p}, and C_{l_β}) are not small when properly compared to the roll and yaw-sideslip derivatives (C_{l_p}, C_{n_r}, and C_{n_β}).

Table 3.3-1 compares the lateral-directional eigenvalues for C_{n_β} and C_{l_β} variations in the presence of non-zero nominal pitch rate. A comparison of the eigenvalues indicates that the effects of steady pitching are independent of the changes in aerodynamic coefficients. In all cases, positive pitch rate destabilizes the Dutch roll and spiral modes and speeds up the roll mode.

TABLE 3.3-1
EFFECTS OF C_{n_β} AND C_{l_β} VARIATIONS IN THE PRESENCE OF STEADY PITCH RATE

		Dutch Roll	Roll	Spiral
Reference Values	$q_0 = 0$	-0.0738±j2.251	-0.443	-0.0545
	$q_0 = 12$ deg/sec	0.114±j2.320	-0.839	0.0220
$C_{n_\beta} = 0.0$ (rad^{-1})	$q_0 = 0$	-0.0043±j1.855	-0.499	-0.127
	$q_0 = 12$ deg/sec	0.214±j1.996	-1.016	0.0063
$C_{l_\beta} = -0.338$ (rad^{-1})	$q_0 = 0$	-0.0505±j1.996	-0.459	-0.0752
	$q_0 = 12$ deg/sec	0.150±j2.638	-0.904	0.0135

The approximations of Eqs. (2.4-2) and (2.4-5) indicate that the change in the Dutch roll mode's real part should be approximately proportional to the change in C_{n_r}. Table 3.3-2 indicates that this is not true in this example, for as C_{n_r} increases by a factor of 20, the Dutch roll mode's real part only doubles. The other significant effect caused by a reduction in yaw damping magnitude is to destabilize the spiral mode.

TABLE 3.3-2
EFFECTS OF C_{n_r} VARIATIONS

C_{n_r}	Dutch Roll	Roll	Spiral
-1.200	-0.0983±j2.2468	-0.4612	-0.1396
-0.646	-0.0738±j2.2508	-0.4425	-0.0545
-0.0602	-0.0477±j2.2523	-0.4304	0.0422

The derivative $C_{n_{\dot{\beta}}}$ is an acceleration derivative (analogous to $C_{m_{\dot{\alpha}}}$) that arises because the aerodynamic flow field exhibits some lag in rearranging itself following a change in aerodynamic angle. Acceleration terms are approximations to these flow field dynamics. Experimentally, acceleration derivatives are difficult to measure, and they usually are combined with the rotary derivatives. Analytical studies often make the assumptions that

$$\hat{C}_{n_{\dot{\beta}}} = 0 \tag{3.3-7}$$

$$\hat{C}_{n_p} = C_{n_p} + \sin \alpha_0 \, C_{n_{\dot{\beta}}} \tag{3.3-8}$$

$$\hat{C}_{n_r} = C_{n_r} - \cos \alpha_0 \, C_{n_{\dot{\beta}}} \tag{3.3-9}$$

Reference 46 examines some of the possible effects of this approximation on aircraft time histories and parameter identification. It is concluded that significant parameter identification errors can occur if the acceleration derivatives are not included in the model when necessary.

Two types of $C_{n_{\dot{\beta}}}$ effects have been examined. In the first type, non-zero $C_{n_{\dot{\beta}}}$ is added to the model with no other change; this effectively decreases the total damping. In the second type, C_{n_p} and C_{n_r} are adjusted by subtracting the $C_{n_{\dot{\beta}}}$ terms given in Eqs. (3.3-8) and (3.3-9) to maintain nearly constant damping. In the variable damping case (in which C_{n_r} and C_{n_p} are constant), the only change is in the Dutch roll eigenvalues. There is significant change in damping and a slight change in frequency. This indicates that $C_{n_{\dot{\beta}}}$ primarily affects the Dutch roll mode. The constant damping cases are quite different, in that the changes in $C_{n_{\dot{\beta}}}$, C_{n_p}, and C_{n_r} effectively cancel, as far as the Dutch roll mode is concerned. In this case, however, there are significant changes in the roll and spiral modes. These changes are not due to $C_{n_{\dot{\beta}}}$ (which does not affect the roll and spiral modes) but rather to the corresponding changes in C_{n_r} and C_{n_p}. Therefore, combining $C_{n_{\dot{\beta}}}$ with C_{n_p} and C_{n_r} leads to erroneous eigenvalue calculations in modes not directly affected by $C_{n_{\dot{\beta}}}$ at all.

Table 3.3-3 illustrates the constant damping results with and without steady rolling motion. Non-zero $C_{n_{\dot{\beta}}}$ affects the frequencies of the oscillations only slightly in the presence of rolling motion, but there are significant changes in damping of the various modes. Dutch roll damping ratio changes for non-zero $C_{n_{\dot{\beta}}}$ when the vehicle is rolling, and

TABLE 3.3-3

EFFECTS OF $C_{n_{\dot{\beta}}}$ IN THE PRESENCE OF STEADY ROLLING

(C_{n_p} and C_{n_r} Adjusted to Maintain Constant Damping)

T-0251

Short Period	Dutch Roll	Roll	Spiral	Phugoid
$C_{n_{\dot{\beta}}} = 0$ (rad^{-1}) $p_{W_0} = 0$ deg/sec				
-0.407±j1.099	-0.0738±j2.251	-0.443	-0.0545	-0.0165±j0.137
$C_{n_{\dot{\beta}}} = 0$ (rad^{-1}) $p_{W_0} = -39.6$ deg/sec				
-0.464±j1.294	-0.0319±j2.342	-0.293±j0.144		0.0427±j0.189
$C_{n_{\dot{\beta}}} = 0.55$ (rad^{-1}) $p_{W_0} = 0$ deg/sec				
-0.407±j1.099	-0.0757±j2.256	-0.525	0.0321	-0.0165±j0.137
$C_{n_{\dot{\beta}}} = 0.55$ (rad^{-1}) $p_{W_0} = -39.6$ deg/sec				
-0.481±j1.290	-0.0411±j2.345	-0.287±j0.124		-0.0630±j0.183

this is not observed for the non-rolling, constant damping case. The conclusion is that an improper $C_{n_{\dot{\beta}}}$ identification may not appear in the Dutch roll mode for non-rolling flight, but it can cause a significant change in the Dutch roll mode during a rolling maneuver.

The following points summarize the findings of this report concerning the effects of lateral stability derivative variations:

- The large amount of rolling in the subject aircraft means that $C_{l_{p,dyn}}$ and $C_{n_{r,dyn}}$ are poor indicators of the roll mode's eigenvalue and the Dutch roll mode's real part.
- C_{n_β} and C_{l_β} variations primarily affect the Dutch roll frequency, as indicated by $C_{n_{\beta,dyn}}$. Variations due to steady

pitching motion are independent of the effects caused by changes in C_{n_β} and C_{l_β}.

- Due to the large amount of rolling motion in the Dutch roll mode, C_{l_p} has a larger than expected effect on Dutch roll damping, while the effect of C_{n_r} is smaller than might be expected.

- $C_{n_{\dot\beta}}$ by itself primarily affects the Dutch roll mode, but subtracting its effect from C_{n_p} and C_{n_r} (holding the damping constant) leads to large roll mode and spiral mode changes and small Dutch roll mode variations.

- In the presence of steady rolling, there is a significant $C_{n_{\dot\beta}}$ effect on the Dutch roll mode even for the constant damping case. Coupled flight conditions should be investigated when the identification of $C_{n_{\dot\beta}}$ is desired.

3.4 VARIATIONS DUE TO MASS AND INERTIA EFFECTS

The variations in the aircraft modes due to mass and rotational inertia changes are examined in this chapter. The rotational inertias considered span the range of aircraft types (from wing-heavy to fuselage-heavy), and the mass variations range from light to heavy wing loadings.

Table 3.4-1 details the aircraft eigenvalue trends as aircraft mass varies. The rotational inertia matrix is held constant (as if a point mass was added or subtracted at the vehicle's center of gravity), so the ratios between the mass and inertia also vary. The mass change represents a change in relative density, μ, which is defined as

$$\mu = m/\rho S\bar{c} \qquad (3.4\text{-}1)$$

TABLE 3.4-1

EFFECTS OF AIRCRAFT MASS ON EIGENVALUE LOCATION

(V_0 = 94 m/s, α_0 = 15 deg)

Mass	Short Period	Phugoid	Dutch Roll	Roll	Spiral
3060. kg	-0.572±j1.07	-0.028±j0.186	-0.120±j2.25	-0.442	-0.054
5055. kg	-0.442±j1.09	-0.019±j0.150	-0.084±j2.25	-0.442	-0.055
8175 kg	-0.367±j1.10	-0.013±j0.120	-0.062±j2.25	-0.443	-0.055

where $\bar{c}$ is a reference length. The relative density relates the aircraft mass to the air density, and therefore indicates the relative magnitude of aerodynamic and inertial effects.

Variations of the aircraft mass have a large effect on the damping of the rotational oscillations -- Dutch roll mode and short period mode -- but only a negligible effect on their frequencies. The spiral and roll modes also are essentially unchanged. Mass variations change the phugoid mode's natural frequency and damping ratio, because this mode involves the interchange of kinetic and potential energy and is highly mass dependent.

The rotational inertia of the aircraft describes the distribution of the aircraft mass about the center of gravity. Most of the inertia is due to the fuselage and the wing, and the relation between them leads to the designation of a specific configuration as "wing-heavy' or "fuselage-heavy."

The yaw inertia is approximately 10 to 15 percent larger than the pitch inertia, and the roll inertia can be from 4 to 12 times smaller than the yaw inertia. High performance fighters emphasize high rolling performance, and tend to be fuselage-heavy. Transport aircraft are built for cruising efficiency and tend to be wing-heavy.

Table 3.4-2 details the results of two rotational inertia investigations, one with constant rolling inertia (I_x) and varying fuselage inertia (I_y and I_z), and one with constant fuselage inertia and varying rolling inertia. In neither of these cases is the phugoid mode significantly affected, underlining the conclusion that the phugoid is a translational mode rather than a rotational mode. For the uncoupled reference flight condition, the short period mode is affected only by a change in pitch inertia; an increase in pitch inertia causes a major decrease in short period frequency and a small decrease in damping ratio.

TABLE 3.4-2
EFFECT OF ROTATIONAL INERTIA ON EIGENVALUES

Fuselage Inertia Varied – I_x Held Constant (V_0 = 81 m/s, α_0 = 25 deg)						
I_z/I_x	I_y/I_x	Short Period	Dutch Roll	Roll	Spiral	Phugoid
4.4	4.0	-0.534±j2.01	0.102±j1.59	-0.483	-0.071	-0.018±j0.156
8.8	8.0	-0.329±j1.43	0.085±j1.54	-0.366	-0.050	-0.018±j0.157
13.2	12.0	-0.261±j1.17	0.0788±j1.52	-0.327	-0.039	-0.017±j0.157

Roll Inertia Varied – I_y and I_z Held Constant (V_0 = 94 m/s, α_0 = 15 deg)						
I_z/I_x	I_y/I_x	Short Period	Dutch Roll	Roll	Spiral	Phugoid
4.4	4.0	-0.407±j1.099	-0.0428±j1.826	-0.313	-0.0587	-0.0165±j0.137
8.8	8.0	-0.407±j1.099	-0.0738±j2.251	-0.443	-0.0545	-0.0165±j0.137

The lateral modes are affected by an increase in rolling inertia, in that both Dutch roll frequency and roll mode response are slowed significantly. There is a significant decrease in Dutch roll damping and very little change in the spiral mode. Larger values of yaw inertia lead to somewhat different effects. Both roll and spiral modes are significantly slower, and there is some decrease in Dutch roll damping ratio and frequency.

The effects of a large rolling inertia on the rolling/slipping stability are shown in Fig. 3.4-1. The stability boundaries are generally similar to those shown in Fig. 2.4-10, although they differ in detail. The Dutch roll mode is stable for the higher rolling inertia. The phugoid instability combines with an unstable spiral mode at high sideslip angles and roll rates to form a fast, highly unstable oscillation.

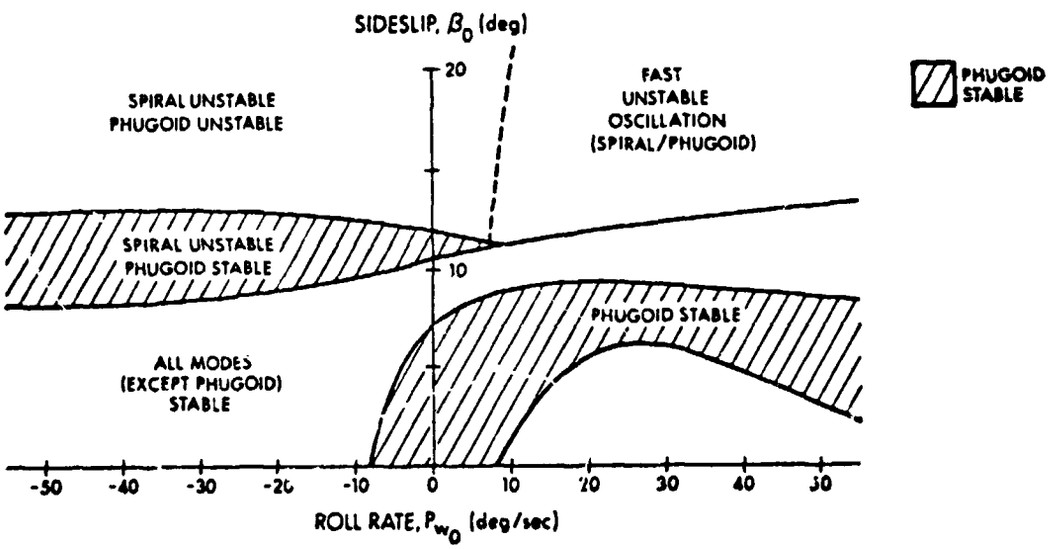

Figure 3.4-1 Effects of Large Rolling Inertia on Aircraft Stability (I_X = 14,370 kg-m^2)

Conclusions concerning the effects of mass and inertia variations are summarized as follows:

- Mass increases reduce Dutch roll and short period damping, but mass variations do not have large effect on the short period or Dutch roll mode frequencies. They do not cause significant changes in the roll or spiral modes.

- The phugoid mode is a translational mode and is greatly affected by mass variations. The phugoid eigenvalue does not depend strongly on rotational inertia.
- Increases in pitch inertia reduce short period frequency and damping.
- Increases in roll inertia increase the roll mode time constant, decrease the Dutch roll frequency significantly, and modify the effects of mode coupling due to asymmetric flight.
- Increases in yaw inertia primarily slow the roll and spiral modes, and there is some effect on Dutch roll damping and frequency.

3.5 CLASSIFICATION OF DEPARTURES

Departure from controlled flight can occur in two ways. Unforced departures are due to instabilities in the basic aircraft. Even if the pilot does not move the controls, small perturbations in the aircraft states build up until the aircraft can no longer be controlled. In a forced departure, the basic aircraft may or may not be unstable, but the addition of a pilot loop closure creates an unstable vehicle-pilot system. The two following sections discuss these departure classes.

3.5.1 Unforced Departure Modes

Unforced departures occur when the pilot cannot or does not stabilize an unstable vehicle. The vehicle eigenvalues directly indicate the open-loop system stability in this case, so that many of the stability boundaries that have been shown in this report can be classed as unforced departure boundaries.

The speed of the fast modes (Dutch roll mode, short period mode and roll mode) is such that the stability of these modes is critical, and the least stable of these usually is the Dutch roll mode. This mode can become unstable in two ways, either resulting from negative "spring terms" or resulting from negative damping, both of which can be influenced by aerodynamics and coupling effects.

The approximate equations for the Dutch roll mode (Eqs. (2.4-1) and (2.4-2)) indicate a pure static instability for large, negative C_{n_β}, but the exact result is somewhat more complex. As in the case of longitudinal mode coupling due to positive C_{m_α} (Section 3.2), directional instability can cause the Dutch roll mode to couple with the classical roll and spiral modes, and it can lead to a new oscillatory mode, analogous to the so-called "roll-spiral" or "lateral-phugoid" mode. Figure 3.5-1 illustrates a case in which negative C_{n_β} causes an oscillatory mode that has low natural frequency and is highly unstable. By comparison to the conventional Dutch roll mode (Fig. 2.4-3), there is a significant change in mode shape. There

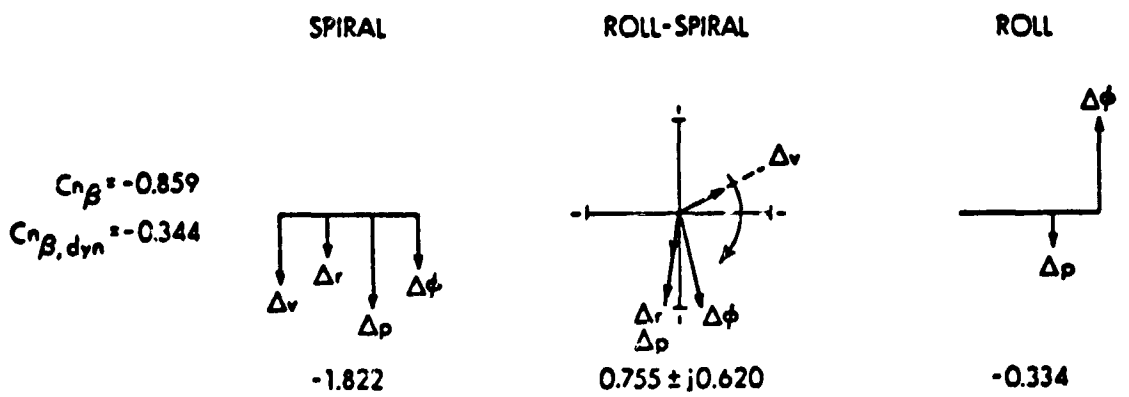

Figure 3.5-1 An Example of Lateral-Directional Eigenvalues for Negative Directional Stability

is a 180-deg phase change in the yaw-rate component, as well as a substantial roll angle change. In addition, the spiral mode has gained significant Δv, Δr, and Δp components.

The departure caused by this type of instability is shown in Fig. 3.5-2. Although the linear model indicates that this motion is an oscillation, it is so unstable that only part of a period appears on the time history plot. The first few seconds of the motion exhibit a rapid roll-yaw angular motion. The pilot would sense a rapid rotational divergence about this axis and might refer to it as a rolling "nose slice" or yaw departure.

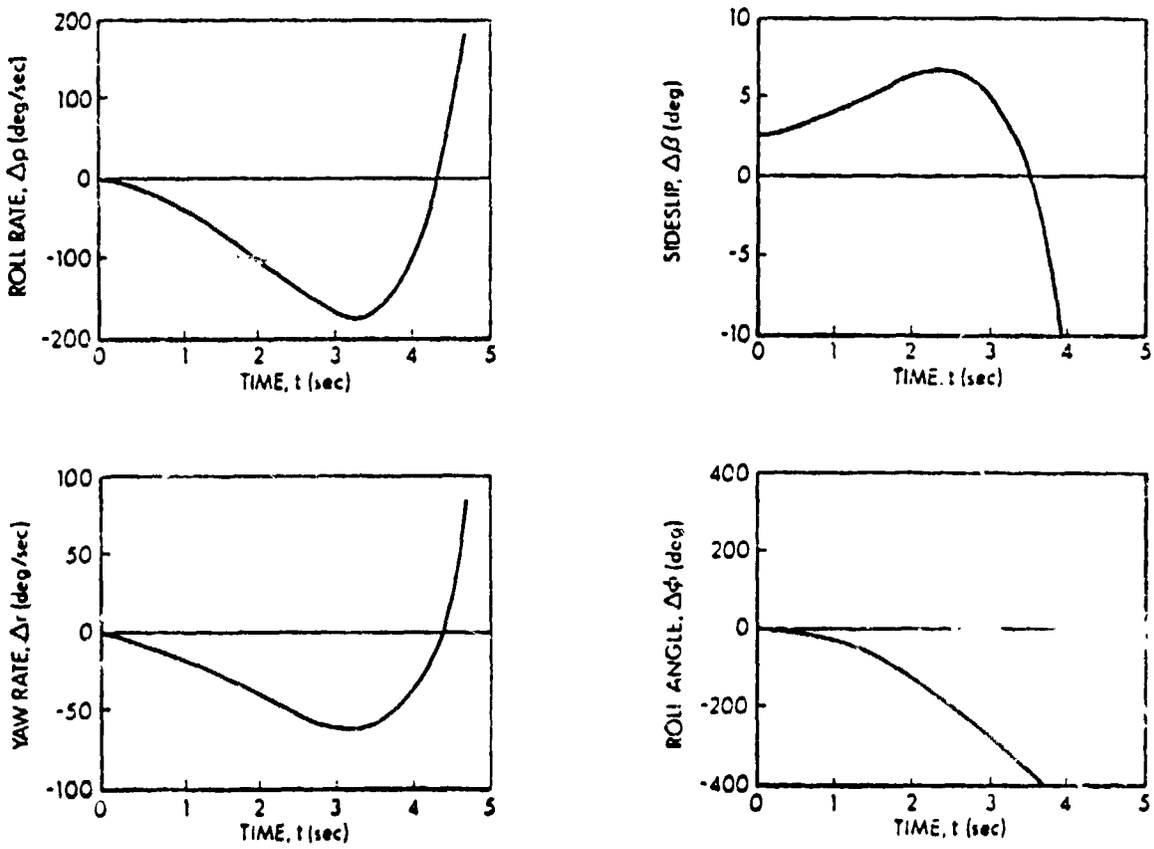

Figure 3.5-2 An Unforced Departure Due to Negative C_{n_β}

Negative yaw damping leads to a more conventional destabilizing of the Dutch roll mode, which retains its characteristic mode shape. The time history of a departure due to dynamic Dutch roll instability is shown in Fig. 3.5-3, and the difference in shape from the departure due to static instability is apparent.

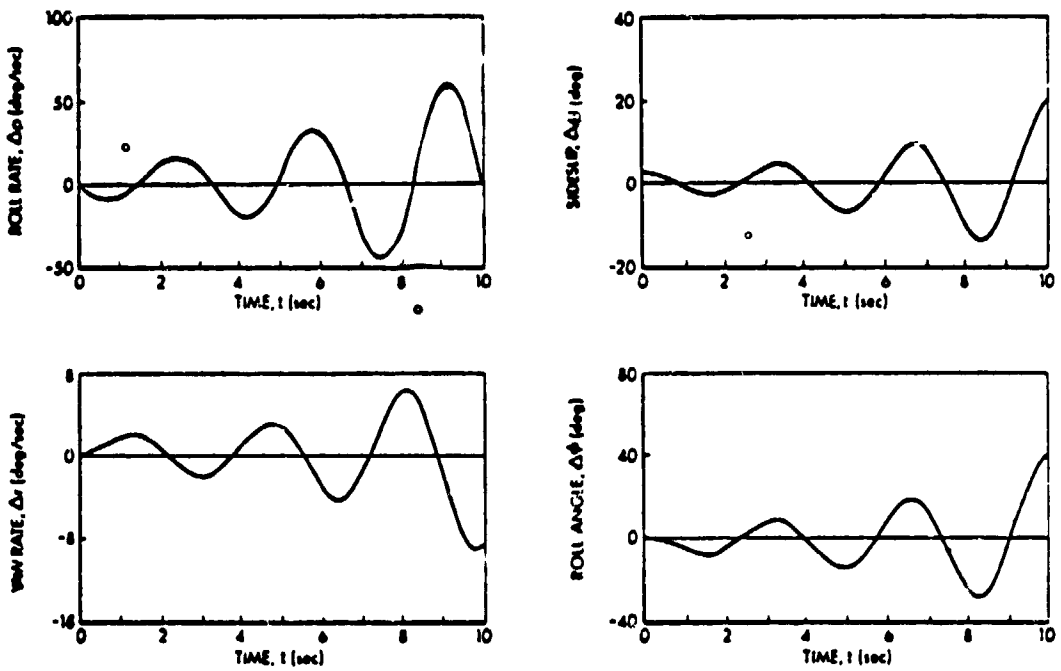

Figure 3.5-3 An Unforced Departure Due to Negative Dutch Roll Damping

The large amount of rolling motion in the Dutch roll mode indicates that this may be what pilots refer to as "wing rock." This is uncertain, however, since "wing rock" also could be a roll-spiral oscillation or a limit cycle caused by an aerodynamic non-linearity. In any case, a pilot sensing such an oscillation probably would unload the aircraft by reducing the angle of attack, removing the aircraft from the region of instability.

A third type of unforced departure can occur at high sideslip angles. The modes of motion are shown in Fig. 3.5-4, and the unstable roll mode is seen to exhibit a mixed rolling-yawing departure characteristic. This divergence is rapid and, as shown in the stability boundaries of Fig. 2.4-2, can appear with only small aerodynamic angle changes from a much more benign flight condition.

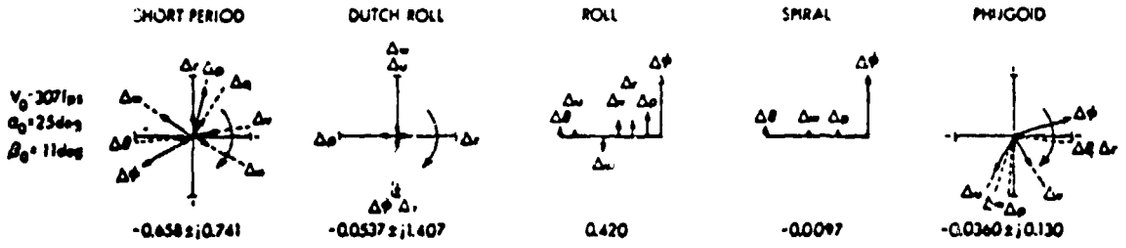

Figure 3.5-4 Eigenvalues and Eigenvectors for a Flight Condition with Large Sideslip Angle

This unstable roll mode is essentially a pure roll about the stability x-axis, but, because of the large nominal aerodynamic angles, it appears as a roll-yaw motion in body axes. It is possible that a pilot flying an aircraft at these large angles would interpret a stability-axis rolling departure as a "nose slice."

3.5.2 Forced Departure Modes

Control inputs from a pilot or control system can force an aircraft to depart from controlled flight in two ways. In the first way, adverse response to pilot inputs moves the nominal flight condition into an unstable region where an unforced departure can occur. The second possible cause of a forced departure is an improper loop closure that creates an unstable closed-loop system. Departure prevention procedures are quite different for the two cases; in

the former case, positive control action is necessary for recovery, while a neutralization of control inputs might allow a recovery from the latter departure.

An example of an improper loop closure was presented in Section 2.6. In that case, the target-tracking pitch attitude-to-elevator loop closure caused lateral mode stability problems at coupled flight conditions. This underlines the necessity of including control cross-couplings in situations where the system itself is coupled.

The target-tracking example can be considered as a situation in which the pilot learns to control the aircraft at one flight condition but does not change his control strategy as the flight condition changes. This is emphasized by the observation that coupled flight conditions often exhibit drastic changes in the shapes of the normal modes, so that a pilot might apply the wrong control action.

The investigation of Section 2.5 demonstrates that control effectiveness problems may leave the pilot no alternative but to apply a poor control combination. For example, at 25-deg angle of attack, the roll moment due to aileron is essentially zero. The rudder would have to be used for roll control but this brings an unavoidable sideslip response with it. This sideslip could drive the vehicle into the roll divergence region cited in the last section.

As an example of unexpected control response, Fig. 3.5-5 shows a departure caused by an aileron input. Normally, the result would be a significant negative roll rate, but the sideslip and yaw rate build up so rapidly that the instability of the basic aircraft results in a rapid rolling departure with positive roll rate.

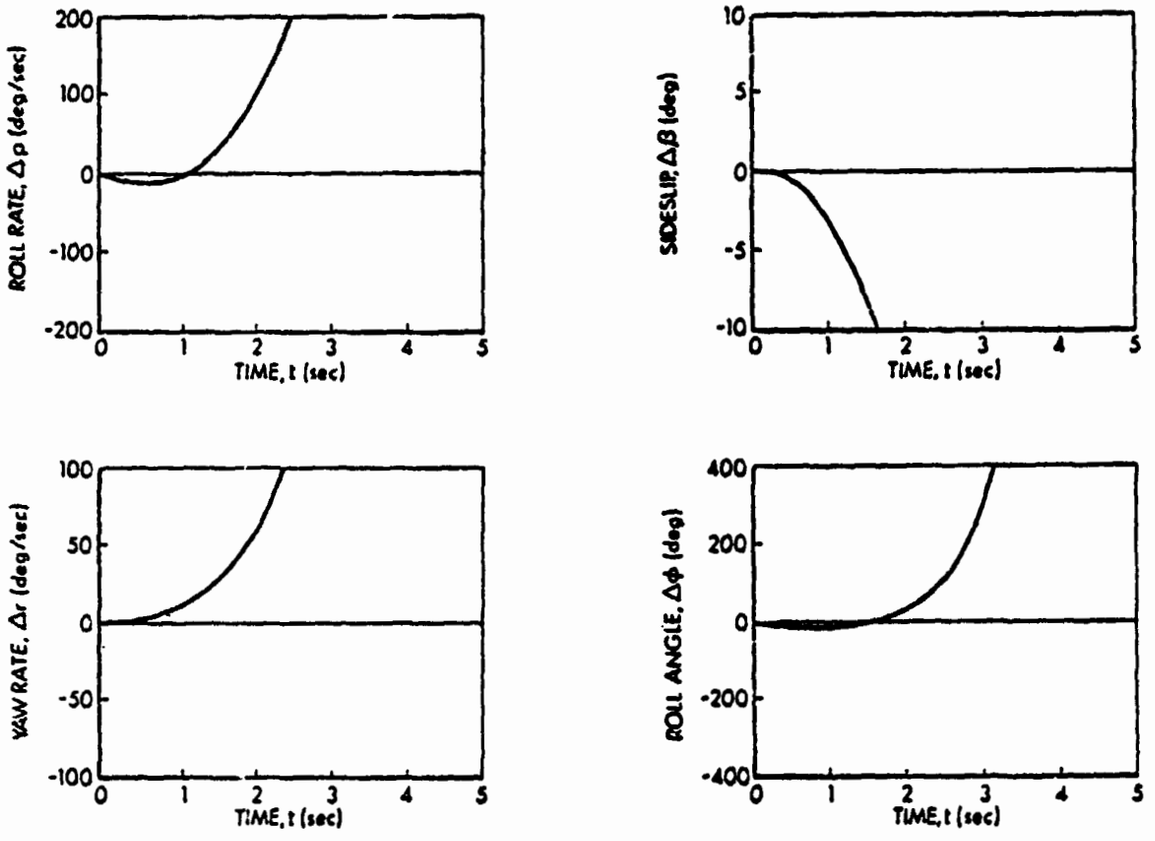

Figure 3.5-5 Aileron Input for Negative C_{n_β}

Situations in which improper pilot inputs are likely are discussed in Section 2.5. These situations are characterized by reduced stability of the open-loop system (due to high angle of attack or pitch rate) and highly coupled modes caused by an asymmetric flight condition (such as non-zero β_0 or p_{W_0}). Nonminimum-phase zeros often appear and can cause great difficulty if "tight" control is attempted.

The conclusions regarding departure modes are summarized as follows:

- An unforced departure (one due to an unstable open-loop system) is most likely to appear in the lateral oscillatory mode. Static instability results in a rapid rolling-yawing departure, while dynamic instability causes an unstable "wing rock" motion.

- An unstable wind-axis roll divergence can appear at extreme aerodynamic angles.

- Forced departures can occur when degraded control response causes the pilot to fly the aircraft into a flight condition where unforced departures are likely.

- Mode coupling or unexpected nonminimum-phase zeros can change the control response so that a "normal" control loop closure leads to an unstable closed-loop system.

3.6 CHAPTER SUMMARY

This chapter has presented effects of configurational variations on aircraft dynamics. Relationships between mode approximations and exact results are discussed for longitudinal, lateral, and coupled motions, and examples of various departure types are presented. It is shown that the effects of aerodynamic parameter variations are modified by the coupling which results in asymmetric flight, particularly in regard to the transfer of damping (due to rotary derivatives) from longitudinal to lateral-directional modes (and vice-versa). Time histories of linearized-model response illustrate departure characteristics similar to those experienced in flight.

4. PREVENTION OF DEPARTURE FROM CONTROLLED FLIGHT

4.1 OVERVIEW

As indicated by earlier developments in this report and the summary of prior work in Section 2.2, there is ample reason to consider designing stability augmentation systems for the specific purpose of preventing departure. Aircraft design is dominated by performance requirements, and even unconstrained configuration modifications may not provide adequate stability or control response (especially during extreme maneuvering). Appendix A and Chapters 2 and 3 demonstrate how linear-time-invariant models of aircraft dynamics can be derived for studying stability and control response during difficult maneuvers. These models are used to illustrate stability augmentation system concepts in the present chapter.

Unlike earlier studies of departure prevention, the powerful tools of linear-optimal control theory are applied to the problem in this chapter. Since new ground is broken and methods which are unfamiliar (in the departure prevention context) are presented, the objective is to provide preliminary guidelines for Departure-Prevention Stability Augmentation System (DPSAS) development. Therefore, a simple optimal controller -- the continuous-time linear-optimal regulator -- is applied to departure prevention. A linear-optimal regulator is a feedback control law of the form

$$\Delta \underline{u}(t) = -K\Delta \underline{x}(t) \qquad (4.1\text{-}1)$$

where $\Delta\underline{u}(t)$ is the vector of control command perturbations, $\Delta\underline{x}(t)$ represents the vector of the aircraft's dynamic states, and K is the gain matrix which scales the state measurements for proper stabilization and compensation of the aircraft's motion. (An equivalent discrete-time linear-optimal regulator, for which the state is measured and control is commanded at a fixed sampling interval, can be derived for a digital flight control system.) This control law has several qualities which are desirable for the present study, in which it is assumed that system dynamics are known exactly and that all states are measured precisely:

- The control gains guarantee stability of the closed-loop system.
- Complete longitudinal/lateral-directional coupling is assumed and is accounted for in the design process.
- The control design technique identifies all significant crossfeeds and interconnects, as well as feedback gains.
- Tradeoffs between the amplitudes of state perturbations and of control motions are specified in the design process.

In addition, a gain-scheduling algorithm which accounts for varying maneuver conditions is developed.

The control design techniques applied to the DPSAS can be generalized to full command augmentation systems for a high-performance aircraft. Reference 58 shows how practical command-response control laws can be developed for a highly coupled aircraft, a tandem-rotor helicopter. These control laws satisfy classical step-response criteria, adapt to flight condition, honor rate- and displacement-limits on control actuators, and use incomplete (possibly noisy)

feedback measurements. A command-response system for a high performance fighter is described in Ref. 59. It adapts to flight condition to provide uniform handling qualities throughout the flight regime. These control laws are developed for direct implementation in a digital computer and use low sampling rates. This extension of the DPSAS to a complete flight control system, while promising, is a subject for future study.

The remainder of this chapter is directed to a brief explanation of linear-optimal regulator design and extensive application of this control design approach to DPSAS examples. Section 4.2 presents the linear-optimal regulator and a discussion of the parameters used in computing control gains. Control designs are developed for a reference aircraft over a wide range of angles of attack, pitch rates, sideslip angles, and roll rates at a single altitude-velocity point -- the central flight condition of 6100 m, 94 m/s -- in Section 4.3. The symmetric and asymmetric variations in flight condition are considered separately, in order to make the differentiation between pullup and sideslip-rolling effects more apparent. Control gains are computed at 32 maneuvering conditions to obtain the results of Section 4.3; with eight states fed back to four control effectors, over 1000 gains are generated. In Section 4.4, these gains are correlated with each other and with maneuver conditions to identify candidate interconnects and gain-scheduling relationships. Negligible and constant gains also are identified in the process. The chapter is summarized in Section 4.5.

4.2 THE LINEAR-OPTIMAL REGULATOR

Optimal control theory provides a useful and practical multi-input, multi-output control system design tool. Linear-optimal control methods are based on the differential equations that describe the vehicle in the time domain (Eq. (A.3-3)), and they produce feedback controllers which exhibit desirable properties.

The problem is to find a controller for the system described by Eq. (A.3-3), which exhibits a linear feedback structure (Eq. (4.1-1)) and minimizes a scalar-valued cost functional of the state and the control:

$$J = \int_0^\infty (\Delta \underline{x}^T Q \Delta \underline{x} + \Delta \underline{u}^T R \Delta \underline{u})\, dt \qquad (4.2\text{-}1)$$

This controller is called a linear-optimal regulator, and it is derived in Refs. 60 to 62.

The designer's freedom rests in his choice of the weighting matrices, Q and R. The design procedure consists of the choice of Q and R, the computation of the Riccati matrix, an evaluation of closed-loop performance, and the adjustment of Q and R as discussed in Section A.4.4.

The linear-optimal regulator is a tool for designing a Departure-Prevention Stability Augmentation System (DPSAS). It is not a limiter, because no limits are placed on the pilot's control authority, and it is not an automatic spin-recovery system, because open-loop anti-spin control settings are not implemented. The DPSAS is intended to augment stability and to minimize the gyrations which precede loss of pilot control. The DPSAS makes full use of

available control power, and, in this respect, could compete with the pilot's control commands; however, the designer can specify the amount of control-surface displacement which normally is available to the DPSAS. Basing the system on the linear-optimal regulator, the DPSAS can be designed to use less than full control authority for expected magnitudes of aircraft maneuvers, leaving a percentage of control authority free for manual commands.

The primary objective of this chapter is to identify the basic effects of varying flight condition on the structure of a DPSAS. To keep the number of varying parameters to a minimum in this demonstration, the state and control weighting factors (Eq. (A.4-21) and (A.4-22)) are chosen at a single symmetric flight condition and held constant throughout the sweep of 32 maneuvering conditions. Q and R elements which provide satisfactory eigenvalues, acceptable time response, and reasonable control gains are chosen at the central flight condition of this sweep (α_0 = 15 deg, V = 94 m/s fps, H = 6100 m). Thus, it is expected that eigenvalues and control gains will vary with flight condition, but the rms-values of state and control perturbations should remain relatively constant.

The Q and R elements are used as design parameters which can be interpreted as the following maximum allowable rms perturbations:

- Throttle setting: 100% of full scale
- Elevator deflection: 20 deg
- Aileron deflection: 60 deg
- Rudder deflection: 30 deg
- Euler angle: 30 deg
- Body angular rate: 25 deg/sec
- Body velocity: 9 m/s

These values indicate that throttle setting, elevator, aileron, and rudder are allowed to vary between their limits and that angles of attack and sideslip must be held within 5.6 deg (the 9 m/s body velocities correspond to aerodynamic angles of this number). Table 4.2-1 indicates that the primary effects of the loop closures at the central flight condition are to increase short period, Dutch roll, and phugoid damping and to quicken the roll and spiral modes.

TABLE 4.2-1

EFFECTS OF DPSAS AT THE CENTRAL FLIGHT CONDITION

Dynamic Mode	Open-Loop Characteristics			Closed-Loop Characteristics		
	Natural Frequency, rad/sec	Damping Ratio, -	Time Constant, sec	Natural Frequency, rad/sec	Damping Ratio, -	Time Constant, sec
Short Period	1.17	0.35	-	2.67	0.72	-
Dutch Roll	2.25	0.03	-	2.35	0.69	-
Roll	-	-	2.26	-	-	0.36
Spiral	-	-	18.34	-	-	1.07
Phugoid	0.14	0.12	-	0.16	0.99	-

This illustrates implicitly that the linear-optimal regulator design can produce stricter tracking than indicated by the choice of Q and R elements. The $\Delta\alpha$ and $\Delta\beta$ requirements can be met only by increasing damping and decreasing time constants. This infers that Euler angles and body angular rates also are closely regulated, even though the weighting of the corresponding elements in Q is light. Table 4.2-1 also indicates that the selection of equal weights on Δv and Δw (and, therefore, on $\Delta\alpha$ and $\Delta\beta$) drives the natural frequencies and damping ratios of the short period and Dutch roll to similar values.

The DPSAS gain matrix for this flight condition is listed in Table 4.2-2. The gain matrix illustrates why damping is increased in the closed-loop system; rate feedbacks are large. The classical longitudinal/lateral-directional partition can be observed in the gains; the control algorithm actually computes coupling gains on the order of 10^{-7} due to the use of single-precision arithmetic. These gains can be ignored. The elevator is seen to be the primary longitudinal controller, as throttle feedback gains are small (the principal effect of throttle control is to damp the phugoid mode). Lateral-directional control largely partitions along the roll and yaw axes. Although the gains shown in Table 4.2-2 have reasonable magnitudes, they could be reduced by reducing the values of q_{ii} (Eq. (A.4-21)). Transient response would be altered, but the system would remain stable.

TABLE 4.2-2

DPSAS GAIN MATRIX AT THE CENTRAL FLIGHT CONDITION

Control Output	Pitch Angle, deg	Body x-axis Velocity, m/s	Pitch Rate, deg/sec	Body z-axis Velocity, m/s	Body y-axis Velocity, m/s	Yaw Rate, deg/sec	Roll Rate, deg/sec	Roll Angle, deg
Throttle Setting, Fraction of Full Scale	-0.019	0.069	-0.005	0.020	0	0	0	0
Elevator Angle, deg	-0.700	1.322	-1.540	-0.988	0	0	0	0
Aileron Angle, deg	0	0	0	0	-0.509	0.138	2.540	1.894
Rudder Angle, deg	0	0	0	0	1.942	-3.096	0.225	-0.100

The performance of the linear-optimal regulator is demonstrated by comparing open- and closed-loop response to perturbations in angle of attack, sideslip angle, and roll rate. Figure 4.2-1 illustrates that a 1.1-deg $\Delta\alpha$ perturbation is moderately damped without the regulator and well-damped with

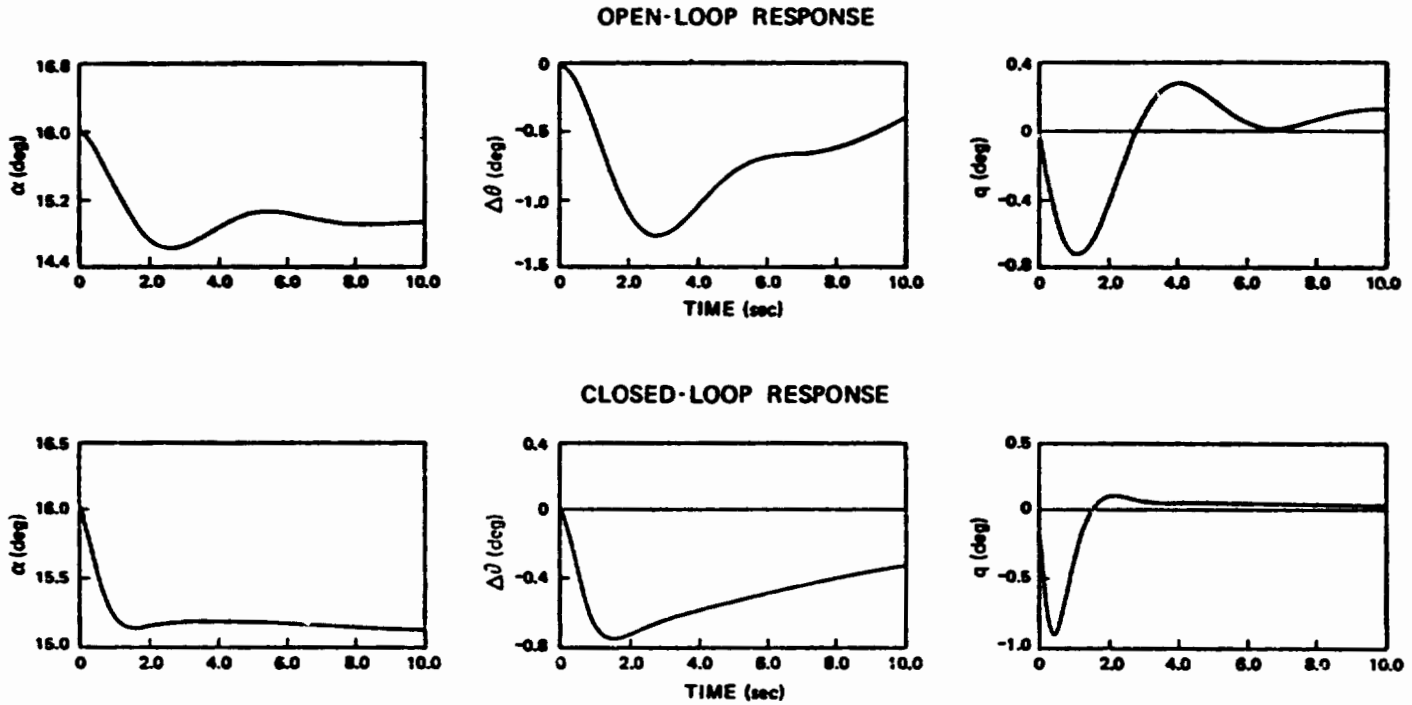

Figure 4.2-1 Longitudinal Response at the Central Flight Condition

the regulator. Figure 4.2-2 shows that the lightly damped natural motion resulting from a 1-deg $\Delta\beta$ initial condition creates a substantial amount of roll as well as yaw. The regulator damps the oscillation and limits the roll angle excursion to 20 percent of its open-loop value, providing significant decoupling of lateral and directional motions. This decoupling effect is confirmed by the aircraft's closed-loop response to a roll-rate disturbance of 1 deg/sec (Figure 4.2-3). This initial condition creates a small sideslip oscillation and triggers the spiral mode (indicated by the underlying exponential response trend in roll angle). The regulator damps the oscillation, reduces the sideslip response by 70 percent, and stabilizes the roll angle.

Having obtained a representative design point for the DPSAS at the central flight condition, the effects of maneuvering on control gains, aircraft stability, and time response are examined in the next section.

4.3 DPSAS CONTROL LAWS

The control gains obtained at the central flight condition would stabilize the aircraft for some range of nominal angles and angular rates; however, changes in the aircraft's dynamics (reflected by variations in F and G) would lead to less-than-optimal regulation. It is necessary, therefore, to redesign the control gain matrix at each maneuvering condition in order to assess the full possibilities for preventing departure with the linear-optimal control law.

Two separate maneuvering condition sweeps have been conducted, using the reference aircraft flying at 6100 m

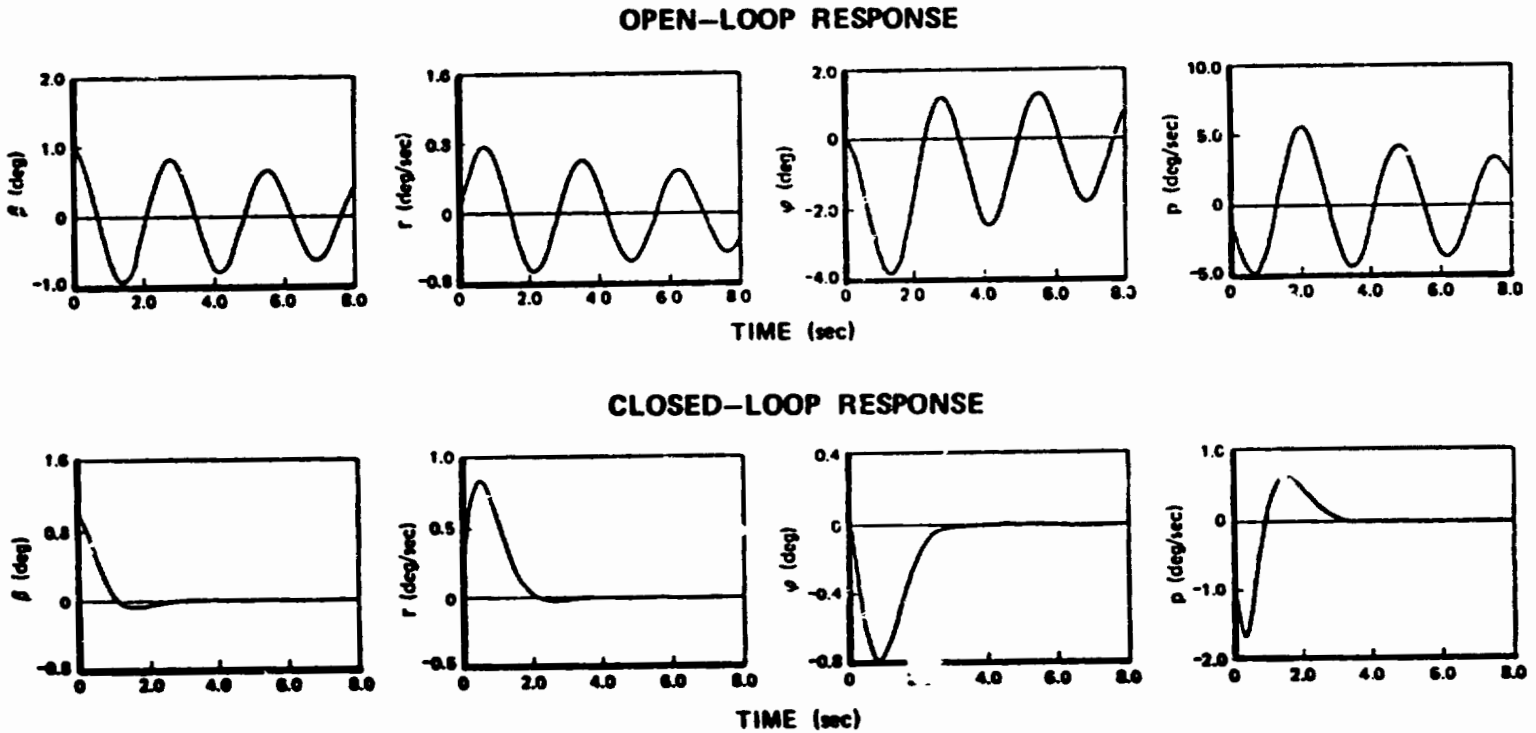

Figure 4.2-2 Directional Response at the Central Flight Condition

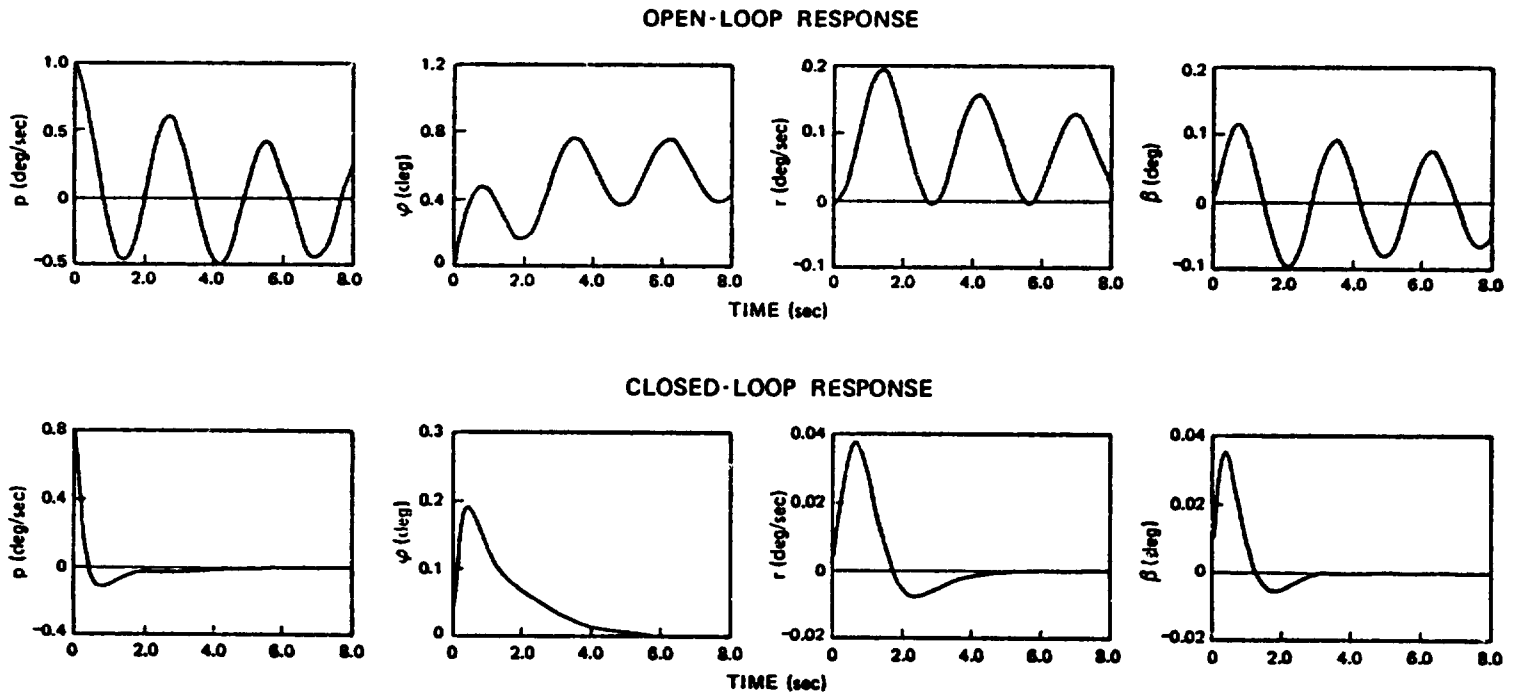

Figure 4.2-3 Lateral Response at the Central Flight Condition

and 94 m/s in both cases. The first is a longitudinal sweep, in which a range of angles of attack and pitch rate are considered. As indicated in Chapters 3 and 4, there is a significant change in lateral-directional dynamics during pullup maneuvers, although the longitudinal and lateral-directional axes remain uncoupled. The lateral-directional sweep varies sideslip angle and stability-axis roll rate, introducing full coupling about all three axes. In the first sweep, control gains and closed-loop characteristics change, but the DPSAS structure is conventional, i.e., gains are partitioned along usual lines. The second sweep generates unconventional DPSAS structures as well as gain variations. (In both cases, the control law is described by Eq. (4.1-1). K contains zero sub-matrices in the first sweep but not in the second.)

4.3.1 Longitudinal Sweep

This section presents the effects of angle of attack and pitch rate on closed-loop eigenvalues, DPSAS control gains, and aircraft response. Section 2.4 showed that the reference aircraft has an unstable Dutch roll mode at high α_0 and unstable Dutch roll, roll, and spiral modes at high q_0. These conditions are stabilized by the DPSAS. Using the state and control weighting factors discussed in the previous section, linear-optimal regulators are designed for 15 maneuver conditions (α_0 varies from 5 to 25 deg, in 5-deg increments, and q_0 is 0, 12, and 24 deg/sec). This sweep represents relatively low load factors ($n_z = 0.4$ to 1.4 "g's"), it covers the normal α_0 range, and it exceeds the normal q_0 range. Consequently, these flight conditions do not literally represent coordinated pullup maneuvers, although they introduce the same symmetric coupling terms in the F matrix (Eq. (A.3-4)) that occur in the pullup.

Closed-loop stability at the 15 conditions is summarized by Table 4.3-1, where it can be seen that all modes are stable and at least moderately damped. Control power does not change with q_0, but it does change with α_0; consequently, the closed-loop stability at a given α_0 is relatively independent of q_0. There is a gradual decrease in Dutch roll damping as α_0 increases, and roll response becomes more sluggish. This happens because rudder and aileron are less effective at the higher angles, while the elements of R which weight the cost of using these surfaces remain unchanged. A heavily damped roll-spiral oscillatory mode occurs at α_0 of 20 and 25 deg. A coupled roll-spiral mode can degrade handling qualities, so adjustment of

TABLE 4.3-1

CLOSED-LOOP STABILITY IN THE LONGITUDINAL SWEEP

Maneuver Condition		Short Period		Dutch Roll		Roll	Spiral	Phugoid	
α_o, deg	q_o, deg/sec	ω_n, rad/sec	ζ –	ω_n, rad/sec	ζ –	τ, sec	τ, sec	ω_n, rad/sec	ζ –
5	0	2.43	0.71	1.90	0.52	0.14	1.18	5.54*	8.06*
	12	2.43	0.69	1.95	0.53	0.14	1.23	.43*	16.82*
	24	2.44	0.67	2.02	0.55	0.14	1.32	.65*	18.31*
10	0	2.60	0.72	1.94	0.57	0.17	1.44	0.17	0.95
	12	2.60	0.71	1.99	0.58	0.17	1.20	2.36*	14.95*
	24	2.60	0.69	2.08	0.59	0.17	1.30	1.60*	17.25*
15	0	2.67	0.72	2.35	0.69	0.36	1.07	0.16	0.99
	12	2.67	0.71	2.42	0.67	0.37	1.17	2.31*	19.23*
	24	2.68	0.70	2.51	0.66	0.34	1.30	1.57*	21.15*
20	0	2.72	0.72	2.95	0.57	1.08†	0.97†	0.16	0.98
	12	2.72	0.72	2.97	0.56	0.82	1.06	2.22*	18.49*
	24	2.72	0.71	3.00	0.55	0.66	1.34	1.50*	20.21*
25	0	2.75	0.62	2.22	0.40	0.80†	0.90†	6.09*	9.58*
	12	2.78	0.61	2.23	0.39	0.79†	0.93†	2.57*	67.57*
	24	2.81	0.60	2.25	0.39	0.78†	0.99†	1.79*	58.41*

*2 Real Roots

†Roll-Spiral ω_n and ζ

Q and R could be necessary to eliminate this characteristic.

The normally oscillatory phugoid mode degenerates into two real modes at most maneuvering conditions considered here. The over-damped phugoid mode may result from the "cost" associated with Δu perturbations, which could be relaxed in future DPSAS designs.

There are 16 non-trivial DPSAS gains generated for the pullup maneuver. Scheduling of these gains is discussed in Section 4.4, and 12 of the gains (four each for elevator, aileron, and rudder) are presented here. Table 4.3-2 lists these gains for α_0 of 5, 15, and 25 deg and q_0 of 0, 12, and 24 deg/sec. The first subscript of k indicates the control effector (in the order used in Table 4.2-2) and the second subscript indicates the feedback variable (also ordered in Table 4.2-2).

Longitudinal Gains (k_{21} to k_{24}) - The gains maintain an orderly progression with both α_0 and q_0; none change sign and most follow a single increasing or decreasing trend with the two flight variables. Table 4.3-2 shows that the pitch-rate gain (k_{23}) is dominant at all maneuver conditions and has a maximum variation of less than 25 percent, which is representative of the variations of most gains at most conditions.

Directional Gains (k_{45} to k_{48}) - Substantial variations in rudder gains can be expected with increasing α_0. The fuselage blocks the flow over the vertical tail at high α_0, and the rudder side force transforms into stability axis roll and yaw moments differently at different angles of attack. Unlike the longitudinal gains, there is a dramatic change in the directional gains as α_0 increases from 15 to

TABLE 4.3-2

DPSAS GAINS FOR THE LONGITUDINAL SWEEP (THROTTLE GAINS OMITTED)

α_o, deg	q_o, deg/sec	$\Delta\delta_h/\Delta\theta$ k_{21}	$\Delta\delta_h/\Delta u$ k_{22}	$\Delta\delta_h/\Delta q$ k_{23}	$\Delta\delta_h/\Delta w$ k_{24}	$\Delta\delta_a/\Delta v$ k_{35}	$\Delta\delta_a/\Delta r$ k_{36}	$\Delta\delta_a/\Delta p$ k_{37}	$\Delta\delta_a/\Delta\phi$ k_{38}	$\Delta\delta_r/\Delta v$ k_{45}	$\Delta\delta_r/\Delta r$ k_{46}	$\Delta\delta_r/\Delta_p$ k_{47}	$\Delta\delta_r/\Delta\phi$ k_{48}
5	0	-0.771	0.912	-1.633	-1.070	0.020	0.151	2.408	2.054	1.673	-2.917	0.201	0.195
	12	-0.911	1.480	-1.702	-1.089	0.591	-0.727	2.466	2.276	1.631	-2.856	0.244	0.102
	24	-0.899	1.654	-1.769	-1.243	1.109	-1.446	2.549	2.511	1.575	-2.748	0.279	0.0001
15	0	-0.700	1.322	-1.540	-0.988	-3.789	0.138	2.540	1.894	1.942	-3.096	0.225	-0.100
	12	-0.822	1.808	-1.62	-0.965	-0.138	-0.546	2.610	2.067	1.850	-2.996	0.289	-0.200
	24	-0.826	1.988	-1.69	-1.099	0.157	-1.100	2.711	2.265	1.768	-2.894	0.344	-0.306
25	0	-0.395	1.280	-1.400	-0.715	-2.274	2.499	0.101	0.339	4.879	-5.763	0.505	-0.381
	12	-0.651	1.755	-1.468	-0.436	-2.244	2.413	-0.006	0.417	4.859	-5.747	0.813	-0.506
	24	-0.763	2.028	-1.537	-0.384	-2.290	2.393	-0.091	0.515	4.967	-5.851	1.099	-0.660

25 deg (Table 4.3-2). The yaw gains (k_{45} and k_{46}) have significant changes with both α_0 and q_0. The roll-angle gain (k_{48}) is noted to change sign as α_0 progresses from 5 to 15 deg, while the increased roll-rate gain (k_{47}) attempts to provide stability-axis yaw damping.

Lateral Gains (k_{35} to k_{38}) - Trends in the aileron gains also have large variation with α_0 due to geometric transformation, loss of rudder effectiveness, and aileron yaw effects. More gains change sign, and pitch rate has a greater effect on gain magnitude. There is an abrupt reduction in the use of aileron for roll control (k_{37} and k_{38}) at an α_0 of 25 deg, which is accompanied by increased aileron use for yaw control (k_{35} and k_{36}).

It was noted earlier that pitch rate destabilizes the Dutch roll, roll, and spiral modes. The coupled nature of this phenomenon has an interesting effect on the secondary lateral-directional control paths, i.e., the yaw feedback to the roll moment controller (and the converse), such as k_{35}, k_{36}, k_{47}, and k_{48} at the lower angles of attack. These gains have as great or greater variation with q_0 as with the change from 5- to 15-deg α_0, which is not the case for the primary control paths (yaw-to-rudder and roll-to-aileron).

As in the previous section, the performance of the DPSAS in the pullup flight condition is assessed by comparing open- and closed-loop time responses. Figure 4.3-1 illustrates the aircraft's open- and closed-loop responses to an initial sideslip perturbation when α_0 is 15 deg and q_0 is 12 deg/sec. The oscillation grows at a moderate rate without stability augmentation but is damped in one cycle with the control loops closed. At higher angle of attack (25 deg) and the same pitch rate, the open-loop oscillation

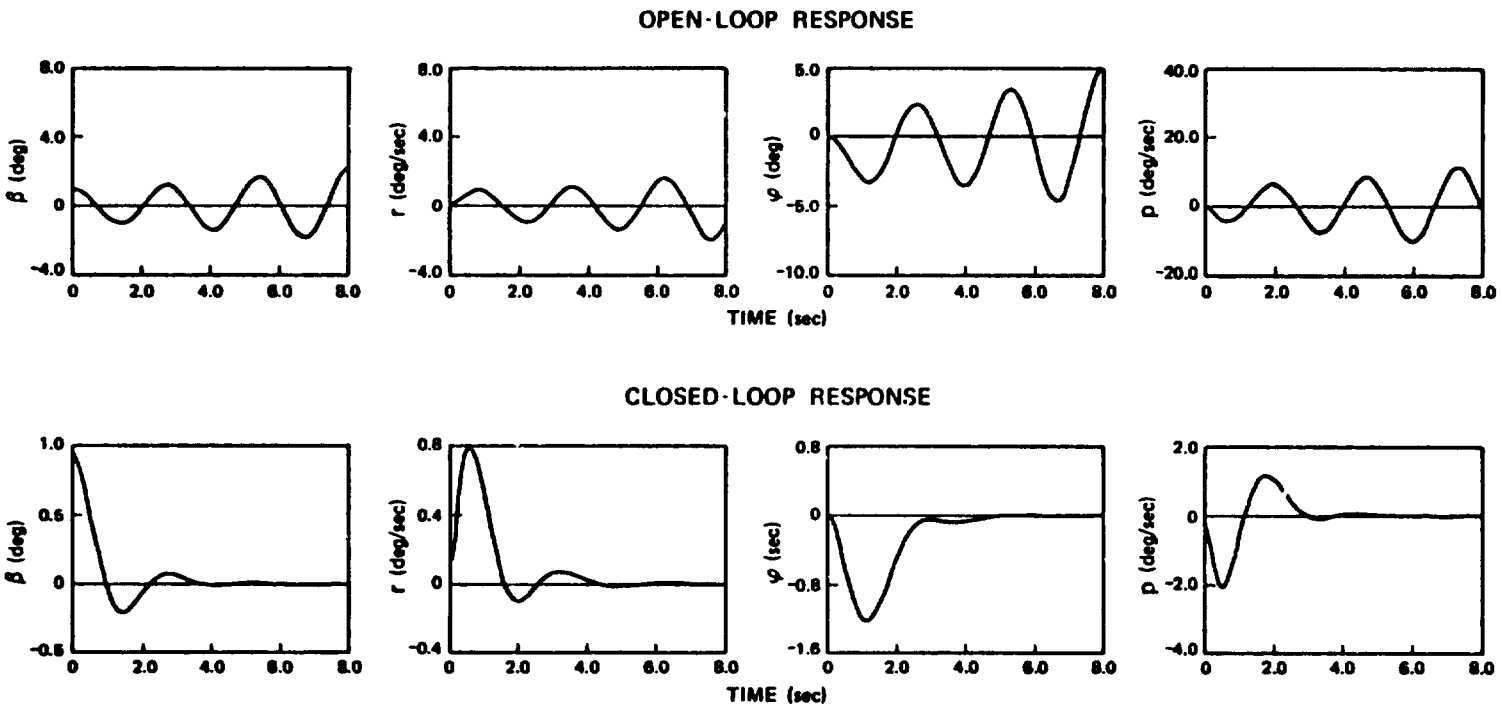

Figure 4.3-1 Pitch-Rate Effect on Directional Response ($\alpha_0 = 15$ deg, $q_0 = 12$ deg/sec)

grows at a faster rate, and the closed-loop oscillation takes two cycles to disappear (in keeping with the reduced damping ratio of the Dutch roll mode).

4.3.2 Lateral-Directional Sweep

Nominal values of sideslip angle and stability-axis roll rate are varied in this section, and their effects on closed-loop eigenvalues, DPSAS control gains, and aircraft response are presented. The development of this section follows the previous section, although the results presented for asymmetric flight are somewhat different from those of the longitudinal sweep. The Q and R matrices are the same as before, and linear-optimal regulators are designed at 18 points. Sideslip angles of 0, 5, and 10 deg are considered in combination with stability-axis roll rates of 0, ±13, ±26, and ±39 deg/sec. (For a given sideslip angle, roll rates of opposite sign have different dynamic effects.) Angle of attack, velocity, and altitude are fixed at 15 deg, 94 m/s, and 6100 m, respectively.

Table 4.3-3 presents the natural frequencies, damping ratios, and time constants of the aircraft, with the linear-optimal regulator loops closed. The most striking result, in comparison with Table 4.3-1, is that the lateral-directional closed-loop roots evidence relatively little variation with maneuver condition. There are no roll-spiral or phugoid degeneracies, and all parameters stay within 40 percent of their mean values. Short period, Dutch roll, and phugoid natural frequencies decrease with increasing β_0 magnitude and increase with increasing p_{W0} magnitude. Roll time constant and damping of the short period and phugoid modes are largely independent of β_0 magnitude but decrease with p_{W0} magnitude. Dutch roll

TABLE 4.3-3

CLOSED-LOOP STABILITY IN THE LATERAL-DIRECTIONAL SWEEP

Maneuver Condition		Short Period		Dutch Roll		Roll	Spiral	Phugoid	
β_o, deg	p_{w_o}, deg/sec	ω_n, rad/sec	ζ, —	ω_n, rad/sec	ζ, —	τ, sec	τ, sec	ω_n, rad/sec	ζ, —
0	39	2.95	0.56	2.52	0.91	0.51	1.13	0.34	0.77
	26	2.79	0.60	2.35	0.84	0.40	1.09	0.26	0.80
	13	2.64	0.66	2.40	0.75	0.37	1.07	0.19	0.89
	0	2.67	0.72	2.35	0.69	0.36	1.07	0.16	0.99
5	-39	2.95	0.56	2.48	0.93	0.52	1.07	0.35	0.77
	-26	2.79	0.61	2.28	0.85	0.38	1.06	0.27	0.78
	-13	2.65	0.66	2.35	0.76	0.36	1.06	0.20	0.87
	0	2.64	0.72	2.35	0.69	0.35	1.07	0.16	0.99
	13	2.59	0.66	2.45	0.75	0.36	1.09	0.19	0.91
	26	2.76	0.60	2.39	0.83	0.38	1.14	0.26	0.81
	39	2.92	0.56	2.51	0.90	0.46	1.22	0.34	0.78
10	-39	2.87	0.56	1.94	0.92	0.32	1.06	0.35	0.76
	-26	2.71	0.62	2.06	0.83	0.31	1.05	0.28	0.78
	-13	2.60	0.69	2.16	0.73	0.30	1.06	0.20	0.86
	0	2.63	0.73	2.16	0.67	0.30	1.08	0.16	0.99
	13	2.50	0.71	2.31	0.70	0.31	1.11	0.19	0.92
	26	2.65	0.61	2.25	0.81	0.32	1.18	0.27	0.82
	39	2.82	0.56	2.21	0.89	0.34	1.30	0.35	0.79

damping increases with p_{w_0} magnitude and is little affected by β_0. The spiral mode time constant increases with p_{w_0} magnitude, although its minimum value occurs at more negative p_{w_0} as β_0 increases.

Examples of the DPSAS gain variations with sideslip angle and roll rate are plotted in Fig. 4.3-2 and 4.3-3. The most apparent trend is that primary gains, i.e., those which would be non-zero in symmetric flight, change very little with β_0 and p_{w_0} while crossfeed gains have sub-

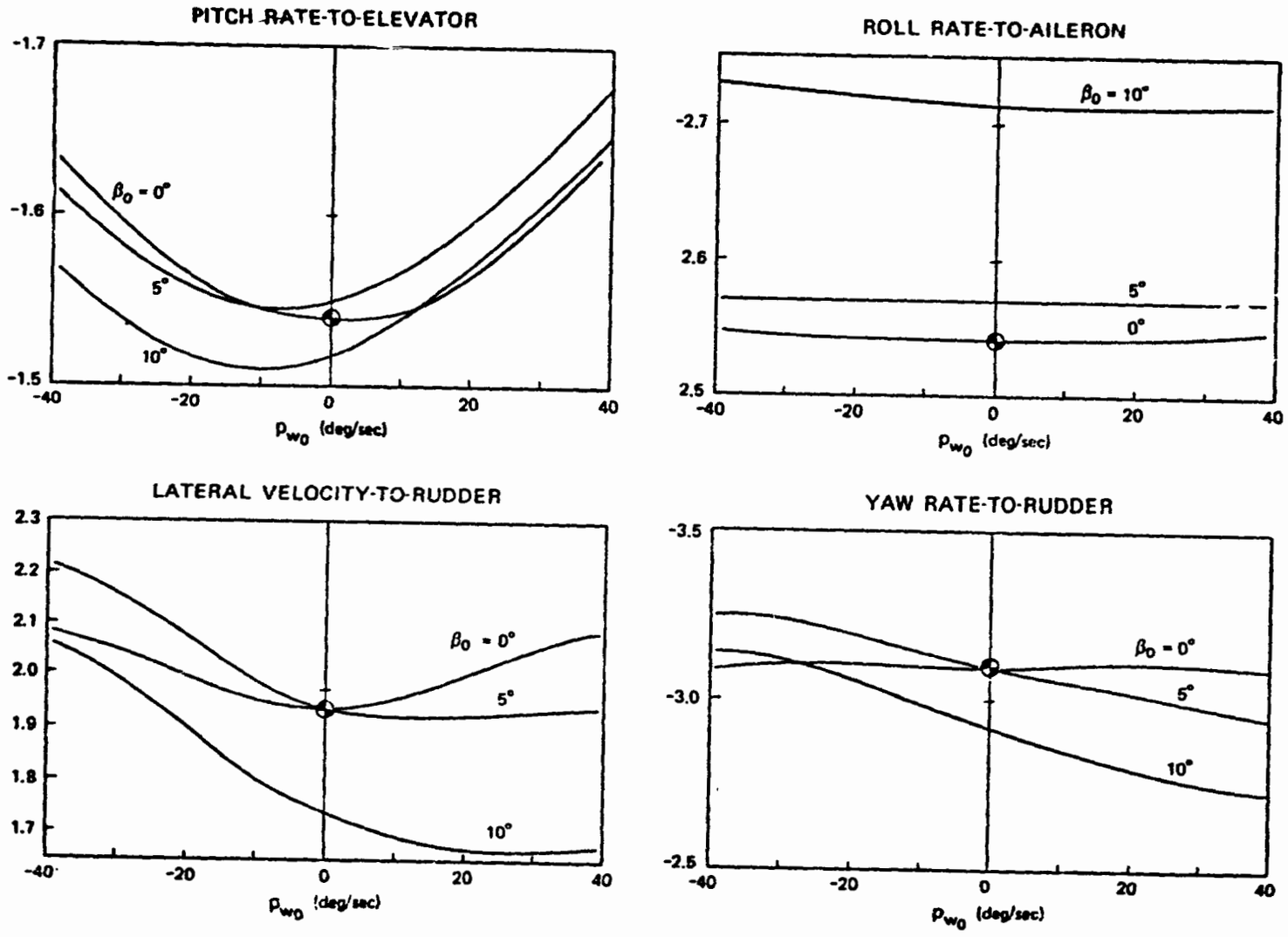

Figure 4.3-2 Examples of Primary Gain Variation in Lateral-Directional Sweep

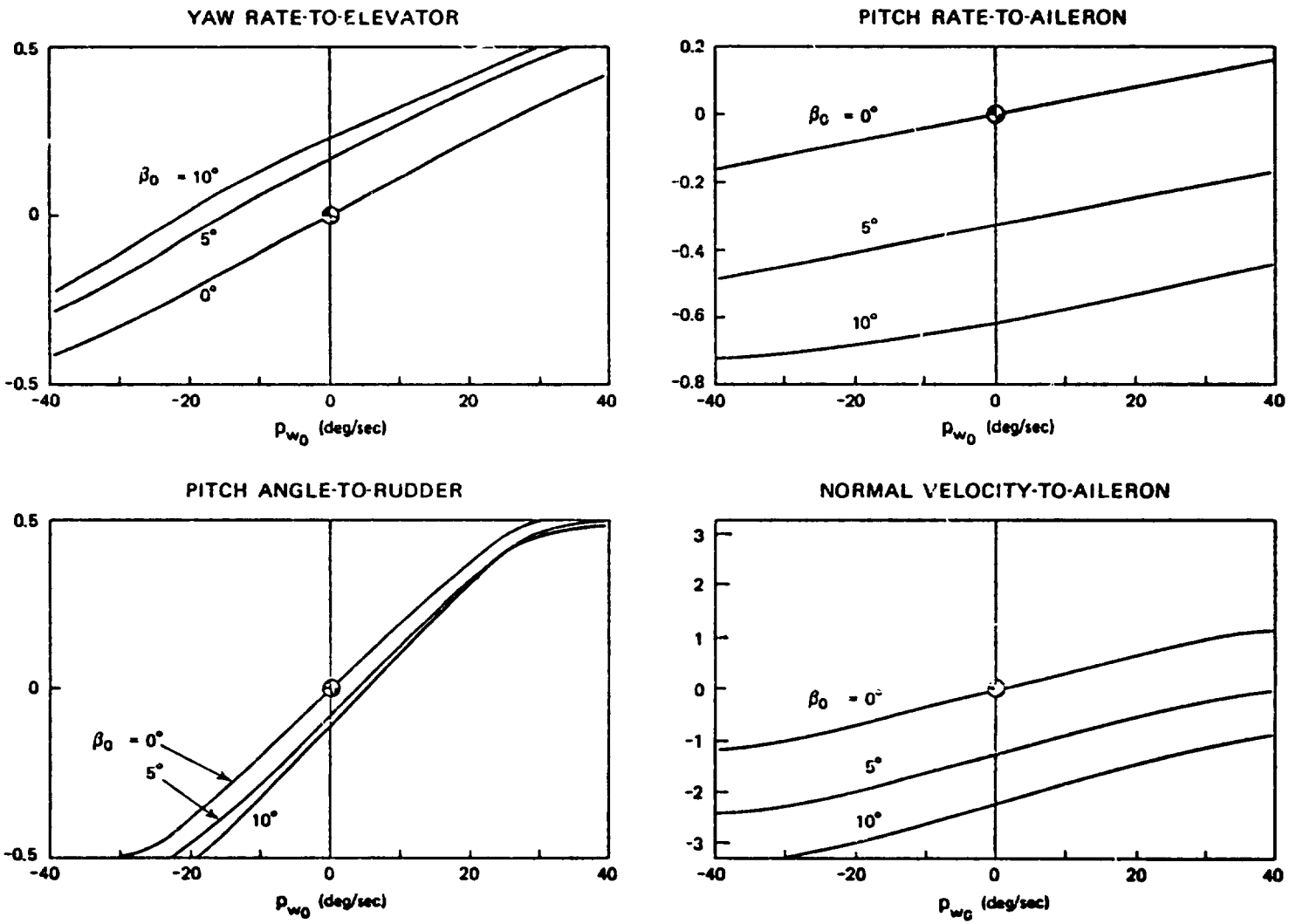

Figure 4.3-3 Examples of Crossfeed Gain Variation in Lateral-Directional Sweep

stantial variation with maneuver condition. The standard deviation of each gain, computed over the 18 lateral-directional sweep conditions, is an indication of its variation from a constant value. The average standard deviation for the primary gains is 16 percent, and for the crossfeed gains it is 422 percent. As discussed in Section 4.6, this is a first indication of gain-scheduling requirements, suggesting that many primary gains are nearly constant and that most secondary gains must be scheduled (unless they are negligible).

Gain variations are seen to depend on whether the vehicle is sideslipped "into" or "out of" the roll. (The vehicle is sideslipped into the roll when β_0 and p_{W_0} have opposite sign, e.g., when the nose is left and the left wing is moving down; it is sideslipped out of the roll when the signs are equal.) Figures 4.3-2 and 4.3-3 illustrate gain variations for positive β_0 only; for negative β_0, the variations with p_{W_0} are changed. The graphs of primary gains for negative β_0 are mirror images of those for positive β_0 (Fig. 4.3-2). The graphs of crossfeed gains for negative β_0 shift up or down, in opposition to the β_0 trend shown in Fig. 4.2-3 Primary gains can be monotonic or convex functions of p_{W_0}; crossfeed gains are monotonic in p_{W_0} and always pass through zero when both β_0 and p_{W_0} are zero (Gains for symmetric flight are inidcated by "●" in Fig. 4.3-3).

The crossfeed gains are shown to be non-trivial for even moderate values of β_0 and p_{W_0}, and those shown in Fig. 4.3-3 can be interpreted as nonlinear control elements. Note that each gain could be approximated by a function of the form

$$\text{Gain} = c_1\beta_0 + c_2 p_{W_0} \qquad (4.3\text{-}1)$$

where c_1 and c_2 are appropriate constants. Then the control signals represented by these four graphs would be

$$\Delta\delta_h = c_1\beta_0\Delta r + c_2 p_{W_0}\Delta r \qquad (4.3\text{-}2)$$

$$\Delta\delta_a = c_3\beta_0\Delta q + c_4 p_{W_0}\Delta q \qquad (4.3\text{-}3)$$

$$\Delta\delta_r = c_5\beta_0\Delta\theta + c_6 p_{W_0}\Delta\theta \qquad (4.3\text{-}4)$$

$$\Delta\delta_a = c_7\beta_0\Delta w + c_8 p_{W_0}\Delta w \qquad (4.3\text{-}5)$$

where the constants are derived by regression analysis (Section 4.6). The $p_{W_0}\Delta w$ and $p_{W_0}\Delta\theta$ terms can be recognized as analogous to so-called "pseudo-$\dot{\beta}$" or "pα" crossfeeds, which have been incorporated in the SAS of modern high-performance aircraft. (An additional "pα"-type primary gain is indicated in Table 4.3-2. The roll rate-to-rudder gain could be approximated by $c\alpha_0$; therefore, the associated rudder command would be $c\alpha_0\Delta p$.) Nonlinearities in the curves of Fig. 4.3-3 suggest that higher-order fits than Eq. (4.3-1) to (4.3-5) are required if design performance is to be obtained over a wide range of β_0 and p_{W_0}.

Examples of open- and closed-loop response at two asymmetric flight conditions are shown in the next two figures. Figures 4.3-4 and 4.3-5 show that roll rate introduces substantial longitudinal response to a directional input and that the addition of sideslip angle leads to qualitative changes in response shapes. Roll rate alone introduces regular oscillations in the aircraft's open-loop response (Fig. 4.3-4). The DPSAS damps the oscillation within 1½ cycles, although excitation of the phugoid mode leads to a slow decay in $\Delta\alpha$ (The effective time constant $(-\zeta\omega_n)$ of the phugoid is 6 sec at this flight condition).

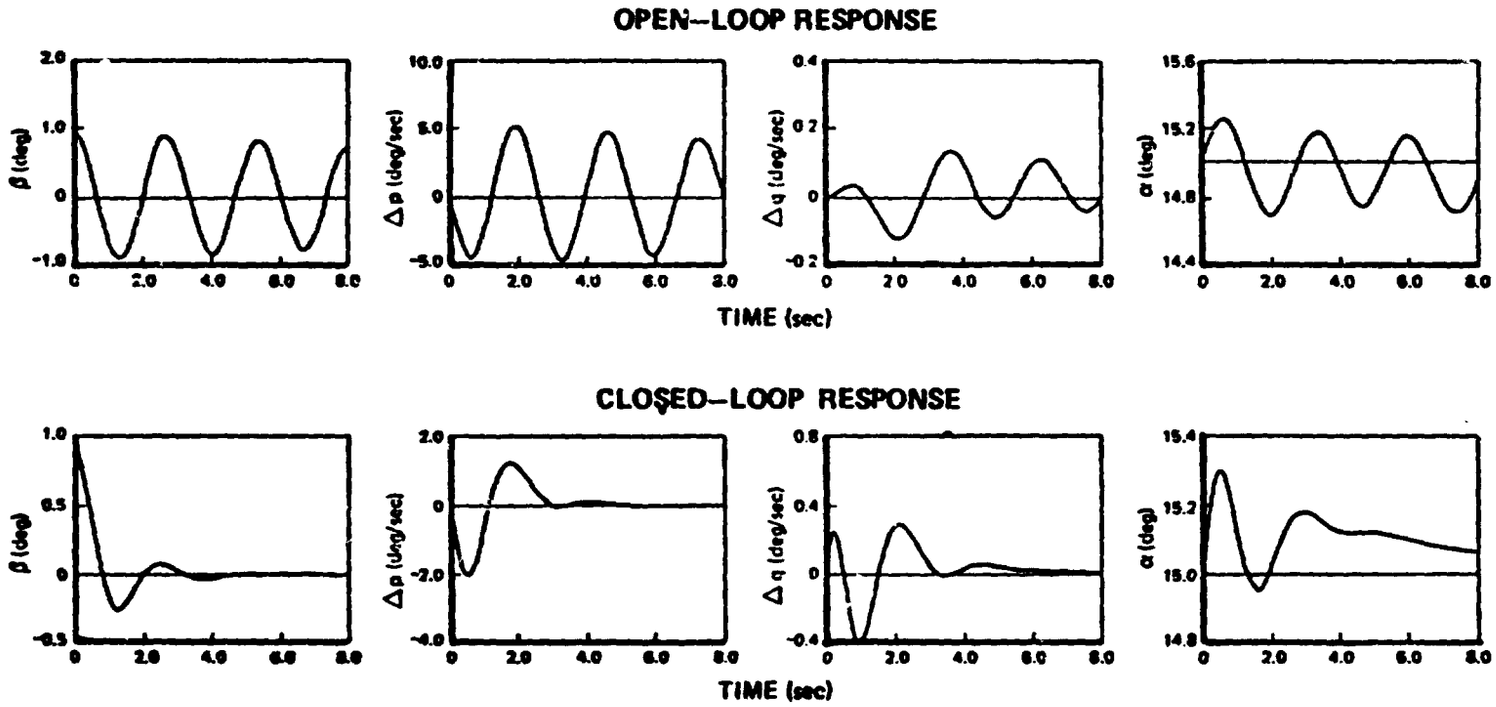

Figure 4.3-4 Roll-Rate Effect on Directional Response
($\alpha_0 = 15$ deg, $\beta_0 = 0$ deg, $p_{w_0} = 39.6$ deg/sec)

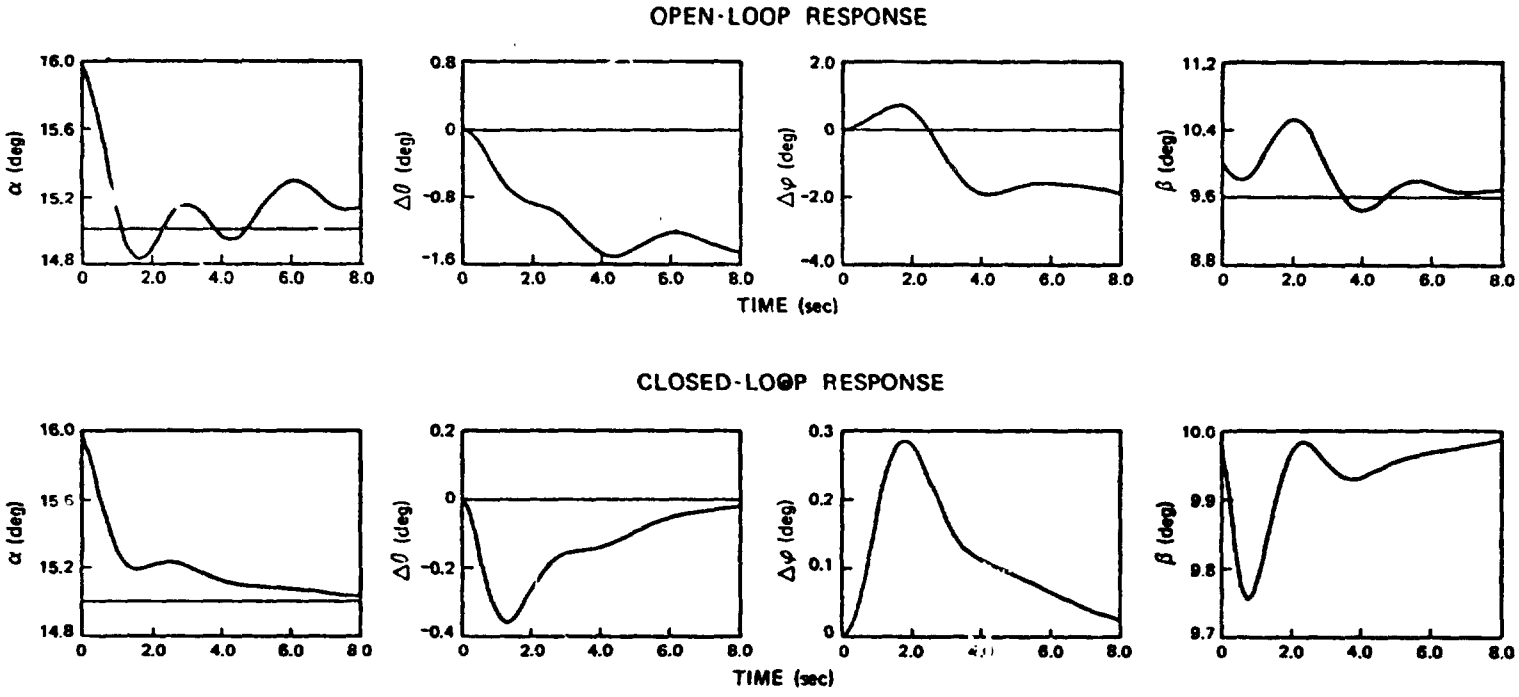

Figure 4.3-5 Roll-Rate/Sideslip Effect on Longitudinal Response ($\alpha_0 = 15$ deg, $\beta_0 = 10$ deg, $p_{w_0} = 39.6$ deg/sec)

When the aircraft has developed a large mean sideslip angle as well as roll rate, the open-loop perturbation motions tend to meander, as several modes are involved in each motion (Fig. 4.3-5). For example, the initial $\Delta\alpha$ appears to be damping out, but after 5 sec, it begins to wander. Pitch and roll angle develop offsets which are continuing to increase at the end of the time period shown. The DPSAS restricts the maximum initial excursions of $\Delta\theta$, $\Delta\phi$, and $\Delta\beta$ to less than half their open-loop values and eliminates the meandering characteristic.

Plotting β rather than $\Delta\beta$ in Fig. 4.3-5 is a reminder that the DPSAS provides stability about a reference flight condition, in this case, 10-deg sideslip angle and -39.6-deg/sec roll rate. With the assumption that these values are commanded by the pilot, it can be seen that the DPSAS does not limit aircraft maneuverability -- in fact, it expands the flight envelope by stabilizing the aircraft in conditions which could not be controlled by the unaided pilot. Although non-zero β_0 is not normally desired in maneuvering current high-performance aircraft, future aircraft, particularly those with direct side force control, could use this capability to tactical advantage.

This section has presented linear-optimal DPSAS designs for the reference aircraft and for a variety of maneuvering conditions. The next section of this chapter demonstrates how control gains can be adapted to flight condition.

4.4 CONTROL-LAW ADAPTATION FOR VARYING FLIGHT CONDITIONS

This section presents results for a procedure which adapts the control gains of a high-performance aircraft to varying flight conditions, including gain correlations for the reference aircraft model. The gains are scheduled by finding functional relationships between aircraft flight variables and the control gains at the corresponding flight conditions.

Previous methods for scheduling control gains have been successful and indicate that gain scheduling is a sound approach. The methodology typically is based on single input/single output concepts, e.g., maintaining constant loop gain. These previous methods, however, provide inadequate insight for scheduling a multivariable system.

The method is a logical extension of previous work to multivariable systems. It involves three steps, and it places minimum reliance on past experience and intuition. The three steps are:

- The determination of means and standard deviations of the control system gains.
- The determination of correlation coefficients between gains and flight variables.
- The determination of functional relationships (or curve fits) between the chosen flight variables and the gains.

This new gain scheduling procedure, discussed in Section A.4.5,

is simple to use, the results are easy to implement on a digital computer, and the procedure can have broad application.

The longitudinal and lateral-directional sweep control gains discussed in Section 4.3 have been correlated with a number of flight variables. In order to identify the individual effects of longitudinal and lateral-directional mean motions, the correlations for each sweep are done separately. In a flight system, the gains should be correlated jointly, and additional factors -- such as weight, altitude, and velocity -- must be considered.

For each sweep, a list of candidate independent variables is established, and various functions of their variables are correlated with the 32 gains associated with each flight condition. Functions considered included polynomials of order one and two,

$$\text{Gain} = b_0 + b_1 m \tag{4.4-1}$$

$$\text{Gain} = b_0 + b_1 m + b_2 m^2 \tag{4.4-2}$$

and linear regressions in two variables,

$$\text{Gain} = b_0 + b_1 m_1 + b_2 m_2 \tag{4.4-3}$$

Given a flight variable, y, independent variables, m, of the form y, y^2, $1/y$, $1/y^2$, and $y|y|$ are considered in the polynomial regressions. Equation (4.4-3) is used with $m_1 = y_1$ and $m_2 = y_2$. The objective of the computations is to find the functional approximation to each gain which has the greatest correlation with the linear-optimal gain at all conditions in the particular sweep. In many cases, alternate functions have similar correlation coefficients, so more than one schedule could be considered in implementation.

The correlation between gains also is of interest, as it suggests which gains can be scheduled as functions of other gains, and it helps to identify control interconnects. This correlation can be computed, using Eq. (A.4-37), by defining the first gain as k and the second as $\hat{k}$. The following results indicate that an aileron-rudder interconnect could be considered for the stability augmentation system of the reference aircraft.

4.4.1 Longitudinal Sweep

The procedure followed in establishing gain-scheduling requirements is to compute means and standard deviations (as percentages of the means) of the gains, to correlate gains with flight variable functions, and to correlate gains with other gains. Sixteen crossfeed gains are identically zero, leaving sixteen gains for scheduling.

Table 4.4-1 summarizes the findings for DPSAS gains in the longitudinal sweep, presenting the mean and standard deviation of each gain. The independent variables which provide the best gain schedule are listed, along with the correlation between the actual and scheduled gain values. Also listed is the gain which exhibits the highest cross-correlation, (calculated by applying Eq. (A.4-37) to all pairs of gains) and the value of that cross-correlation. For example, the gain $\Delta\delta_T/\Delta\theta$ exhibits a mean of -0.016 and a standard deviation of 32% over the chosen set of longitudinal flight conditions. A gain schedule using normal load factor (n_{z_0}) and pitch rate (q_0) produces a scheduled gain whose correlation factor with the actual gain is 0.89. Finally, $\Delta\delta_T/\Delta\theta$ exhibits strongest cross-correlation with $\Delta\delta_T/$ u, and the correlation factor is 0.98. The flight variables considered as possible scheduling variables are

TABLE 4.4-1

GAIN CORRELATIONS FOR THE LONGITUDINAL SWEEP

Longitudinal Gains

Gain	$\Delta\delta_T/\Delta\theta$	$\Delta\delta_T/\Delta u$	$\Delta\delta_T/\Delta q$	$\Delta\delta_T/\Delta w$	$\Delta\delta_h/\Delta\theta$	$\Delta\delta_h/\delta_u$	$\Delta\delta_h/\Delta q$	$\Delta\delta_h/\Delta w$
Mean of Gain	-0.016	0.062	-0.006	0.013	-0.763	1.640	-1.621	-0.928
Standard Deviation of Gain, % of Mean	32	16	18	54	17	20	6	26
Best Scheduling Variables	n_z, q*	n_z, q	n_z, q	n_z, q	n_z, q	n_z, q	cos α	cos α
Scheduled/Actual Gain Correlation	0.89	0.93	0.95	0.95	0.85	0.94	0.88	0.89
Gain of Highest Cross Correlation	$\Delta\delta_T/\Delta u$	$\Delta\delta_T/\Delta\theta$	$\Delta\delta_h/\Delta u$	$\Delta\delta_h/\Delta q$	$\Delta\delta_h/\Delta q$	$\Delta\delta_T/\Delta q$	$\Delta\delta_a/\Delta r$	$\Delta\delta_a/\Delta\phi$
Gain Cross Correlation	0.98	0.98	0.91	0.89	0.84	0.91	0.92	0.94

Lateral Gains

Gain	$\Delta\delta_a/\Delta v$	$\Delta\delta_a/\Delta r$	$\Delta\delta_a/\Delta p$	$\Delta\delta_a/\Delta\phi$	$\Delta\delta_r/\Delta v$	$\Delta\delta_r/\Delta r$	$\Delta\delta_r/\Delta p$	$\Delta\delta_r/\Delta\phi$
Mean of Gain	-0.446	0.076	2.054	1.764	2.480	-3.567	0.404	-0.206
Standard Deviation of Gain, % of Mean	251	1713	50	40	50	32	60	111
Best Scheduling Variables	cos α	cos α	cos α	cos α	cos α	cos α	n_z	n_z,q
Scheduled/Actual Gain Correlation	0.93	0.83	0.82	0.90	0.93	0.91	0.94	0.98
Gain of Highest Cross Correlation	$\Delta\delta_a/\Delta\phi$	$\Delta\delta_a/\Delta\phi$	$\Delta\delta_r/\Delta r$	$\Delta\delta_r/\Delta r$	$\Delta\delta_r/\Delta r$	$\Delta\delta_r/\Delta v$	$\Delta\delta_h/\Delta w$	$\Delta\delta_T/\Delta u$
Gain Cross Correlation	0.94	0.98	0.98	0.99	1.00	1.00	0.89	0.90

*All independent variables evaluated at nominal flight condition, "0" subscript omitted.

angle of attack (α_0), pitch rate (q_0), normal load factor (n_{z_0}), $\sin\alpha_0$, and $\cos\alpha_0$. This set of independent variables includes those actually varied (α_0 and q_0) and some likely functions of them, and it serves to illustrate the DPSAS gain scheduling procedure.

The only gain which is reasonably constant in Table 4.4-1 is $\Delta\delta_h/\Delta q$, the pitch rate-to-elevator gain, as its standard deviation is just 6 percent of the mean value. As is the case for all gains which are most highly correlated with $\cos\alpha_0$, the best functional fit is given by

$$\text{Gain} = b_0 + b_1/\cos^2\alpha_0 + b_2/\cos^4\alpha_0 \qquad (4.4\text{-}4)$$

The roll rate-to-rudder gain, $\Delta\delta_r/\Delta p$, is best approximated by a polynomial in load factor,

$$\text{Gain} = b_0 + b_1 n_{z_0}^2 + b_2 n_{z_0}^4 \qquad (4.4\text{-}5)$$

and the remaining gains are "best" fit by linear functions of n_{z_0} and q_0. This is not to say that alternate functions, e.g., $n_{z_0}^2$ and q_0, would not be better. These correlations are "best" for the independent variables and functions considered, and the average correlation with actual gain values is over 0.9.

All gains have a correlation greater than 0.89 with at least one other gain except $\Delta\delta_h/\Delta\theta$, which has a correlation above 0.8 with several gains. The suitability of a SAS aileron-rudder interconnect is evaluated by noting the correlation between the aileron and rudder gains for each feedback variable (Δv, Δr, Δp, and $\Delta\phi$). The correlations (not necessarily the maximums, and not necessarily in the table) are 0.93(Δv), 0.95(Δr), 0.83(Δp), and 0.70($\Delta\phi$), indicating a good possibility for combining Δv and Δr feedbacks

with little performance degradation, and a moderate possibility for combining Δp and $\Delta\phi$ feedbacks as well.

4.4.2 Lateral-Directional Sweep

Correlation results for the lateral-directional sweep are shown in Table 4.4-2 which indicates that no gain means are identically zero, although several appear negligible. The flight variables considered for scheduling are sideslip angle (β_0) and stability-axis roll rate (p_{W_0}), which are chosen to illustrate the DPSAS gain scheduling method. In an actual application, additional independent variables could be included in the search.

Unlike the longitudinal sweep, it appears that 13 gains could be considered constant, with standard deviations of less than 8 percent of the mean value. Five gains are inadequately scheduled by the chosen independent variables and functions, as their correlations are below 0.75. Two of these are the rudder gains shown in Fig. 4.3-2, which can be seen to be more complex than the polynomials and linear combination considered here. Higher-order curves would fit these gains, although they are candidates for the constant-value approximation because their standard deviations are low.

Seventeen gains are most closely correlated with p_{W_0} and are fitted best by second-order polynomials in p_{W_0}. The eleven gains which are most correlated with β_0 are fitted almost as well by second-order polynomials in β_0, β_0^2, $1/\beta_0$, $1/\beta_0^2$, or $\beta_0|\beta_0|$. Three of the four linear β_0-p_{W_0} fits are adequate, with $\Delta\delta_r/\Delta r$ requiring an improved fit (along with $\Delta\delta_a/\Delta w$, $\Delta\delta_a/\Delta v$, $\Delta\delta_a/\Delta r$, and $\Delta\delta_r/\Delta v$). Most pairs have strong correlation with at least one other gain. The correlations associated with SAS aileron-rudder interconnect are 0.95(Δv),

TABLE 4.4-2
GAIN CORRELATIONS FOR THE LATERAL-DIRECTIONAL SWEEP

Longitudinal Gains

Gain	$\Delta\delta_T/\Delta\theta$	$\Delta\delta_T/\Delta u$	$\Delta\delta_T/\Delta q$	$\Delta\delta_T/\Delta w$	$\Delta\delta_T/\Delta v$	$\Delta\delta_T/\Delta r$	$\Delta\delta_T/\Delta_p$	$\Delta\delta_T/\Delta\phi$	$\Delta\delta_h/\Delta\theta$	$\Delta\delta_h/\Delta u$	$\Delta\delta_h/\Delta q$	$\Delta\delta_h/\Delta w$	$\Delta\delta_h/\Delta v$	$\Delta\delta_h/\Delta r$	$\Delta\delta_h/\Delta p$	$\Delta\delta_h/\Delta\phi$
Mean of Gain	-0.018	0.069	-0.005	0.020	0.007	0.002	0.0001	0.002	-0.767	1.352	-1.580	-1.004	0.030	0.120	0.049	0.008
Standard Deviation of Gain, % of Mean	4	1	2	5	94	84	215	147	7	3	3	5	562	237	91	1451
Best Scheduling Variables	p*	β	p	p	β	β	p	p	p	p	p	β,p	p	β,p	β	p
Scheduled/Actual Gain Correlation	0.85	0.84	0.81	0.86	0.87	0.99	0.54	0.84	0.98	0.93	0.92	0.73	0.79	0.76	1.00	0.81
Gain of Highest Cross Correlation	$\Delta\delta_T/\Delta_w$	$\Delta\delta_a/\Delta u$	$\Delta\delta_r/\Delta\phi$	$\Delta\delta_T/\Delta\theta$	$\Delta\delta_h/\Delta p$	$\Delta\delta_a/\Delta u$	$\Delta\delta_h/\Delta w$	$\Delta\delta_h/\Delta r$	$\Delta\delta_T/\Delta w$	$\Delta\delta_h/\Delta q$	$\Delta\delta_h/\Delta u$	$\Delta\delta_T/\Delta q$	$\Delta\delta_h/\Delta\phi$	$\Delta\delta_r/\Delta_q$	$\Delta\delta_T/\Delta v$	$\Delta\delta_r/\Delta q$
Gain Cross Correlation	0.98	0.91	0.99	0.98	1.00	0.99	0.50	0.95	0.90	0.98	0.98	0.87	0.94	0.98	1.00	0.99

Lateral Gains

Gain	$\Delta\delta_a/\Delta\theta$	$\Delta\delta_a/\Delta u$	$\Delta\delta_a/\Delta q$	$\Delta\delta_a/\Delta w$	$\Delta\delta_a/\Delta v$	$\Delta\delta_a/\Delta r$	$\Delta\delta a/\Delta_p$	$\Delta\delta_a/\Delta\phi$	$\Delta\delta_r/\Delta\theta$	$\Delta\delta_r/\Delta u$	$\Delta\delta_r/\Delta q$	$\Delta\delta_r/\Delta w$	$\Delta\delta_r/\Delta v$	$\Delta\delta_r/\Delta r$	$\Delta\delta_r/\Delta p$	$\Delta\delta_r/\Delta\phi$
Mean of Gain	-0.025	-0.194	-0.308	-1.142	-0.554	0.293	2.610	2.001	-0.048	-0.262	0.038	0.066	1.942	-3.045	0.217	-0.148
Standard Deviation of Gain, % of Mean	1934	79	86	108	70	62	3	8	871	78	543	157	8	4	7	65
Best Scheduling Variables	p	β	β	β	β	p	β	p	p	β	p	β,p	β	β,p	p	p
Scheduled/Actual Gain Correlation	0.98	0.93	0.92	0.73	0.79	0.76	1.00	0.81	0.97	0.97	0.99	0.82	0.68	0.69	0.80	0.82
Gain of Highest Cross Correlation	$\Delta\delta_r/\Delta\theta$	$\Delta\delta_r/\Delta u$	$\Delta\delta_h/\Delta p$	$\Delta\delta_h/\Delta p$	$\Delta\delta_r/\Delta v$	$\Delta\delta_r/\Delta p$	$\Delta\delta_T/\Delta r$	$\Delta\delta_T/\Delta q$	$\Delta\delta_a/\Delta\theta$	$\Delta\delta_T/\Delta r$	$\Delta\delta_h/\Delta\phi$	$\Delta\delta_r/\Delta\theta$	$\Delta\delta_a/\Delta v$	$\Delta\delta_r/\Delta v$	$\Delta\delta_T/\Delta w$	$\Delta\delta_T/\Delta q$
Gain Cross Correlation	0.9	0.94	0.99	0.97	0.95	0.87	0.93	0.96	0.99	0.99	0.99	0.78	0.95	0.93	0.92	0.99

*All independent variables evaluated at nominal flight condition, "0" subscript omitted

0.50(Δr), 0.13(Δp), and 0.04($\Delta\phi$), indicating that either rudder or aileron would require additional Δr and Δp feedbacks in parallel with the interconnected control path.

4.4.3 Additional Considerations

The longitudinal and lateral-directional sweeps were conducted to illustrate the separate effects of α_0, q_0, β_0, and p_{W0} on DPSAS gains. Furthermore, a limited set of independent variables and scheduling functions were examined. At a minimum, these sweeps should be combined in a single correlation procedure to obtain a single multi-variable schedule for each gain. Altitude, velocity, and weight effects should be added, principally through indicated airspeed, Mach number, and the ratio of weight-to-dynamic pressure. Permutations of the independent variables, e.g., body-axis rather than stability-axis rates, may provide better correlation or may be easier to implement in a particular system.

The present results suggest that primary gains schedule largely on longitudinal variables and that crossfeed gains schedule primarily on lateral-directional variables. This observation derives from the fact that most primary DPSAS gains are nearly constant as β_0 and p_{W0} change, while crossfeed gains are zero in symmetric flight. Any approximations made in gain scheduling must be validated by direct simulation, as this is tantamount to changing the gains from their linear-optimal values, thus altering closed-loop response.

An entirely separate issue is the on-board determination (either through measurement or estimation) of the independent variables to be used for gain scheduling --

particularly α_0 and β_0, which are notably difficult to measure. Two potential problems are inaccurate steady-state measurement, which leads to inaccurate calculation of gains, and superposition of perturbations on the mean values, which could cause longitudinal motions to drive lateral-directional motions (and vice versa) through oscillatory gain changes. The solution to both problems, should they occur, is found through state estimation, which allows all available measurements to be blended in a unified estimate of nominal and perturbation motion variables (Ref. 63). As an example, measurements of α, q, n_z, airspeed, and δ_h could be used to estimate α_0, q_0, $\Delta\alpha$, and Δq. If the DPSAS is incorporated in a full command augmentation system, pilot commands could be direct indicators of the desired (or nominal) state; therefore, they could be used for gain scheduling (Ref. 58). This is a topic for further study.

4.5 CHAPTER SUMMARY

This chapter has presented design principles for stability augmentation systems (DPSAS) which prevent departure from controlled flight. Linear-optimal control theory has been used to develop control structures for departure prevention, and the effects of maneuvering condition on optimal feedback and crossfeed gains have been explored. Examples of aircraft response to longitudinal, lateral, and directional initial conditions illustrate the well-controlled behavior which the DPSAS provides, and closed-loop eigenvalues show that variation in aircraft dynamic characteristics is minimized for a wide range of maneuvering conditions.

In many respects, stabilizing the reference aircraft in a pullup maneuver is a more challenging task than accounting

for the coupling which results from sideslip and roll rate; however, lateral-directional maneuvering results in significant linear-optimal gains which improve aircraft response. In combination with gain-scheduling functions which depend on mean values of angles and angular rates, the DPSAS control algorithms are seen to produce nonlinear crossfeeds which are analogous to control structures being employed in modern high-performance aircraft.

Linear-optimal control theory solves many aircraft control problems which have been difficult to overcome with past design techniques. It is easy to use, it guarantees system stability, and it accommodates aircraft with limited control authority.

5. CONCLUSIONS AND RECOMMENDATIONS

This report has illustrated how linear systems analysis can be used to characterize the stability of aircraft during maneuvering flight. It also presents a design procedure for stability augmentation systems which prevent departure from controlled flight. The key to linearizing the dynamics of the aircraft is that an accelerated flight condition can be used as a reference path. A linear model can provide a good description of the aircraft's perturbation response (to initial conditions, control inputs, and disturbances) even when the aircraft has large aerodynamic angles and angular rates. Control systems designed for fully coupled linear models and adapted to changing flight conditions can provide protection against inadvertent departure from controlled flight.

5.1 CONCLUSIONS

A detailed examination of the dynamics of the reference aircraft has led to generalizations concerning aircraft stability and control. These include the following:

- The aircraft's stability (as shown by its eigenvalues) is most affected by changes in the nominal longitudinal variables (V_0, α_0, and q_0), while the mode shapes (as described by the aircraft eigenvectors) are most affected by non-zero nominal values of the lateral variables (β_0 and p_{W_0}). Asymmetric flight leads to longitudinal-variable response in typically lateral-directional modes, and vice-versa.

- Nonminimum-phase zeros in the aircraft transfer functions occur frequently in asymmetric flight, and the transfer function numerators are changed substantially by non-zero q_0.

- Extreme maneuvers are often characterized by rapid changes in <u>both</u> mode shapes and speeds due to large values of α_0, p_{W_0}, and q_0. Highly coupled, unstable natural modes can result.

- Elementary loop closures which are stabilizing in symmetric flight can lead to unstable system dynamics in asymmetric flight.

- The departure parameter, $C_{n_{\beta dyn}}$, has limited value in predicting aircraft departure. It provides no information regarding Dutch roll damping; hence, it does not predict departure due to negative damping (as is the case for the subject aircraft).

- <u>Unforced departures</u> occur when one of the fast modes (short period, Dutch roll, or roll mode) is unstable. These departures primarily take the form of a Dutch roll instability, with fast rolling-yawing motions or oscillatory divergence. The roll mode can become unstable at extreme angles, where it exhibits a fast roll-yaw divergence.

- <u>Forced departures</u> occur as a result of pilot action. This can happen when degraded response to control inputs causes the pilot to fly the aircraft into a flight regime where unforced departures are likely or when pilot actions destabilize the aircraft directly.

- Guidelines for the design of Departure-Prevention Stability Augmentation Systems (DPSAS) have been presented. An adaptive-control design procedure, using the linear-optimal regulator for

fixed-point design followed by gain scheduling, is shown to provide a nonlinear control structure containing crossfeeds as well as feedback gains. The resulting DPSAS has similarities to the flight control systems of current high-performance aircraft. However, the new design is based on "quadratic synthesis" techniques, which provide a unified set of control gains for all axes from a single set of vector-matrix design equations.

- The linear-optimal DPSAS prevents departure not by limiting the maneuvering ability of the aircraft but by stabilizing the aircraft in all foreseeable maneuver conditions.

- The linear-optimal control law can be readily extended to a full Departure-Prevention Command Augmentation System (DPCAS) which accounts for control actuator rate limits and allows essentially unlimited pilot control authority (within the physical limitations of the aircraft).

- The maneuverability envelope of the subject aircraft could be materially expanded through the incorporation of DPSAS/DPCAS concepts, as identified in this report.

5.2 RECOMMENDATIONS

The following recommendations are made as a result of this study:

- Departure prevention studies for high-performance aircraft should be extended to transonic and supersonic flight regimes.

- The high angle-of-attack/high angular rate problems of additional aircraft types, including transports, helicopters, and general aviation aircraft,

are amenable to coupled linear analysis and bear investigation.

- Design requirements for a DPCAS should be investigated. Digital implementation and incorporation of active control concepts for improved maneuverability should be considered.

- It is recommended that improvements to the subject aircraft's maneuverability envelope due to DPSAS/DPCAS implementation be explored in ground-based piloted simulation and flight test.

Dynamic coupling is a significant factor in the maneuvers of high-performance aircraft, and a full understanding of its effects is an important facet of preventing departure from controlled flight. This report has shown how linear models of the aircraft's motions can be used to investigate the stability and control of maneuvering flight, and it has demonstrated the flexibility and ease with which linear-optimal control theory can be used to design departure-preventing control systems.

APPENDIX A

ANALYTICAL APPROACH TO AIRCRAFT DYNAMICS

A.1 OVERVIEW

This appendix develops the analytical approach taken in this report. The goal of this work is to analyze the aircraft stability and control problems that arise at high angles of attack and during rapid maneuvers. The nonlinear equations of motion of a vehicle in atmospheric flight are developed in Section A.2. A large body of theory and experience relating to linear system analysis and control synthesis exists (Ref. 64 to 67), yet a full and complete linearization of the aircraft problem is not readily available; therefore, a rigorous application of linear analysis should provide new insights regarding departure. Section A.3 presents the full linearized equations of motion in a general form, and it includes a discussion of methods for choosing the point of linearization. Section A.4 presents an overview of linear system analysis and control methods.

A.2 NONLINEAR EQUATIONS OF MOTION

The complete nonlinear rigid-body equations of motion are derived in this section. They are developed using "flat-earth" assumptions, i.e. the effects of earth curvature and rotation are assumed negligible. This means that earth-fixed and inertial reference frames are equivalent.

There are four coordinate systems of interest in the study of rigid-body motions of aerodynamic vehicles. They are described as follows:

- Inertial-Axis System - This frame is fixed in inertial space, and is the frame from which the inertial velocity and angular rate of the vehicle are measured.
- Body-Axis System - The forces and moments on the vehicle, and therefore the dynamic equations, are best expressed in a body-fixed reference frame. The stability-axis system is a special body-fixed reference frame.
- Velocity-Axis System - An especially useful reference frame for navigation and guidance, the velocity-axis system relates the vehicle velocity vector to inertial axes.
- Wind-Axis System - Since the aerodynamic forces and moments depend largely on the body-velocity vector orientation, the wind-axis system, which provides straightforward body-wind relations, is useful.

For the moderate velocities of interest in this report (typically subsonic, i.e., below about 340 m/s), the equivalence of earth-fixed and inertial reference frames is a good assumption. The origin of the inertial reference frame used here is located on the surface of the earth, with the x-, y-, and z-axes in a north-east-down orientation. Since the simplest statement of Netwon's Second Law is given in an inertial reference frame, this frame plays an important part in the derivation of the dynamic equations.

The various body-fixed axis systems have a common origin, located at the body center of mass, and are fixed

in orientation with respect to the vehicle. Generally, the body x-axis extends forward out the vehicle's nose, the y-axis extends out the right wing, and the z-axis extends out the bottom of the vehicle. The x-z plane is usually a plane of geometric symmetry, if the vehicle has one. There are a number of possible body-fixed reference frames, and the one fixed by the builder is simply referred to in this report as the body-axis system. For any nominal flight condition, body-fixed axes can be chosen so that the x-axis is aligned with the velocity vector, and the z-axis is in the body-axis x-z plane. This set of body-fixed axes is referred to as the stability-axis system.

Since body axes are the only axes in which the vehicle rotational inertia matrix is constant, the rotational dynamics equations are usually (though not exclusively) expressed in this frame. The body frame also is the one in which the pilot, and all sensors and control surfaces are located; for this reason, the body frame is considered the basic frame of reference in this report. Figure A.2-1a illustrates the body frame orientation with respect to the inertial-axis system.

The velocity- and wind- axis systems have a common origin (the vehicle center of mass) and a common x-axis, which is oriented along the vehicle's inertial velocity vector. The velocity reference frame y-axis is parallel to the inertial x-y plane. This results in simple relations between inertial and velocity axes, so that these axes are useful for navigation and point-mass trajectory calculations. Figure A.2-1b illustrates the relationship between inertial and velocity axes.

The wind reference frame's z-axis is located in the x-z plane of the body frame; this reference frame is

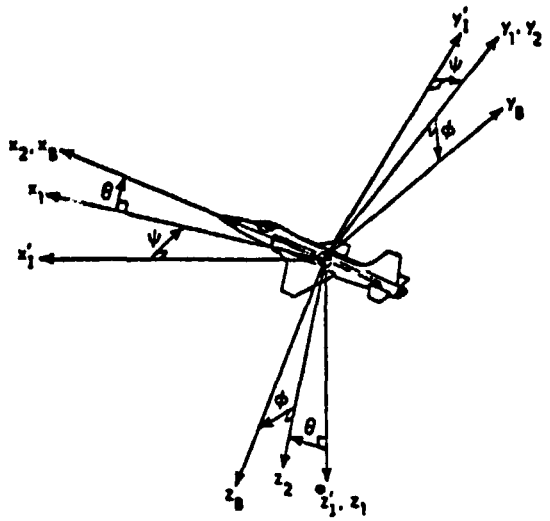

a) Inertial-Body Orientation

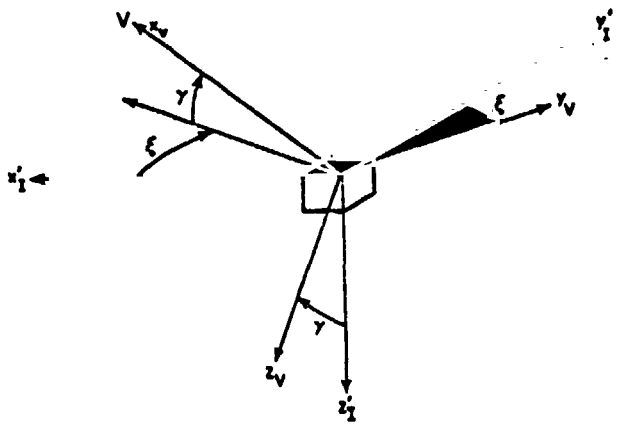

b) Inertial-Velocity Orientation

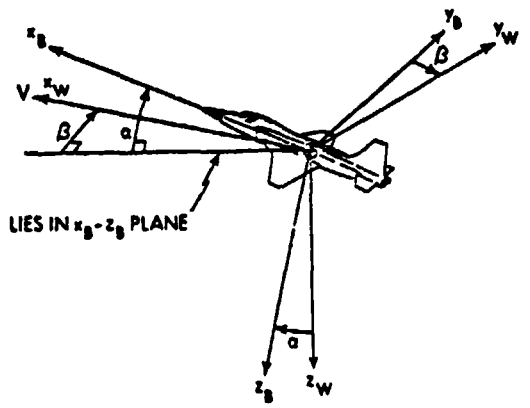

c) Wind-Body Orientation

Figure A.2-1 Reference Frame Relations

very useful in dynamic calculations because the orientation angles between the wind frame and body frame have large influences on the aerodynamic forces and moments. Figure A.2-1c illustrates the orientation between body and wind axes. Figure A.2-2 summarizes the transformations between reference frames. Any necessary transformation can be identfied from this figure, noting that the Euler angles are given in the order of yaw, pitch, and roll, as specified by the arrows. For example, a transformation from inertial to body axes is composed of a right-handed yaw through an angle, ψ, then a right-handed pitch through an angle, θ, and then a right-handed roll through an angle, ϕ. These three single-angle transformations can be combined to form an inertial-body transformation as follows:

$$H_I^B(\phi,\theta,\psi) = H_2^B(\phi)\ H_1^2(\theta)\ H_I^1(\psi)$$

$$= \begin{bmatrix} 1 & 0 & 0 \\ 0 & \cos\phi & \sin\phi \\ 0 & -\sin\phi & \cos\phi \end{bmatrix} \begin{bmatrix} \cos\theta & 0 & -\sin\theta \\ 0 & 1 & 0 \\ \sin\theta & 0 & \cos\theta \end{bmatrix} \begin{bmatrix} \cos\psi & \sin\psi & 0 \\ -\sin\psi & \cos\psi & 0 \\ 0 & 0 & 1 \end{bmatrix} \qquad \text{(A.2-1)}$$

For orthogonal matrices such as these, the matrix inverse, $(\ )^{-1}$, is equal to the transpose, $(\ )^T$.

In the remainder of Section A.2, the vehicle's equation of motion is derived as a single state-vector equation of the form,

$$\dot{\underline{x}} = \underline{f}(\underline{x},\underline{u}) \qquad \text{(A.2-2)}$$

where $\underline{x}$ is the state vector, $\underline{u}$ is the control vector, $\underline{f}$ is the vector system dynamics equation, and disturbances are neglected. The state vector is a 12-element vector, and the nonlinear state equations are readily derived as four

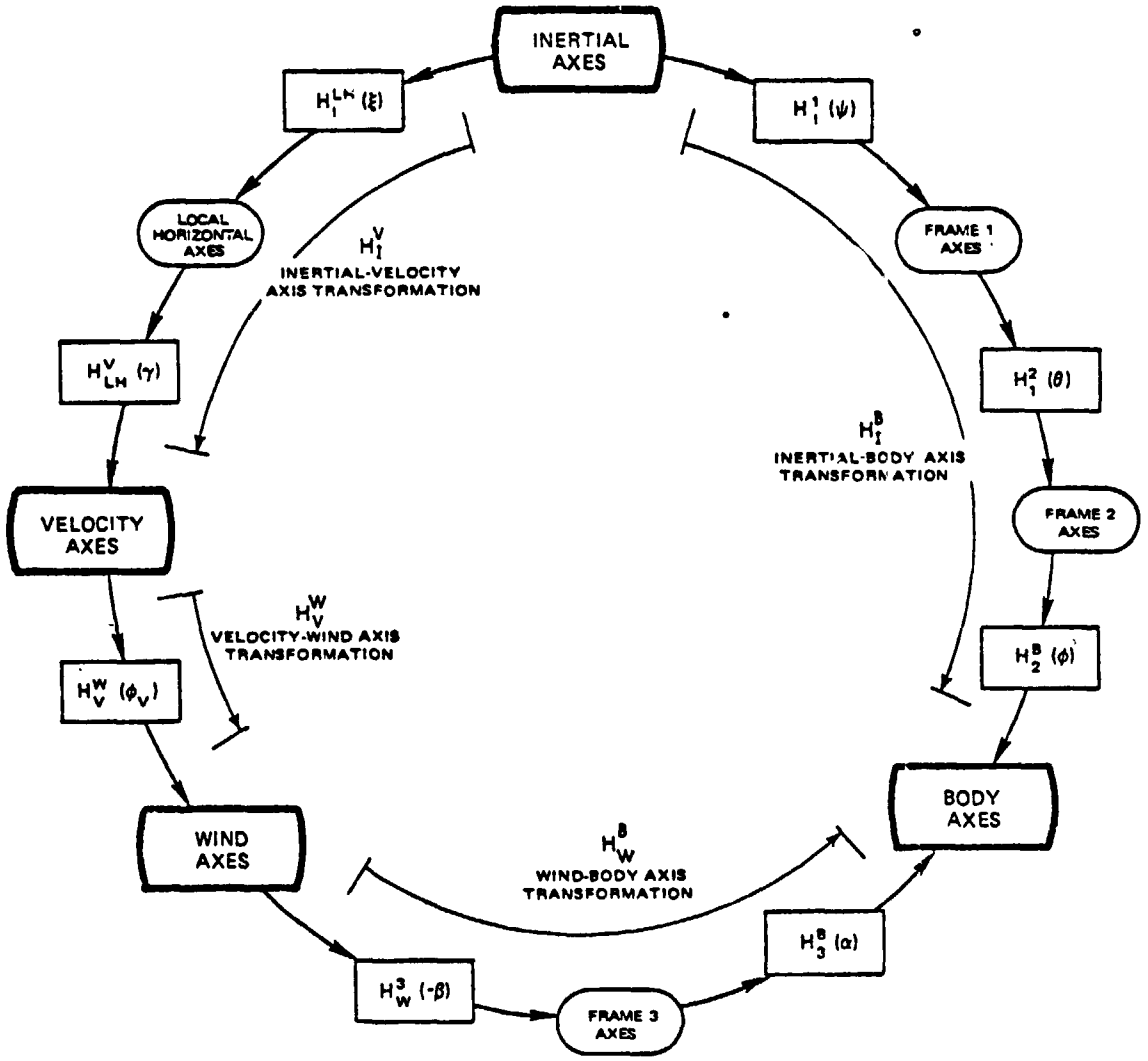

Figure A.2-2 Reference Axis Transformations (Arrows Indicate Right-Hand Rotation)

sets of three equations representing

- Translational Kinematics
- Rotational Kinematics
- Translational Dynamics
- Rotational Dynamics

The kinematic equations relate the vehicle's translational and rotational velocities to its position in inertial space, and they involve body-axis/inertial-axis relationships. The dynamic equations describe the changes of the vehicle velocities caused by the applied forces and moments; they are best derived in a body-fixed frame of reference.

A.2.1 Kinematics

Kinematics is the study of the motion of a body without regard to the forces which cause that motion. In this section, the relations between the vehicle's position and velocity are examined. The translational and angular position of the vehicle are given relative to inertial space by the inertial position vector, $\underline{x}_I$, and by the inertial-body Euler angle vector, $\underline{\nu}_B$:

$$\underline{x}_I = \begin{bmatrix} x_I \\ y_I \\ z_I \end{bmatrix} \tag{A.2-3}$$

$$\underline{\nu}_B = \begin{bmatrix} \phi \\ \theta \\ \psi \end{bmatrix} \tag{A.2-4}$$

It is important to note that the Euler angle "vector" is not a true vector in physical space; it is an ordered triple of right-handed rotations which occur about different axes of different reference frames.

The translational and angular rate vectors are often expressed in body axes, as in the following:

$$\underline{v}_B = \begin{bmatrix} u \\ v \\ w \end{bmatrix} \qquad (A.2\text{-}5)$$

$$\underline{\omega}_B^I = \begin{bmatrix} p \\ q \\ r \end{bmatrix} \qquad (A.2\text{-}6)$$

The body-axis translational rate vector, $\underline{v}_B$, is an expression, in body axes, of the derivative of the inertial position vector. This relationship supplies the first part of the nonlinear state equations of motion:

$$\dot{\underline{x}}_I = H_B^I \, \underline{v}_B \qquad (A.2\text{-}7)$$

where H_B^I is the inverse of the inertial-body transformation derived in Eq. (A.2-1).

The body angular rate vector also can be related to the derivative of the Euler angle vector by noting that the Euler angle derivatives occur in three different reference frames. The resulting transformation is constructed in Eq. (A.2-8), where the individual transformations are the same as those of Fig. A.2-2 and Eq. (A.2-1):

$$\underline{\omega}_B^I = \begin{bmatrix} \dot{\phi} \\ 0 \\ 0 \end{bmatrix} + H_2^B \begin{bmatrix} 0 \\ \dot{\theta} \\ 0 \end{bmatrix} + H_2^B H_1^2 \begin{bmatrix} 0 \\ 0 \\ \dot{\psi} \end{bmatrix}$$

$$= L_B \, \dot{\underline{v}}_B \qquad (A.2\text{-}8)$$

The non-orthogonal transformation, L_B, is

$$L_B = \begin{bmatrix} 1 & 0 & -\sin\theta \\ 0 & \cos\phi & \sin\phi\cos\theta \\ 0 & -\sin\phi & \cos\phi\cos\theta \end{bmatrix} \qquad (A.2\text{-}9)$$

The ordering of the transformations in Eq. (A.2-8) arises from the ordering of the Euler angles. As can be seen from Fig. A.2-1a, the angular rate, $\dot{\phi}$, occurs about the x_B axis, while the rate, $\dot{\theta}$, occurs about the y_2 axis, and $\dot{\psi}$ occurs about the z_1 axis. The inverse of Eq. (A.2-8) supplies the rotational kinematic part of the vehicle nonlinear state equations, and is given by:

$$\underline{\dot{\nu}}_B = L_B^{-1} \, \underline{\omega}_B^I \qquad \text{(A.2-10)}$$

The relations between translational position and velocity, Eq. (A.2-7), and between angular orientation and velocity, Eq. (A.2-10), comprise the kinematic portions of the nonlinear state equations.

A.2.2 Dynamics

The dynamics of the vehicle involve the interaction between the vehicle motion and the forces that produce that motion. This involves the application of Newton's Second Law, which equates the applied force to the time derivative of inertial translational momentum of a body. For rotational motion, this equivalence becomes one between torque and the derivative of angular momentum, measured in an inertial reference frame.

An expression for the inertial translational acceleration, expressed in body-axis variables, is needed. This can be derived from Eq. (A.2-7) by taking the derivative of both sides. It is important to note that the transformation matrix is time-varying. This result is

$$\underline{\ddot{x}}_I = H_B^I \underline{\dot{v}}_B + \dot{H}_B^I \underline{v}_B \qquad \text{(A.2-11)}$$

where

$$\dot{H}_B^I = H_B^I \tilde{\omega}_B^I \tag{A.2-12}$$

and $\tilde{\omega}_B^I$ is the cross-product equivalent matrix for $\underline{\omega}_B^I$ given by

$$\tilde{\omega}_B^I = \begin{bmatrix} 0 & -r & q \\ r & 0 & -p \\ -q & p & 0 \end{bmatrix} \tag{A.2-13}$$

This leads to the body-axis equation:

$$\dot{\underline{v}}_B = H_I^B \underline{g}_I - \tilde{\omega}_B^I \underline{v}_B \tag{A.2-14}$$

The applied specific forces consist of gravitational forces and aerodynamic forces. The gravity force is especially simple in inertial axes, as it is confined to the vertical axis:

$$\underline{g}_I = \begin{bmatrix} 0 \\ 0 \\ g \end{bmatrix} \tag{A.2-15}$$

The specific contact force can be broken into two components, one of which is due to aerodynamic forces and one of which is due to thrust:

$$\underline{F}_B/m = \begin{bmatrix} X/m \\ Y/m \\ Z/m \end{bmatrix} \tag{A.2-16}$$

$$\underline{T}_B/m = \begin{bmatrix} T_{B_x}/m \\ T_{B_y}/m \\ T_{B_z}/m \end{bmatrix} \qquad \text{(A.2-17)}$$

(Capital letters are conventionally used in aerodynamics to denote the force components.)

The translational dynamic equation is formed by equating the sum of the aerodynamic and gravitational specific forces to the inertial translational acceleration of the vehicle. When all vectors are expressed in body axes and the derivatives of the body-axis velocities are isolated on the left-hand side, the vector equation is

$$\dot{\underline{v}}_B = (\underline{F}_B + \underline{T}_B)/m + H_I^B \underline{g}_I - \tilde{\omega}_B^I \underline{v}_B \qquad \text{(A.2-18)}$$

To construct the rotational dynamic equation, an expression for the time derivative of angular momentum measured in inertial axes is necessary. The angular momentum, $\underline{h}_B$, is most easily expressed in body axes; neglecting rotating machinery, it is the product of the moment-of-inertia matrix (constant in body axes) and the angular rate vector,

$$\underline{h}_B = I_B \, \underline{\omega}_B^I \qquad \text{(A.2-19)}$$

where the inertia matrix contains all products and moments of inertia:

$$I_B = \begin{bmatrix} I_x & -I_{xy} & -I_{xz} \\ -I_{xy} & I_y & -I_{yz} \\ -I_{xz} & -I_{yz} & I_z \end{bmatrix} \qquad \text{(A.2-20)}$$

The time derivative of the angular momentum, expressed in inertial axes, is easily derived by noting that the transformation H_B^I is time-varying:

$$\dot{\underline{h}}_I = H_B^I I_B \dot{\underline{\omega}}_B^I + \dot{H}_B^I I_B \underline{\omega}_B^I$$

$$= H_B^I I_B \dot{\underline{\omega}}_B^I + H_B^I \tilde{\omega}_B^I I_B \underline{\omega}_B^I \qquad \text{(A.2-21)}$$

The contact moments consist of aerodynamic and thrust components. These are defined as

$$\underline{M}_B = \begin{bmatrix} L \\ M \\ N \end{bmatrix} \qquad \text{(A.2-22)}$$

$$\underline{G}_B = \begin{bmatrix} G_{B_x} \\ G_{B_y} \\ G_{B_z} \end{bmatrix} \qquad \text{(A.2-23)}$$

(Capital letters are conventionally used for the moment components.) The rotational dynamic equation can be formed by equating the applied torques to the derivative of the angular momentum. All vectors are expressed in body axes, and the derivative of body-axis angular rate is isolated on the left-hand side of the equation, resulting in

$$\dot{\underline{\omega}}_B^I = I_B^{-1}(\underline{M}_B + \underline{G}_B) - I_B^{-1} \tilde{\omega}_B^I I_B \underline{\omega}_B^I \qquad \text{(A.2-24)}$$

A.2.3 Summary of Equations

Section A.2 has presented the various reference frames of interest and has derived the equations of motion of an atmospheric vehicle. The 12-element state vector consists of three positions, three angular orientations, three

translational rates and three angular rates. The state equations were found by examining the translational and rotational kinematics and dynamics, and are repeated here:

$$\dot{\underline{x}}_I = H_B^I \, \underline{v}_B \tag{A.2-25}$$

$$\dot{\underline{v}}_B = L_B^{-1} \, \underline{\omega}_B^I \tag{A.2-26}$$

$$\dot{\underline{v}}_B = (\underline{F}_B + \underline{T}_B)/m + H_I^B \underline{g}_I - \tilde{\omega}_B^I \underline{v}_B \tag{A.2-27}$$

$$\dot{\underline{\omega}}_B^I = I_B^{-1}(\underline{M}_B + \underline{G}_B) - I_B^{-1} \tilde{\omega}_B^I I_B \underline{\omega}_B^I \tag{A.2-28}$$

These equations fall into the general state equation form,

$$\dot{\underline{x}} = \underline{f}(\underline{x},\underline{u}) \tag{A.2-29}$$

by defining the state vector as

$$\underline{x}^T = \left[\underline{x}_I^T \; \underline{v}_B^T \; \underline{v}_B^T \; \underline{\omega}_B^{I\,T} \right] \tag{A.2-30}$$

and noting that the aerodynamic forces and moments are functions of the states, controls, disturbances and, to some extent, the state time history. These nonlinear state equations are useful because they are general enough to allow a thorough analysis of the departure prevention problem. They are expressed in state-space form, which is notationally efficient and which makes the subsequent linearization an easily followed process.

A.3 LINEAR EQUATIONS OF MOTION

While the nonlinear equations derived in the previous section can be solved on a digital computer, they are

not easily analyzed by general techniques, and general closed-form solutions cannot be obtained. Many of the important dynamic attributes of the aircraft can be preserved and the analysis facilitated by developing corresponding linearized equations of motion, as is done in Refs. 64 to 67.

A.3.1 Derivation from Nonlinear Equations

The linearization procedure begins with the construction of a Taylor series expansion representing the nonlinear equations about some nominal trajectory:

$$\dot{\underline{x}} = \dot{\underline{x}}_0 + \Delta\dot{\underline{x}} = \underline{f}(\underline{x}_0, \underline{u}_0) + \left.\frac{\partial \underline{f}}{\partial \underline{x}}\right|_{\substack{\underline{x}=\underline{x}_0 \\ \underline{u}=\underline{u}_0}} \Delta\underline{x} + \left.\frac{\partial \underline{f}}{\partial \underline{u}}\right|_{\substack{\underline{x}=\underline{x}_0 \\ \underline{u}=\underline{u}_0}} \Delta\underline{u} + \text{Higher Order Terms} \tag{A.3-1}$$

where the subscript "0" indicates the nominal value and the prefix "Δ" denotes a small perturbation. All except first-order terms are then neglected by arguing that the higher-order terms are small compared to linear terms. The results of this procedure are separated into a nonlinear equation describing the nominal trajectory (Eq. (A.3-2)) and a linear equation defining the dynamics of the perturbations about the nominal trajectory (Eq. (A.3-3)):

$$\dot{\underline{x}}_0 = \underline{f}(\underline{x}_0, \underline{u}_0) \tag{A.3-2}$$

$$\Delta\dot{\underline{x}} = F\,\Delta\underline{x} + G\,\Delta\underline{u} \tag{A.3-3}$$

where

$$F = \left.\frac{\partial \underline{f}}{\partial \underline{x}}\right|_{\substack{\underline{x}=\underline{x}_0 \\ \underline{u}=\underline{u}_0}} \tag{A.3-4}$$

and

$$G = \left.\frac{\partial \underline{f}}{\partial \underline{u}}\right|_{\substack{\underline{x}=\underline{x}_0 \\ \underline{u}=\underline{u}_0}} \tag{A.3-5}$$

The linearization is straightforward because the nonlinear state equations (Eq. (A.2-25) to A.2-28)) are specified in a general state-space format. Equations for the perturbations of the axis transformations are easily derived by taking the partial derivatives of each transformation with respect to the Euler angles of that transformation and multiplying by the Euler angle perturbations. For the inertial-body transformation and its inverse, these transformation perturbations can be stated as follows:

$$\Delta H_I^B = -\Delta\tilde{\mu}_B \, H_{I_0}^B \tag{A.3-6}$$

where the cross-product operator ($\tilde{}$) is employed,

$$\Delta\underline{\mu}_B = L_{B_0} \, \Delta\underline{\nu}_B \tag{A.3-7}$$

and

$$\Delta H_B^I = H_{B_0}^I \, \Delta\tilde{\mu}_B \tag{A.3-8}$$

These relationships for the transformation perturbations are used to linearize the translational kinematic

equation, Eq. (A.2-25), to give

$$\Delta\dot{\underline{x}}_I = -(\widetilde{\dot{x}_{I_0}})\, H^I_{B_0}\, L_{B_0}\, \Delta\underline{\nu}_B + H^I_{B_0}\, \Delta\underline{v}_B \qquad \text{(A.3-9)}$$

This equation clearly shows that the perturbation inertial velocity depends both on the perturbation body-axis velocity and the inertial-body Euler angle perturbations.

The rotational kinematic equation, Eq. (A.2-26), results in the following linear perturbation equation:

$$\Delta\dot{\underline{\nu}}_B = -\, L^{-1}_{B_0}\, L'_{B_0}\, \Delta\underline{\nu}_B + L^{-1}_{B_0}\, \Delta\underline{\omega}^I_B \qquad \text{(A.3-10)}$$

where

$$L'_{B_0} = \left.\frac{\partial(L_B\, \dot{\underline{\nu}}_B)}{\partial \underline{\nu}_B}\right|_{\underline{\nu}_B = \underline{\nu}_{B_0}} \qquad \text{(A.3-11)}$$

so that

$$-L^{-1}_{B_0}\, L'_{B_0} = \begin{bmatrix} \dot{\theta}_0 \tan\theta_0 & \dot{\psi}_0 \sec\theta_0 & 0 \\ -\dot{\psi}_0 \cos\theta_0 & 0 & 0 \\ \dot{\theta}_0 \sec\theta_0 & \dot{\psi}_0 \tan\theta_0 & 0 \end{bmatrix} \qquad \text{(A.3-12)}$$

The definition of L'_{B_0} takes the form it does because the linear rotational kinematic equation was derived from the original form of the rotational kinematics equation, given in Eq. (A.2-8).

Linearization of the dynamic equations requires consideration of the aerodynamic force and moment relationships. These are functions of the states, controls, and the past history of these variables. This dependence on

past values is caused by aerodynamic flow field effects and their propagation delays; unsteady aerodynamic effects can be represented as functions of the state rates. The formal linearization of the aerodynamic forces and moments is a lengthy but straightforward process which amounts to taking the partial derivatives of every aerodynamic force and moment vector with respect to the states, state rates, and controls. These partial derivatives are called stability derivatives.

The difficulty revolves around the actual values to be used for each of these coefficients. This data is produced primarily by wind tunnel testing, as described, for example, in Refs. 68 and 69. There is a large amount of effort and expense involved in generating this data, so only the most important functional relationships can be examined. This often results in different data sets for each aircraft. For this reason, only general terms for the perturbation forces and moments are included in the following discussion. Appendix B contains a discussion and example of the construction of force and moment stability derivative matrices from real data. Many stability derivative matrices are either known to be zero or are so small as to be neglected in all cases of interest. Assuming that altitude and orientation variations have negligible effect on contact force and moment variations, and assuming insignificant state derivative and angular rate effects on thrust forces and moments, the perturbation aerodynamic forces and moments are as follows:

$$\Delta \underline{F}_B = \left[\frac{\partial \underline{F}_B}{\partial \underline{v}_B}\right] \Delta \underline{v}_B + \left[\frac{\partial \underline{F}_B}{\partial \underline{\omega}_B^I}\right] \Delta \underline{\omega}_B^I + \left[\frac{\partial \underline{F}_B}{\partial \underline{u}}\right] \Delta \underline{u} + \left[\frac{\partial \underline{F}_B}{\partial \dot{\underline{v}}_B}\right] \Delta \dot{\underline{v}}_B + \left[\frac{\partial \underline{F}_B}{\partial \dot{\underline{\omega}}_B^I}\right] \Delta \dot{\underline{\omega}}_B^I \qquad \text{(A.3-13)}$$

$$\Delta \underline{M}_B = \left[\frac{\partial \underline{M}_B}{\partial \underline{v}_B}\right] \Delta \underline{v}_B + \left[\frac{\partial \underline{M}_B}{\partial \underline{\omega}_B^I}\right] \Delta \underline{\omega}_B^I + \left[\frac{\partial \underline{M}_B}{\partial \underline{u}}\right] \Delta \underline{u} + \left[\frac{\partial \underline{M}_B}{\partial \dot{\underline{v}}_B}\right] \Delta \dot{\underline{v}}_B + \left[\frac{\partial \underline{M}_B}{\partial \dot{\underline{\omega}}_B^I}\right] \Delta \dot{\underline{\omega}}_B^I \tag{A.3-14}$$

$$\Delta \underline{T}_B = \left[\frac{\partial \underline{T}_B}{\partial \underline{v}_B}\right] \Delta \underline{v}_B + \left[\frac{\partial \underline{T}_B}{\partial \underline{u}}\right] \Delta \underline{u} \tag{A.3-15}$$

$$\Delta \underline{G}_B = \left[\frac{\partial \underline{G}_B}{\partial \underline{v}_B}\right] \Delta \underline{v}_B + \left[\frac{\partial \underline{G}_B}{\partial \underline{u}}\right] \Delta \underline{u} \tag{A.3-16}$$

The linear translational dynamic equation is derived from Eq. (A.2-27) and incorporates the perturbation aerodynamic force expressions presented above. Note that the state-rate stability derivative matrices enter the equation in a different manner than the other terms; they must be moved to the left-hand side of the dynamic equations. The linear translational dynamic equation becomes

$$\left\{I - \frac{1}{m}\left[\frac{\partial \underline{F}_B}{\partial \dot{\underline{v}}_B}\right]\right\} \Delta \dot{\underline{v}}_B + \left\{-\frac{1}{m}\left[\frac{\partial \underline{F}_B}{\partial \dot{\underline{\omega}}_B^I}\right]\right\} \Delta \dot{\underline{\omega}}_B^I = \tilde{g}_{B_0} L_{B_0} \Delta \underline{v}_B$$

$$+ \left\{\frac{1}{m}\left[\frac{\partial \underline{F}_B}{\partial \underline{v}_B}\right] + \frac{1}{m}\left[\frac{\partial \underline{T}_B}{\partial \underline{v}_B}\right] - \tilde{\omega}_{B_0}^I\right\} \Delta \underline{v}_B$$

$$+ \left\{\frac{1}{m}\left[\frac{\partial \underline{F}_B}{\partial \underline{\omega}_B^I}\right] + \tilde{v}_{B_0}\right\} \Delta \underline{\omega}_B^I$$

$$+ \left\{\frac{1}{m}\left[\frac{\partial \underline{F}_B}{\partial \underline{u}}\right] + \frac{1}{m}\left[\frac{\partial \underline{T}_B}{\partial \underline{u}}\right]\right\} \Delta \underline{u} \tag{A.3-17}$$

The linear rotational dynamic equation is derived similarly, and the state-rate stability derivatives appear in the same way. The linear rotational dynamic equation is

$$\left\{-I_B^{-1}\left[\frac{\partial \underline{M}_B}{\partial \dot{\underline{v}}_B}\right]\right\}\Delta\dot{\underline{v}}_B+\left\{I-I_B^{-1}\left[\frac{\partial \underline{M}_B}{\partial \dot{\underline{\omega}}_B^I}\right]\right\}\Delta\dot{\underline{\omega}}_B^I=I_B^{-1}\left\{\left[\frac{\partial \underline{M}_B}{\partial \underline{v}_B}\right]+\left[\frac{\partial \underline{G}_B}{\partial \underline{v}_B}\right]\right\}\Delta\underline{v}_B$$
$$+I_B^{-1}\left\{\left[\frac{\partial \underline{M}_B}{\partial \underline{\omega}_B^I}\right]+\widetilde{I_B\underline{\omega}_{B_0}^I}-\tilde{\omega}_{B_0}^I I_B\right\}\Delta\underline{\omega}_B^I$$
$$+I_B^{-1}\left\{\left[\frac{\partial \underline{M}_B}{\partial \underline{u}}\right]+\left[\frac{\partial \underline{G}_B}{\partial \underline{u}}\right]\right\}\Delta\underline{u} \qquad \text{(A.3-18)}$$

The four state equations (translational and rotational kinematic and dynamic equations) can be written in standard linear equation form (Eq. (A.3-3)) by using the following state vector:

$$\Delta\underline{x}^T=\left[\Delta\underline{x}_I^T\ \Delta\underline{\nu}_B^T\ \Delta\underline{v}_B^T\ \Delta\underline{\omega}_B^{I^T}\right] \qquad \text{(A.3-19)}$$

The state equations then fall into the form:

$$J_B\Delta\dot{\underline{x}}_B=F_B'\,\Delta\underline{x}_B+G_B'\,\Delta\underline{u} \qquad \text{(A.3-20)}$$

where the state-rate transformation matrix is

$$J_B=\begin{bmatrix} I & 0 & 0 & 0 \\ 0 & I & 0 & 0 \\ 0 & 0 & J_{33} & J_{34} \\ 0 & 0 & J_{43} & J_{44} \end{bmatrix} \qquad \text{(A.3-21)}$$

and the three-by-three sub-matrices are

$$J_{33} = I - \frac{1}{m}\left[\frac{\partial \underline{F}_B}{\partial \dot{\underline{V}}_B}\right] \tag{A.3-22}$$

$$J_{34} = -\frac{1}{m}\left[\frac{\partial \underline{F}_B}{\partial \dot{\underline{\omega}}^I_B}\right] \tag{A.3-23}$$

$$J_{43} = -I_B^{-1}\left[\frac{\partial \underline{M}_B}{\partial \dot{\underline{V}}_B}\right] \tag{A.3-24}$$

$$J_{44} = I - I_B^{-1}\left[\frac{\partial \underline{M}_B}{\partial \dot{\underline{\omega}}^I_B}\right] \tag{A.3-25}$$

The primed state dynamics matrix is

$$F'_B = \begin{bmatrix} 0 & F_{12} & F_{13} & 0 \\ 0 & F_{22} & 0 & F_{24} \\ 0 & F_{32} & F_{33} & F_{34} \\ 0 & 0 & F_{43} & F_{44} \end{bmatrix} \tag{A.3-26}$$

where the three-by-three sub-matrices are

$$F_{12} = -\tilde{\dot{x}}_{I_0} H^I_{B_0} L_{B_0} \tag{A.3-27}$$

$$F_{13} = H^I_{B_0} \tag{A.3-28}$$

$$F_{22} = -L^{-1}_{B_0} L'_{B_0} \tag{A.3-29}$$

$$F_{24} = L^{-1}_{B_0} \tag{A.3-30}$$

$$F_{32} = H^{B}_{I_0} \tilde{g}_I H^{I}_{B_0} L_{B_0} \tag{A.3-31}$$

$$F_{33} = \left\{ \frac{1}{m} \left[\frac{\partial \underline{F}_B}{\partial \underline{v}_B} \right] + \frac{1}{m} \left[\frac{\partial \underline{T}_B}{\partial \underline{v}_B} \right] - \tilde{\omega}^{I}_{B_0} \right\} \tag{A.3-32}$$

$$F_{34} = \left\{ \frac{1}{m} \left[\frac{\partial \underline{F}_B}{\partial \underline{\omega}^{I}_B} \right] + \tilde{v}_{B_0} \right\} \tag{A.3-33}$$

$$F_{43} = I_B^{-1} \left\{ \left[\frac{\partial \underline{M}_B}{\partial \underline{v}_B} \right] + \left[\frac{\partial \underline{G}_B}{\partial \underline{v}_B} \right] \right\} \tag{A.3-34}$$

$$F_{44} = I_B^{-1} \left\{ \left[\frac{\partial \underline{M}_B}{\partial \underline{\omega}^{I}_B} \right] + \widetilde{I_B \underline{\omega}^{I}_{B_0}} - \tilde{\omega}^{I}_{B_0} I_B \right\} \tag{A.3-35}$$

and

$$G'_B = \begin{bmatrix} 0 \\ 0 \\ G_3 \\ G_4 \end{bmatrix} \tag{A.3-36}$$

The sub-matrices (of three rows and as many columns as controls) are

$$G_3 = \left\{ \frac{1}{m} \left[\frac{\partial \underline{F}_B}{\partial \underline{u}} \right] + \frac{1}{m} \left[\frac{\partial \underline{T}_B}{\partial \underline{u}} \right] \right\} \tag{A.3-37}$$

$$G_4 = \left\{ I_B^{-1} \left[\frac{\partial \underline{M}_B}{\partial \underline{u}} \right] + I_B^{-1} \left[\frac{\partial \underline{G}_B}{\partial \underline{u}} \right] \right\} \tag{A.3-38}$$

The complete state equation is produced by pre-multiplying Eq. (A.3-20) by the inverse of the state-rate

transformation matrix, giving the following result:

$$\Delta\dot{\underline{x}}_B = J_B^{-1} F_B' \, \Delta\underline{x}_B + J_B^{-1} G_B' \, \Delta\underline{u}$$

$$= F_B \, \Delta\underline{x}_B + G_B \, \Delta\underline{u} \qquad \text{(A.3-39)}$$

This resulting linear system is analyzed throughout this report. It is important to note that this system specifies the state and control perturbations about their nominal values. Methods of properly choosing these nominal values are examined next.

A.3.2 Generalized Trim Conditions

An aircraft is in the trimmed condition when its controls are set to produce equilibrium in the equations of motion. Steady trim occurs when the aircraft is under no inertial acceleration, i.e., when translational velocities are constant and rotational rates are zero. The trim concept can be extended to dynamic flight conditions by defining generalized trim as the condition in which control settings produce constant velocities and angular rates. In this case, the vehicle is not necessarily in steady equilibrium, due to changing roll and pitch angles.

The importance of these trim classifications lies in the use of trimmed flight conditions as nominal trajectories for linearization, since trim implies that the nominal velocities, angular rates, and controls are constant, or, at most, slowly varying. Thus, the use of the trimmed condition as a nominal flight condition causes the linear equations to represent almost all of the system dynamics at that flight condition. This can be seen by writing the general equations for the total state rate:

$$\dot{\underline{v}}_B = \dot{\underline{v}}_{B_0} + \Delta\dot{\underline{v}}_B \qquad \text{(A.3-40)}$$

$$\dot{\underline{\omega}}^I_B = \dot{\underline{\omega}}^I_{B_0} + \Delta\dot{\underline{\omega}}^I_B \qquad \text{(A.3-41)}$$

If a set of nominal states and controls can be found so that the generalized trim condition

$$\dot{\underline{v}}_{B_0} = \dot{\underline{\omega}}^I_{B_0} = 0 \qquad \text{(A.3-42)}$$

is satisfied, then the perturbation state rates are <u>equal</u> to the total state rates. This can be seen by inserting Eq. (A.3-42) into Eqs. (A.3-40) and (A.3-41).

Another desirable characteristic of using the trimmed flight condition as a nominal for linearization is that the total state and control trajectories over a significant interval of time are the sums of the <u>constant</u> nominal values and the linear perturbation time histories. This relation is given as:

$$\underline{v}_B(t) \cong \underline{v}_{B_0} + \Delta\underline{v}_B(t) \qquad \text{(A.3-43)}$$

$$\underline{\omega}^I_B(t) \cong \underline{\omega}^I_{B_0} + \Delta\underline{\omega}^I_B(t) \qquad \text{(A.3-44)}$$

$$\underline{u}(t) \cong \underline{u}_0 + \Delta\underline{u}(t) \qquad \text{(A.3-45)}$$

where $\underline{v}_{B_0}$, $\underline{\omega}^I_{B_0}$ and $\underline{u}_0$ are <u>constant</u>.

A solution method for the generalized trim problem can be derived by examining general forms of the nonlinear translational and rotational dynamic equations, which are derived in Section A.2.2 as

$$\dot{\underline{v}}_B = \underline{f}_1(\underline{\nu}_B, \underline{v}_B, \underline{\omega}_B^I, \underline{u}) \qquad \text{(A.3-46)}$$

$$\dot{\underline{\omega}}_B^I = \underline{f}_2(\underline{v}_B, \underline{\omega}_B^I, \underline{u}) \qquad \text{(A.3-47)}$$

The aerodynamic forces and moments are assumed to be functions of $\underline{v}_B$, $\underline{\omega}_B^I$, and $\underline{u}$. One element of the Euler angle vector, ψ, does not appear in the equations, and altitude is a parameter.

Two different generalized trim problems then become possible, the first of which is the following:

- Find the values of velocity and angular rate ($\underline{v}_B$ and $\underline{\omega}_B^I$) that produce generalized trim ($\dot{\underline{v}}_B = \dot{\underline{\omega}}_B^I = 0$) for given controls and Euler angles ($\underline{u}$, $\underline{\nu}_B$).

This problem consists of six equations (the dynamic equations) in six unknowns (the velocity and angular rates), and therefore it can be expected to have a solution. The controls and Euler angles are the set points that determine the generalized trim solution, and it should be noted that altitude also has an effect on the solution.

The second generalized trim problem can provide the trim controls that produce specific state values:

- Find the values of the controls and Euler angles ($\underline{u}$ and $\underline{\nu}_B$) that satisfy the generalized trim conditions ($\dot{\underline{v}}_B = \dot{\underline{\omega}}_B^I = 0$) for given values of the velocity and angular rate vectors ($\underline{v}_B$ and $\underline{\omega}_B^I$).

The existence of a solution to the second problem depends on the degrees of freedom and power of the controls. Many aerodynamic vehicles have a four-element control vector; along with the Euler angles, ϕ and θ, this results in a problem of six equations (the dynamic equations) in six unknowns (throttle, elevator, aileron, rudder, pitch angle, and roll angle).

One approach for solving either of these generalized trim problems is to use functional minimization. This approach, also called parametric optimization, requires all elements of $\underline{u}$ and $\underline{v}_B$ (or of $\underline{v}_B$ and $\underline{\omega}_B^I$) to be specified as given or desired, but it is not tied to any particular flight path. In this case, Eqs. (A.3-46) and (A.3-47) are solved directly using an iterative process, e.g., a steepest-descent, accelerated gradient algorithm, or direct numerical search (Ref. 70). A scalar cost function, J, measures trim error; a quadratic form is appropriate for computing a norm of the vector error:

$$J = \dot{\underline{v}}_B^T Q_1 \dot{\underline{v}}_B + \dot{\underline{\omega}}_B^{I\,T} Q_2 \dot{\underline{\omega}}_B^I$$

In both generalized trim problems, the trim value is determined when J reaches a minimum.

A.3.3 Body-Axis Equations

It is advantageous to express the vehicle state equations in body-fixed axes. These are the axes in which the pilot, the sensors, and the control surfaces are located. Body axes are the only axes in which the moment-of-inertia matrix is constant. Aerodynamic data collected from sting-mounted wind tunnel models or from flight test usually is

expressed in body axes. Consequently, body axes are considered to be the basic axes in this report, and all of the equations given so far have been in body axes.

A.3.4 Stability-Axis Equations

Stability axes also are body-fixed axes, so that they retain the convenient characteristics mentioned above. The axes are fixed in the body so that the x-axis is aligned with the nominal velocity vector. Although the axes are fixed in the body, they have different orientations at different nominal flight conditions. Further, the perturbation velocity vector is not expressed as three orthogonal velocity perturbations but as a velocity magnitude perturbation and two body-velocity orientation angles: perturbation angles of attack ($\Delta\alpha$) and sideslip ($\Delta\beta$). This vector is referred to here as $\Delta\underline{v}_W$. It is important to note that stability axes are also the same as wind axes for a specific nominal flight condition: $\dot{\alpha}_o=\dot{\beta}_o=0$. This is the justification for using a "W" subscript throughout this report for stability axis variables.

Stability axes simplify certain aspects of the linear equations. In level nominal flight, stability x- and y-axes are horizontal and the z-axis is vertical. The lift and drag forces act along stability axes. Finally, it often is true that stability axes are close to the normal mode axes. This means that the basic modes of motion appear as motion about or along a single axis of the stability reference frame. The frequency and damping of the basic modes then become simple functions of the aerodynamic stability derivatives expressed along stability axes; therefore aerodynamic stability derivatives expressed in the stability-axis frame can be used as approximate indications of stability or instability. For example, assuming that

body axes coincide with principal axes, the stability-axis rotational dynamic equations appear in part as:

$$\Delta\dot{p}_W = \frac{1}{2}\rho V_0^2 Sb \frac{1}{I_x}\left[\cos\alpha_0 C_{l_\beta} + \frac{I_x}{I_z}\sin\alpha_0 C_{n_\beta}\right]\Delta\beta + \ldots \qquad \text{(A.3-49)}$$

$$\Delta\dot{r}_W = \frac{1}{2}\rho V_0^2 Sb \frac{1}{I_z}\left[\cos\alpha_0 C_{n_\beta} - \frac{I_z}{I_x}\sin\alpha_0 C_{l_\beta}\right]\Delta\beta + \ldots \qquad \text{(A.3-50)}$$

where Appendix B details the definition of the individual symbols. The departure parameter $C_{n_{\beta,dyn}}$ (Section 2.2) is recognized as an element in the yaw equation. This is significant because these equations are derived by a simplification of the complete equations, and it is possible that other useful departure parameters can be derived from the same approach.

Since stability axes are body-fixed axes with a particular nominal orientation, it is convenient to derive the linear equations in body axes and simply rotate them to obtain a stability-axis set. This can be done by applying the transformation matrix, K_B, to the body-axis system matrices, F_B and G_B, as follows:

$$F_W = K_{BW}^{-1} F_B K_{BW} \qquad \text{(A.2-51)}$$

$$G_W = K_{BW}^{-1} G_B \qquad \text{(A.3-52)}$$

where

$$K_{BW} = \begin{bmatrix} I & 0 & 0 & 0 \\ 0 & I & 0 & 0 \\ 0 & 0 & H^B_{W_0} J_{W_0} & 0 \\ 0 & 0 & H^I_{B_0} L_{W_0} & H^B_{W_0} \end{bmatrix} \qquad \text{(A.3-53)}$$

and, from Fig. 2.2-2, the wind-body transformation is

$$H^{B}_{W_0} = \begin{bmatrix} \cos\alpha_0 \cos\beta_0 & -\cos\alpha_0 \sin\beta_0 & -\sin\alpha_0 \\ \sin\beta_0 & \cos\beta_0 & 0 \\ \sin\alpha_0 \cos\beta_0 & -\sin\alpha_0 \sin\beta_0 & \cos\alpha_0 \end{bmatrix} \qquad \text{(A.3-54)}$$

while

$$L_{W_0} = \begin{bmatrix} 0 & \sin\alpha_0 & 0 \\ 0 & 0 & 1 \\ 0 & -\cos\alpha_0 & 0 \end{bmatrix} \qquad \text{(A.3-55)}$$

and J_{W_0} is a diagonal matrix whose elements are $[1, V_0, V_0\cos\beta_0]$. These relations (which assume $\alpha_0=\beta_0=0$) are used to transform body-axis equations to stability-axis equations for further analysis.

A.3.5 State Ordering and Dimension

The order of the states given by Eq. (A.2-30) is the one that proceeds from considering translation before rotation and kinematics before dynamics. This order does not, however, group related states together. For example, many aircraft demonstrate a natural mode that is primarily composed of Δu and $\Delta\theta$ oscillations (the phugoid mode), and it is logical to regroup the states so that Δu and $\Delta\theta$ fall next to each other.

For some reference flight conditions, a further major division between longitudinal and lateral-directional variables can be made. The former variables describe motion within the vehicle plane of symmetry, while the lateral-directional variables describe motion out of the plane of symmetry. This division is useful because it allows a quick appraisal of the extent and nature of cross couplings that arise in maneuvering flight.

With this condition in mind, the ordering of states given in Table A.3-1 is suggested for aircraft and similar vehicles. The six longitudinal states are first, followed by the six lateral-directional states.

TABLE A.3-1
STATE ORDERING

Body Axes	Stability Axes
Δx_I	Δx_I
Δz_I	Δz_I
$\Delta\theta$	$\Delta\theta$
Δu	ΔV
Δq	Δq_W
Δw	$\Delta\alpha$
Δv	$\Delta\beta$
Δr	Δr_W
Δp	Δp_W
$\Delta\phi$	$\Delta\phi$
$\Delta\psi$	$\Delta\psi$
Δy_I	Δy_I

In any reduced-order approximation, this state ordering also is useful. The four "outermost" states, for example, do not affect the inner eight, but are merely integral functions of them. Thus, Δx_I, Δz_I, Δy_I and $\Delta\psi$ can be removed without changing the basic modes of motion of the vehicle. The first two of the remaining eight states are the primary states involved in the phugoid mode, while the next two represent the primary short period longitudinal mode. The four lateral-directional states often exhibit a Dutch roll oscillatory mode and roll and spiral convergence modes. Except in special cases, each of these modes involves most of the lateral-directional states.

The formation of models of order less than eight depends on an examination of the individual problem. For example, when there is no coupling between lateral-directional and longitudinal modes, the eighth-order model can be split into two independent fourth-order models with no loss of accuracy. If the time-span of interest is short, it may be possible to neglect the slower modes (phugoid mode and spiral convergence) without decreasing the accuracy of the results; however, as the eigenvectors of earlier chapters show, one runs the risk of missing significant coupling effects when "inner eight" states are eliminated.

A different order reduction suggests itself when the generalized trim problem is examined. As discussed in Section A.3.2, the goal of the generalized trim procedure is to find a nominal flight condition with constant velocity and angular rates. Because they do not affect the velocity and angular rate states, x_I, y_I, z_I and ψ are dropped immediately. To completely control the six desired states, six controls are necessary, but most atmospheric flight vehicles have less than six control effectors. Noting that the two Euler angles, θ and ϕ, are involved primarily in the slow modes, these two states may be regarded as parameters. This results in a problem of four controls (throttle, elevator, aileron, rudder), two parameters (θ, ϕ), six states (u,v,w,p,q,r), and six state equations ($\dot{u}$,$\dot{v}$,$\dot{w}$,$\dot{p}$,$\dot{q}$,$\dot{r}$) to define trim.

A.4 TOOLS FOR LINEAR ANALYSIS OF AIRCRAFT STABILITY AND CONTROL

The previous sections of this chapter have developed the linear aircraft model and demonstrated its validity along highly dynamic trajectories. The use of a linear model is desirable because the large body of theory and experience relating to the analysis and control of linear systems then can be applied to the departure prevention problem. These tools are discussed in this section.

A.4.1 Eigenvalues, Eigenvectors, and Normal Modes

The initial-condition response of a linear-time-invariant system is composed of a linear combination of a limited number of natural, or normal modes. Each normal mode is characterized by its time scale, given by the eigenvalue of that mode, and the relative involvement of each state in that mode, indicated by the eigenvector of that mode. In physically realizable systems, the modes are described either by individual real eigenvalues or by pairs of complex eigenvalues. A first-order mode exhibits either an exponentially increasing response (positive eigenvalue) or an exponentially decreasing response (negative eigenvalue). A complex (second-order) mode oscillates at a frequency determined by the imaginary part of the eigenvalue within an exponential envelope determined by the real part of the eigenvalue. Therefore, the oscillation can diverge, converge, or maintain constant amplitude.

As an example of the eigenvalues involved in the normal modes of fighter aircraft, Fig. A.4-1 illustrates the areas in the complex plane which contain the five modes and eight basic eigenvalues of a small high-performance

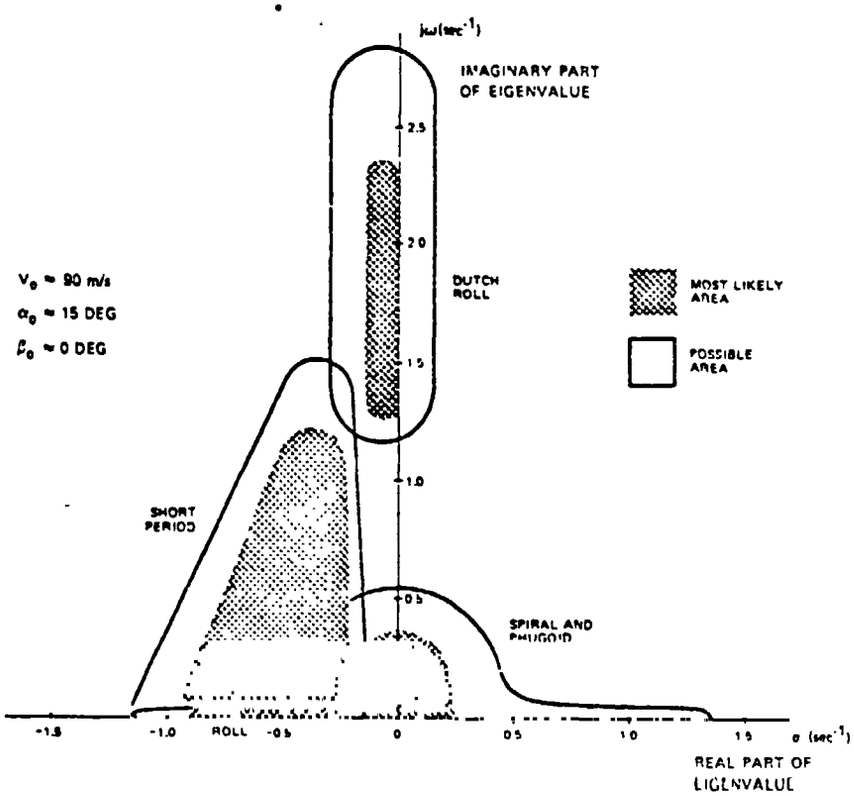

Figure A.4-1 Approximate Root Locations of a High-Performance Aircraft

aircraft. Because complex eigenvalues occur in pairs of complex conjugates, the lower half of the complex plane is symmetric with the upper half and is not shown.

The eigenvectors indicate the relative involvement of the aircraft states in a given mode. Each of the modes shown in Fig. A.4-1 may involve the motion of every state, but the following generalizations can be made for straight-and-level flight. The longitudinal states ($\Delta\theta$, Δu, Δq, Δw) exhibit two second-order modes. The phugoid mode is a slow, lightly damped interchange of kinetic energy (speed) and potential energy (altitude) and primarily involves $\Delta\theta$ and Δu. The short period mode is the rapid, well-damped angular oscillation, and is exhibited primarily by Δq and Δw.

The lateral-directional modes usually consist of a second-order and two first-order modes. The former is called the Dutch roll mode and is a fast, poorly damped yaw oscillation about the stability z-axis. The roll convergence mode is a fast, stable mode, and it represents the aircraft response (generally about the stability x-axis) to a roll moment. Due to the angle between body and stability axes, the Dutch roll mode and the roll convergence modes appear in the three states Δv, Δr, and Δp. The spiral mode is slow and frequently unstable. An unstable spiral mode is important in a piloted aircraft only if the time constant is so short that the pilot has difficulty keeping the wings level.

These mode shapes change considerably as the flight condition varies from straight-and-level flight. Asymmetric flight conditions result in coupled longitudinal/lateral-directional modes, and angular rates cause large changes in the eigenvalues. In certain cases, modes combine: the roll and spiral modes can form a roll-spiral oscillation, for example.

The eigenvalues of the outer four states (Δx_I, Δy_I, and $\Delta\psi$) are zero, i.e., these states have no effect on the other variables and are pure integrations of the other state variables. As a consequence, control-loop closures have no direct effect on these modes unless the outer variables are fed back directly.

The eigenvalues are the roots of the characteristic equation of the system dynamics matrix, F,

$$|\lambda I - F| = 0 \qquad \text{(A.4-1)}$$

where I is the identity matrix of the same order as the system matrix, and λ is a scalar which must equal an eigenvalue for Eq. (A.4-1) to be satisfied.

As shown in Ref. 71, there is a set of vectors associated with the eigenvalues which have special properties. The eigenvectors, $\underline{z}_i$, are linear combinations of the elements of the state vector and are solutions to the equations

$$[\lambda_i I - F]\underline{z}_i = 0 \qquad \text{(A.4-2)}$$

As in the case of eigenvalues, the eigenvectors of a second-order mode appear as complex conjugate pairs. The eigenvectors contain the same information about the normal modes that is given by the time vectors of classical aircraft stability analysis (Ref. 65).

The modal matrix is the matrix of eigenvectors arranged columnwise. The inverse of this matrix transforms the state vector into normal mode space, in which each element of the vector, $\Delta\underline{y}$, represents a normal mode of the system:

$$\Delta\underline{y} = M^{-1}\,\Delta\underline{x} \qquad \text{(A.4-3)}$$

(Instead of the two complex-conjugate eigenvectors of a second-order mode, it may be useful to use two real vectors, one composed of the eigenvector real part and one the imaginary part.)

The linear equation of motion, Eq. (A.3-3) can be transformed as well:

$$\Delta\dot{\underline{y}} = M^{-1}FM\,\Delta\underline{y} + M^{-1}G\,\Delta\underline{u} \qquad \text{(A.4-4)}$$

The normal-mode system matrix, $M^{-1}FM$, is composed of first- or second-order diagonal blocks containing the system eigenvalues, and the normal mode input matrix, $M^{-1}G$, indicates which inputs affect which normal modes. This alternate form

of the state equation is useful because it demonstrates a method of analyzing normal mode excitation. The excitation due to the state initial condition can be calculated from Eq. (A.4-3), while the excitation due to control inputs is given by the normal mode input matrix, $M^{-1}G$.

This section has discussed eigenvalue and eigenvector concepts. Examples of the application of these analytical tools to the analysis of linearized aircraft models are contained in Sections 2.4 and 2.5.

A.4.2 Controllability

In a multi-input, multi-output system, certain normal modes may be unaffected by the system controls without this being apparent from the system dynamics and input matrices. This can not occur in an n^{th}-order linear-time-invariant system whose controllability test matrix, Γ, has full rank:

$$\Gamma = \left[G \,\vdots\, FG \,\vdots\, \ldots \,\vdots\, F^{n-1}G \right] \qquad \text{(A.4-5)}$$

The presence of controllability is necessary for the construction of a complete system controller, and this property almost always exists in physical systems of interest. (Controllability tests show that the high-performance fighter investigated in this report is controllable throughout the range of flight conditions.)

Of more interest is the investigation of control effectiveness throughout the flight regime. The difficulty is in devising a simple measure of control effectiveness, but this can be overcome, to some extent, by using the normal mode control input matrix, $M^{-1}G$, which was introduced above. The rows of this matrix indicate the relative

importance of the aircraft's controls in affecting each of the normal modes.

A.4.3 Transfer Functions

Specific input-output relationships in linear-time-invariant dynamic systems can be described by transfer functions, which are typically given as ratios of polynomials in the Laplace operator, s. The Laplace transform of the ordinary differential equation of motion (Eq. (A.3-3)) is

$$(sI-F)\,\Delta\underline{x}(s) = G\,\Delta\underline{u}(s) \tag{A.4-6}$$

where I, F, and G have been defined, and $\Delta\underline{x}(s)$ and $\Delta\underline{u}(s)$ are Laplace transforms of the state and control vectors, $\Delta\underline{x}(t)$ and $\Delta\underline{u}(t)$. The input, $\Delta\underline{u}(s)$, and the output, $\Delta\underline{x}(s)$, are related by a transfer function matrix, H(s), which is obtained when Eq. (A.4-6) is pre-multiplied by the inverse of (sI-F):

$$\begin{aligned}\Delta\underline{x}(s) &= (sI-F)^{-1}G\,\Delta\underline{u}(s)\\ &= H(s)\,\Delta\underline{u}(s)\end{aligned} \tag{A.4-7}$$

where

$$H(s) = (sI-F)^{-1}G \tag{A.4-8}$$

Any scalar transfer function of interest (for example, the effect of the i^{th} control on the j^{th} motion variable), can be obtained from Eq. (A.4-8) by evaluating two determinants derived from the matrices of Eq. (A.4-6) (Ref. 72),

$$\frac{\Delta x_j(s)}{\Delta u_i(s)} = \frac{|sI-F+g_{ij}| - |sI-F|}{|sI-F|} \tag{A.4-9}$$

where g_{ij} is an n by n matrix whose elements are zero, except for the j^{th} column, which contains the i^{th} column of the G matrix. This transfer function is a ratio of polynomials in s, and the numerator and denominator can be factored to identify the poles, p, and zeros, z, which describe the relationship between $\Delta u_i(s)$ and $\Delta x_j(s)$:

$$\frac{\Delta x_j(s)}{\Delta u_i(s)} = \frac{K_I(s-z_1)(s-z_2)....(s-z_m)}{(s-p_1)(s-p_2)....(s-p_n)} \qquad \text{(A.4-10a)}$$

Alternatively, dividing by the individual poles and zeros, Eq. (A.4-10a) becomes

$$\frac{\Delta x_i(s)}{\Delta u_j(s)} = \frac{K_F\left(1 - \frac{s}{z_1}\right)\left(1 - \frac{s}{z_2}\right)\ldots\left(1 - \frac{s}{z_m}\right)}{\left(1 - \frac{s}{p_1}\right)\left(1 - \frac{s}{p_2}\right)\ldots\left(1 - \frac{s}{p_n}\right)} \qquad \text{(A.4-10b)}$$

The poles of the transfer function are the roots of the system's characteristic equation, i.e., they are the system's eigenvalues, and they are identical for all transfer functions of the system described by F. The zeros depend on G as well as F; therefore, they vary from one transfer function to the next. The transfer function gain, K_F, is the steady-state value of the transfer function after all transients damp out, assuming that all transients are stable. The transfer function gain, K_I, is (for most aircraft transfer functions) the initial state rate response to a control step.

The initial value gain, K_I, is important because it determines the initial slope of a given state variable's step response. This can be seen by applying the initial value theorem (Ref. 11) to the state variable's transform, which states that

$$\lim_{t \to 0} x(t) = \lim_{s \to \infty} s\, x(s) \qquad \text{(A.4-11)}$$

if the limit exists. The Laplace transform for the perturbation state, Δx_i, given a unity step input in control, Δu_j, is given as

$$\Delta x_i(s) = \frac{\Delta x_i(s)}{\Delta u_j(s)} \left(\frac{1}{s}\right) \qquad \text{(A.4-12)}$$

Since there are more poles than zeros in the transfer functions of interest, the initial value of $\Delta x_i(t)$ is zero. Physically, this is an indication that the vehicle states do not change instantaneously in response to a control input. The lowest order non-zero state derivative is equal to the excess of poles over zeros. For most aircraft transfer functions of interest, the excess is one, and

$$\Delta \dot{x}_j(s) = s\, \Delta x_j(s) = \frac{\Delta x_i(s)}{\Delta u_j(s)} \frac{s}{s} = \frac{\Delta x_i(s)}{\Delta u_j(s)} \qquad \text{(A.4-13)}$$

This leads to the calculation of the initial value of the state derivative response to a unity step input as

$$\Delta \dot{x}_i(t=0) = K_I = \lim_{s \to \infty} \frac{\Delta x_i(s)}{\Delta u_j(s)} \qquad \text{(A.4-14)}$$

Coupled aircraft transfer functions typically have seven zeros and eight non-zero poles, so K_I and K_F are related as follows:

$$K_I = \frac{K_F(-p_1)(-p_2) \ldots (-p_8)}{(-z_1)(-z_2) \ldots (-z_7)} \qquad \text{(A.4-15)}$$

A comparison of the signs of K_I and K_F, which are related by the signs of the poles and zeros, as indicated by Eq. (A.4-15), is important because these signs give an indication of the expected transient response. If the transfer function is stable and minimum phase, the signs of K_I and K_F are the same. The resulting response is similar to the solid line in Fig. 2.5-1. A nonminimum-phase zero causes K_I and K_F to have opposite signs, and the resulting response resembles one of the dashed lines in Fig. 2.5-1. In these responses, the initial response direction is away from the desired final value.

The transfer function has been a fundamental tool of control system design in the past, and, although linear-optimal control theory serves that purpose in this report (Chapter 4), transfer functions can be valuable for understanding details of the aircraft's dynamics. For example, nonminimum-phase zeros and sign changes in K_I can degrade handling qualities (Section 2.2). When poles and zeros are nearly equal, there is a cancelling effect which tends to remove the associated normal mode from the output variable's response to the given input. Conversely, feedback paths between the transfer function's output and input have negligible effect on that normal mode. In other words, the transfer function provides the information regarding the quality of controllability which was missing in Eq. (A.4-5). These capabilities are put to use in Chapter 2.

A.4.4 Optimal Control Theory

A regulator is a feedback control law which is designed to maintain asymptotically stable output of a dynamic system, i.e., it bounds the fluctuations in the output, and it assures that the output goes to zero as time

increases. An optimal regulator minimizes a cost (or penalty) functional of the output and control in stabilizing the dynamic system. A linear-optimal regulator minimizes a particular cost function -- the time integral of quadratic functions of the output and control -- for a linear dynamic system, and it takes the form of Eq. (4.1-1) (Ref. 80). A linear-optimal regulator can be designed for an aircraft near, at, or beyond its open-loop departure boundary. This design indicates the control loops which must be closed (either automatically or by the pilot) to prevent departure, providing asymptotic stability and minimizing a quadratic cost functional of the output and control.

The basic design objective for the linear-optimal regulator is to define the feedback control law which minimizes a quadratic cost functional, J, of the perturbation output vector, $\Delta\underline{y}(t)$, and the perturbation control vector, $\Delta\underline{u}(t)$:

$$J = \int_0^\infty \left[\Delta\underline{y}^T(t)\, Q\Delta\underline{y}(t) + \Delta\underline{u}^T(t)\, R\Delta\underline{u}(t)\right] dt \qquad (A.4\text{-}16)$$

The control vector contains all available aircraft control displacements -- in this case, throttle setting ($\Delta\delta_T$), elevator ($\Delta\delta_h$), aileron ($\Delta\delta_a$), and rudder ($\Delta\delta_r$). The output vector represents the measured aircraft variables and can be formulated as a linear combination of the aircraft's perturbation states, $\Delta\underline{x}(t)$, state rates, $\Delta\dot{\underline{x}}(t)$, and controls, $\Delta\underline{u}(t)$: the present development uses the simplifying assumption, $\Delta\underline{y}(t) = \Delta\underline{x}(t)$, where

$$\Delta\underline{x}^T = \left[\Delta\theta\ \Delta u\ \Delta q\ \Delta w\ \Delta v\ \Delta r\ \Delta p\ \Delta\phi\right] \qquad (A.4\text{-}17)$$

The state-weighting matrix is nonnegative-definite and symmetric.

$$Q = \begin{bmatrix} q_{11} & 0 & \cdots & 0 \\ 0 & q_{22} & \cdots & 0 \\ \cdots & \cdots & \cdots & \cdots \\ 0 & 0 & \cdots & q_{nn} \end{bmatrix} \qquad \text{(A.4-18)}$$

and the control-weighting matrix is positive-definite and symmetric:

$$R = \begin{bmatrix} r_{11} & 0 & \cdots & 0 \\ 0 & r_{22} & \cdots & 0 \\ \cdots & \cdots & \cdots & \cdots \\ 0 & 0 & \cdots & r_{mm} \end{bmatrix} \qquad \text{(A.4-19)}$$

Equatio (A.4-19) can be written as

$$J = \int_0^\infty \left[q_{11}\Delta x_1^2(t) + \cdots + q_{nn}\Delta x_n^2(t) + r_{11}\Delta u_1^2(t) + \cdots + r_{mm}\Delta u_m^2(t) \right] dt \qquad \text{(A.4-20)}$$

and the cost functional is seen to be a weighted sum of the integrated-square values of the perturbation state and control. In the present case, minimizing the weighted sum of integrated-square values is equivalent to minimizing the weighted sum of root-mean-square (rms) values of the state and control.

Equation (A.4-20) provides a means of trading off the cost of output errors against the cost of control, and it is simply this: choose each weighting coefficient in Q and R as the inverse of the maximum allowable mean-square value of the weighted variable, i.e.,

$$q_{ii} = 1/\Delta x^2_{i_{max}}, \quad i = 1 \text{ to } n \qquad \text{(A.4-21)}$$

$$r_{jj} = 1/\Delta u^2_{j_{max}}, \quad j = 1 \text{ to } m \qquad \text{(A.4-22)}$$

This normalizes each term in Eq. (A.4-20), so that its contribution to the integrand is unity when the variable equals its maximum value. The elements of R are specified by the control authority which can be assigned to the DPSAS. For example, if 10 deg of elevator perturbation can be assigned to departure prevention, the corresponding element of R is $1/(10)^2 = 0.01$. If there is prior information regarding allowable state perturbations (as in a tracking task), the elements of Q are determined similarly.

An alternate approach is to use the elements of Q and R as design parameters which can be varied until desirable transient response or eigenvalues are achieved. In such case, the equivalence of Q elements to allowable mean-square values is not lost, and it is possible to gain insight regarding the correspondence of rms-output errors and classical figures of merit in each particular case.

The minimization of J must be accomplished subject to the dynamic constraint provided by the linear equation of motion,

$$\Delta\dot{\underline{x}}(t) = F\Delta\underline{x}(t) + G\Delta\underline{u}(t) \qquad \text{(A.4-23)}$$

(It is assumed that F and G form a controllable pair.) The method of finding the control which minimizes J subject to Eq. (A.4-23) is derived in numerous texts (e.g., Refs. 60 to 62). In the special case of quadratic cost and linear system dynamics, the control solution is a linear feedback law (Eq. (4.1-1)). The gain matrix of this control law is

$$K = R^{-1}G^{T}P \qquad \text{(A.4-24)}$$

where the symmetric matrix, P, is the steady-state solution of the matrix Riccati equation

$$\dot{P} = -PF - F^{T}P + PGR^{-1}G^{T}P - Q \qquad \text{(A.4-25)}$$

In other words, the DPSAS gain matrix is easily found by two matrix multiplications once P is found (Eq. (A.4-24)), but the solution for P (Eq. (A.4-25)) appears formidable. There are, however, four recognized methods for steady-state solution of Eq. (A.4-15)), all of which require digital computation (Ref. 60): these are direct integration of Eq. (A.4-25), the Newton-Raphson method, the Kalman-Englar method, and the diagonalization/eigenvalue method. The choice between these methods must be based on grounds of numerical convenience and efficiency.

The Kalman-Englar method (Ref. 73) has been used to generate the results which follow in later sections. In this technique, P is propagated to steady state using the recursive equation,

$$P_{k+1} = \left[\Theta_{21} + \Theta_{22}P_k\right]\left[\Theta_{11} + \Theta_{12}P_k\right]^{-1} \qquad \text{(A.4-26)}$$

The matrices Θ_{11}, Θ_{12}, Θ_{21}, and Θ_{22} are the appropriate $(n \times n)$ sub-matrices of

$$\Theta(\Delta t) = e^{-Z\Delta t} \qquad \text{(A.4-27)}$$

where

$$Z = \begin{bmatrix} F & -GR^{-1}G^{T} \\ Q & -F^{T} \end{bmatrix} \qquad \text{(A.4-28)}$$

and the propagation interval, Δt, is small compared to the natural periods of the aircraft motion.

The DPSAS design procedure is summarized and shown to be a straightforward technique once the appropriate general-purpose computer routines are programmed:

- Define control authority available to the DPSAS, thus specifying R.
- Define allowable state perturbations, thereby specifying Q.
- For the aircraft dynamics specified by the stability and control matrices, F and G, compute the feedback gain matrix, K, using Eq. (A.4-26), (A.4-27), (A.4-26), and (A.4-24).
- The control law for the DPSAS is given by Eq. (4.1-1), using the gain matrix calculated in the previous step.

The resulting DPSAS stabilizes the aircraft without using mroe control authority than that specified by R for state perturbations defined by Q.

A.4.5 Gain Scheduling Procedure

Means and Standard Deviations - Two features which suggest that a gain be held constant are its standard deviation and mean value. Certain gains do not exhibit wide variations as the flight conditions change. This can be determined by constructing a table of means and standard deviations for the gains, as illustrated by Table A.4-1. In the table, Gain 6 displays a low standard deviation and a large mean value. This indicates that the gain should probably not be scheduled, i.e., that its mean value can be used at all flight conditions.

Another feature of each gain is its relative magnitude compared to other gains of a similar class. Gain 4 is small compared to Gain 6 and also exhibits a wide variation in magnitude; thus it may be desirable to schedule Gain 4, if its variation with flight condition is coherent, or set it to zero. Simulations should be done to fully

TABLE A.4-1
EXAMPLE OF MEAN-STANDARD DEVIATION TABLE

	Mean	Standard Deviation	S.D. Per Cent of Mean
Gain 4	-.00598	.0269	449.0
Gain 5	-.1013	.032	31.7
Gain 6	2.55	.046	1.82
⋮ etc.			

determine the zeroed gains' effects on controlling the aircraft. Gain 5 is a logical candidate for scheduling. The gain magnitude is not negligible, and it displays enough variation to warrant scheduling.

Correlation Between Gains and Flight Variables - The aircraft dynamic model varies in a complex but deterministic way with flight conditions. If the closed-loop response of the aircraft is maintained essentially invariant by automatic control, it is reasonable to assume that the necessary control gains also vary in a complex but deterministic way with flight conditions; hence the gains and flight conditions should be correlated.

The search for gain/flight variable dependencies begins by determining correlation coefficients between the

gains and all available flight variables. One method of determining the correlation coefficient between a set of gains (dependent variables), k_i, and a flight variable (independent variable), m, is given by the following:

$$\rho(k,m) = \frac{|\mathrm{cov}[k,m]|}{\sigma(k)\sigma(m)} = \frac{\left|\sum_{i=1}^{I}(k_i-\bar{k})(m_i-\bar{m})\right|}{\sqrt{\sum_{i=1}^{I}(k_i-\bar{k})^2}\sqrt{\sum_{i=1}^{I}(m_i-\bar{m})^2}} \qquad \text{(A.4-29)}$$

In Eq. (A.4-29), I is the number of flight conditions for which the gains are known, k_i is the value of the gain observed at flight point i, and m_i is the value of the flight variable at flight point i. The variable $\bar{k}$ is the mean value of the gain, given by

$$\bar{k} = \frac{1}{I}\sum_{i=1}^{I} k_i \qquad \text{(A.4-30)}$$

and $\bar{m}$ is the mean value of the flight variable. The closer the magnitude of ρ is to one, the better the correlation between the gain and the flight variable. Independent variables which can be considered for gain scheduling include indicated airspeed (IAS), body-axis velocities (u,v,w) angles of attack and sideslip (α,β), angular rates (p,q,r), and control trim positions. These variables can be inverted, squared, and so on, in the search for high correlation. An example of a correlation coefficient table is shown in Table A.4-2. The circled values are the high correlation coefficients between gains and independent variable functions.

TABLE A.4-2

EXAMPLE OF CORRELATION COEFFICIENTS TABLE

	α	α^2	$1/\alpha$	IAS	IAS^2	p	q	r	...etc.
Gain 1	.838	(.939)	.297	(.939)	(.912)	.804	.018	.0359	
Gain 2	.879	.743	.168	.745	.541	(.890)	.028	.245	
Gain 3	.672	.786	.069	.782	(.904)	.724	.447	.339	
⋮									
etc.									

Curve Fitting - The third step in the gain-scheduling procedure is to construct a smooth relationship between the gains which are to be scheduled and the most highly correlated flight variables. Multiple regression

$$\hat{k} = b_0 + b_1 m_1 + b_2 m_2 + \ldots + b_n m_n \qquad \text{(A.4-31)}$$

and polynomial regression,

$$\hat{k} = b_0 + b_1 m_1 + b_2 m_1^2 + \ldots + b_n m_i^n \qquad \text{(A.4-32)}$$

can be used. Equation (A.4-31), the multiple regression, uses n different independent variables, while Eq. (A.4-32), the polynomial regression, uses powers of the highest correlated independent flight variable, m_i, to estimate the gain, k. A method for determining the regression coefficients, b_i, is shown next.

A multiple regression analysis determines the regression coefficients $b_0, b_1, \ldots, b_n$ in Eq. (A.4-31) so that the sum of the squared error between the regression estimate, $\hat{k}$, and the true value of k is minimized. For I flight conditions, the function to be minimized is

$$J = \sum_{i=1}^{I} (k_i - \hat{k}_i)^2 \qquad \text{(A.4-33)}$$

To minimize J, set

$$\frac{\partial J}{\partial b_0} = \frac{\partial J}{\partial b_1} = \ldots \frac{\partial J}{\partial b_n} = 0 \qquad \text{(A.4-34)}$$

Then the expression for the regression coefficients becomes

$$A\,\underline{b} = \underline{C} \qquad \text{(A.4-35)}$$

or

$$\underline{b} = A^{-1}\underline{C} \qquad \text{(A.4-36)}$$

where A and $\underline{C}$ are defined as in the least-squares formulas of Ref. 63. These are the values of b_i which minimize the squared error.

To determine just how good the b_i values are, the correlation coefficient for the multiple regression fit can be found, as in Eq. (A.4-29):

$$\rho(k,\hat{k}) = \frac{\sum_{i=1}^{I} (k_i - \bar{k})(\hat{k}_i - \bar{\hat{k}})}{\sqrt{\sum_{i=1}^{I} (k_i - \bar{k})^2}\sqrt{\sum_{i=1}^{I} (\hat{k}_i - \bar{\hat{k}})^2}} \qquad \text{(A.4-37)}$$

The closer ρ is to one, the better the fit of the multiple regression model. When using a multiple regression, the more independent variables chosen, the higher the value of ρ will be, until n=I and ρ=1.

An alternate way of estimating gain values is to use only one of the flight variables in a polynomial regression. An n^{th}-order polynomial regression analysis determines the regression coefficients, $b_0, b_1, \ldots, b_n$ in Eq. (A.4-32) so that the sum of the squared error between the regression estimate, $\hat{k}$, of Eq. (A.4-31) and the true value of k is minimum. In this case, there is only one kind of independent variable, m_i, for each gain value, but it is raised to various powers, i.e., $m_1 = m_i$, $m_2 = m_i^2$, until adequate correlation is achieved.

The analysis for the polynomial regression proceeds as in the multiple regression, starting at Eq. (A.4-33). The polynomial regression can be considered a special case of the multiple regression.

A.4.6 Program ALPHA

The construction of the complete linear equations of motion, their analysis, and the design of feedback controllers has been programmed in ALPHA--Analysis Program for High Angle-of-Attack Stability and Control. Figure 4.4-2 illustrates the structure of this program. Input data consists of aircraft inertial and aerodynamic characteristics. The aerodynamic data can be entered as conventional stability derivatives, dimensionless derivatives, or full tables of nonlinear force and moment characteristics.

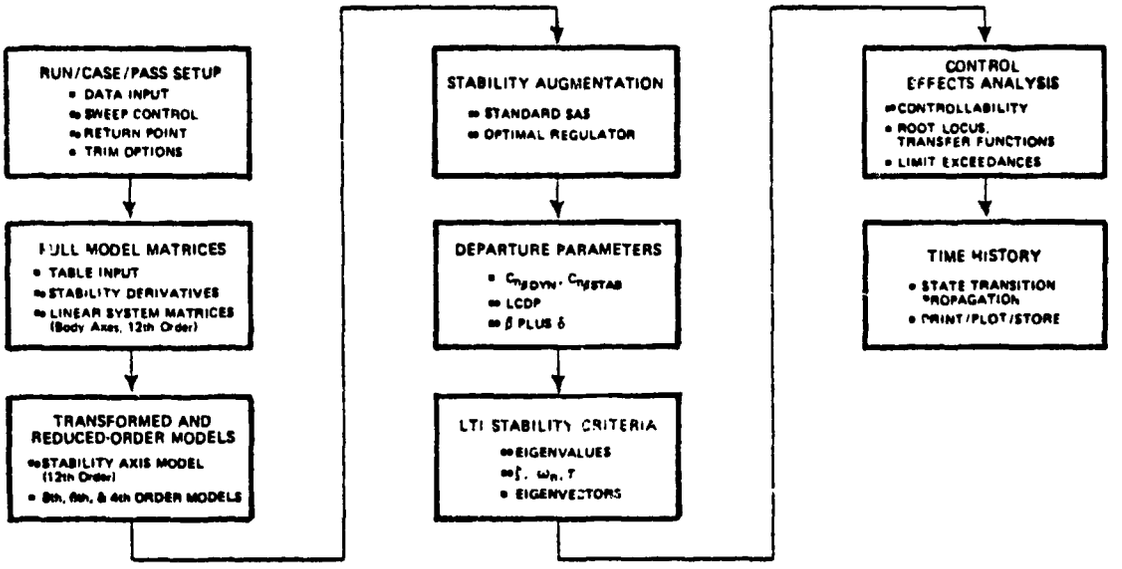

Figure A.4-2 ALPHA - Analysis Program for High Angle-of-Attack Stability and Control

The program executes a three-step procedure. The first step consists of steady or generalized trim calculation, if desired, and the construction of the complete body-axis system dynamics and control input matrices. During the second step, the linear system is modified, if required, to include any axis transformation, order reduction,or fixed stability augmentation loop closure. The final step consists of the analysis of the resulting system. Eigenvalues, eigenvectors, transfer functions, linear-optimal stability augmentation systems, and time histories can be calculated and plotted.

The executive structure of ALPHA includes logic to modify the dynamic model on succeeding passes through the program and to vary the analysis type as certain parameters are varied over a given range of interest. Program ALPHA provides an efficient tool for the thorough analysis of aircraft high angle-of-attack stability and control.

APPENDIX B

AIRCRAFT AERODYNAMIC MODEL

The reference aircraft is a small, supersonic fighter type designed for air superiority missions. Mass, dimensional, and inertial characteristics are listed in Table B-1. The aerodynamic data set is a composite of sub-scale wind tunnel measurements for two configurations of the reference aircraft; hence, the numerical results presented here do not represent a specific aircraft in detail.

TABLE B-1
CHARACTERISTICS OF THE REFERENCE AIRCRAFT

Mass, kg	6,124.
I_x, kg-m^2	7,186.
I_y, kg-m^2	57,350.
I_z, kg-m^2	63,450.
I_{xz}, kg-m^2	-149.
Reference Area, m^2	17.30
Mean Aerodynamic Chord, m($\bar{c}$)	2.46
Wing Span, m(b)	.3
Length, m	.73
Reference Center of Gravity (c.g.)	0.25$\bar{c}$
Flight c.g.	0.17$\bar{c}$

The control variables are elevator (or horizontal tail, δ_h), leading/trailing edge flaps (δ_f), ailerons (δ_a), rudder (δ_r), speed brake (δ_{SB}), and thrust setting (δ_T). The ranges of these variables are listed in Table B-2.

TABLE B-2
CONTROL VARIABLE RANGES

δ_h	-20 to +5 deg
δ_f	0 to 100 percent
δ_a	-60 to +60 deg
δ_r	-30 to +30 deg
δ_{SB}	0 to 45 deg
δ_T	0 to 100 percent

The aerodynamics of the aircraft are represented by 45 coefficients which are functions of angle of attack, sideslip angle, elevator deflection, and flap setting. Using simplified conventional notation, the 6 total coefficients are described as follows:

$$C_{X_T} = C_X(\alpha,\beta) + \Delta C_X(\alpha,\beta,\delta_f) + \Delta C_X(\alpha,\delta_{SB}) + \Delta C_X(\alpha,\delta_f,\delta_h) + \frac{\bar{c}q}{2V} C_{X_q}(\alpha) \qquad \text{(B-1)}$$

$$C_{Y_T} = C_{Y_0}(\alpha,\delta_f) + \Delta C_Y(\alpha,\beta) + \Delta C_Y(\alpha,\beta,\delta_f) + \Delta C_Y(\alpha,\delta_f,\delta_a) + \Delta C_Y(\alpha,\delta_r) + \frac{b}{2V}\left[C_{Y_r}(\alpha)r + C_{Y_p}(\alpha)p + C_{Y_{\dot\beta}}(\alpha)\dot\beta\right] \qquad \text{(B-2)}$$

$$C_{Z_T} = C_Z(\alpha,\beta) + \Delta C_Z(\alpha,\beta,\delta_f) + \Delta C_Z(\alpha,\delta_{SB}) + \Delta C_Z(\alpha,\delta_a,\delta_h)$$

$$+ \frac{\bar{c}q}{2V} C_{Z_q}(\alpha) \qquad \text{(B-3)}$$

$$C_{l_T} = C_{l_0}(\alpha,\delta_f) + C_l(\alpha,\beta) + \Delta C_l(\alpha,\beta,\delta_f) + \Delta C_l(\alpha,\delta_f,\delta_a)$$

$$+\Delta C_l(\alpha,\delta_r) + \frac{b}{2V}\left[C_{l_r}(\alpha)r + C_{l_p}(\alpha)p + C_{l_{\dot\beta}}(\alpha)\dot\beta\right] \qquad \text{(B-4)}$$

$$C_{m_T} = C_{m_0} + C_m(\alpha,\beta) + C_{Z_T}(\Delta\bar{x}) + \Delta C_m(\alpha,\beta,\delta_f) + \Delta C_m(\alpha,\delta_f,\delta_h)$$

$$+\Delta C_m(\alpha,\delta_{SB}) + \frac{\bar{c}q}{2V} C_{m_q}(\alpha) \qquad \text{(B-5)}$$

$$C_{n_T} = C_{n_0}(\alpha,\delta_f) + C_n(\alpha,\beta) + \Delta C_{Y_T}(\Delta\bar{x})\frac{\bar{c}}{b} + \Delta C_n(\alpha,\beta,\delta_f)$$

$$+\Delta C_n(\alpha,\delta_f,\delta_a) + \Delta C_n(\alpha,\delta_r)$$

$$+ \frac{b}{2V}\left[C_{n_r}(\alpha)r + C_{n_p}(\alpha)p + C_{n_{\dot\beta}}(\alpha)\dot\beta\right] \qquad \text{(B-6)}$$

The first step in finding the individual terms of the perturbation forces and moments, Eqs. (A.3-13) to (A.3-16), is to evaluate the derivatives of the force and moment coefficients with respect to the nondimensional states at the nominal flight condition. This results in nondimensional stability derivatives, such as the following:

$$C_{X_u} = \frac{\partial C_{X_T}}{\partial (u/V_0)} = \left[- \frac{\bar{c} q_0}{2V_0} C_{X_q}(\alpha_0) \right] \frac{\partial (V/V_0)}{\partial (u/V_0)}$$

$$+ \left[\frac{\partial C_X(\alpha_0, \beta_0)}{\partial \beta} + \frac{\partial \Delta C_X(\alpha_0, \beta_0, \delta f_0)}{\partial \beta} \right] \frac{\partial \beta}{\partial (u/V_0)}$$

$$+ \left[\frac{\partial C_X(\alpha_0, \beta_0)}{\partial \alpha} + \frac{\partial \Delta C_X(\alpha_0, \beta_0, \delta f_0)}{\partial \alpha} \right.$$

$$+ \frac{\partial \Delta C_X(\alpha_0, \delta_{SB})}{\partial \alpha} + \frac{\partial \Delta C_X(\alpha_0, \delta f_0, \delta f_0)}{\partial \alpha}$$

$$\left. + \frac{\bar{c} q_0}{2V_0} \frac{\partial C_{m_q}(\alpha_0)}{\partial \alpha} \right] \frac{\partial \alpha}{\partial (u/V_0)} \qquad \text{(B-7)}$$

$$C_{X_q} = \frac{\partial C_{X_T}}{\partial \left(\frac{q\bar{c}}{2V} \right)} = C_{X_q}(\alpha_0) \qquad \text{(B-8)}$$

Many of these derivatives contain the partial derivatives of the nondimensional wind-axis translational velocities $(V/V_0, \beta, \alpha)$ with respect to the nondimensional body-axis translational velocities $(u/V_0, v/V_0, w/V_0)$. This matrix of derivatives, evaluated at the nominal flight condition, is

$$\left. \frac{\partial (V/V_0, \beta, \alpha)^T}{\partial (u/V_0, v/V_0, w/V_0)^T} \right|_{V_0, \alpha_0, \beta_0} = \begin{bmatrix} \cos\alpha_0 \cos\beta_0 & \sin\beta_0 & \sin\alpha_0 \cos\beta_0 \\ -\cos\alpha_0 \sin\beta_0 & \cos\beta_0 & -\sin\alpha_0 \sin\beta_0 \\ -\sin\alpha_0/\cos\beta_0 & 0 & \cos\alpha_0/\cos\beta_0 \end{bmatrix}$$

(B-9)

The dimensional stability derivatives are formed by taking the derivatives of the dimensional aerodynamic forces and moments with respect to the dimensional state variables. These dimensional derivatives contain the non-dimensional derivatives; $\frac{\partial F_X}{\partial u}$ and $\frac{\partial F_X}{\partial q}$ are examples of these derivatives:

$$\frac{\partial F_X}{\partial u} = \frac{\partial}{\partial u}\left[\tfrac{1}{2}\rho V^2 S\, C_{X_T}\right]$$

$$= \rho_0 u_0 S\, C_{X_T}\left(\alpha_0,\ \beta_0,\ \delta_{f_0},\ \delta_{h_0},\ \delta_{SB_0},\ \frac{q_0 b}{2V_0}\right)$$

$$+ \tfrac{1}{2}\rho_0 V_0 S\, C_{X_u} \qquad \text{(B-10)}$$

$$\frac{\partial F_X}{\partial q} = \frac{\partial}{\partial q}\left[\tfrac{1}{2}\rho V^2 S\, C_{X_T}\right]$$

$$= \tfrac{1}{2}\rho_0 V_0^2 S\, C_{X_q}\frac{\bar{c}}{2V_0} \qquad \text{(B-11)}$$

The complete dimensional stability derivative matrices are

$$\left[\frac{\partial \underline{F}_B}{\partial \underline{v}_B}\right] = \rho_0 S \begin{bmatrix} u_0 C_{X_0} + \tfrac{1}{2}V_0 C_{X_u} & v_0 C_{X_0} + \tfrac{1}{2}V_0 C_{X_v} & w_0 C_{X_0} + \tfrac{1}{2}V_0 C_{X_w} \\ u_0 C_{Y_0} + \tfrac{1}{2}V_0 C_{Y_u} & v_0 C_{Y_0} + \tfrac{1}{2}V_0 C_{Y_v} & w_0 C_{Y_0} + \tfrac{1}{2}V_0 C_{Y_w} \\ u_0 C_{Z_0} + \tfrac{1}{2}V_0 C_{Z_u} & v_0 C_{Z_0} + \tfrac{1}{2}V_0 C_{Z_v} & w_0 C_{Z_0} + \tfrac{1}{2}V_0 C_{Z_w} \end{bmatrix}$$

(B-12)

$$\left[\frac{\partial \underline{F}_B}{\partial \underline{\omega}_B^I}\right] = \frac{\rho_0}{4} V_0 S \begin{bmatrix} bC_{X_p} & \bar{c}C_{X_q} & bC_{X_r} \\ bC_{Y_p} & \bar{c}C_{Y_q} & bC_{Y_r} \\ bC_{Z_p} & \bar{c}C_{Z_q} & bC_{Z_r} \end{bmatrix} \qquad \text{(B-13)}$$

$$\left[\frac{\partial \underline{F}_B}{\partial \underline{u}}\right] = q_{\infty_0} S \begin{bmatrix} C_{X_{\delta T}} & C_{X_{\delta h}} & C_{X_{\delta a}} & C_{X_{\delta r}} \\ C_{Y_{\delta T}} & C_{Y_{\delta h}} & C_{Y_{\delta a}} & C_{Y_{\delta r}} \\ C_{Z_{\delta T}} & C_{Z_{\delta h}} & C_{Z_{\delta a}} & C_{Z_{\delta r}} \end{bmatrix} \qquad \text{(B-14)}$$

$$\left[\frac{\partial \underline{F}_B}{\partial \dot{\underline{v}}_B}\right] = \frac{\rho_0}{4} S \begin{bmatrix} \bar{c}C_{X_{\dot{u}}} & bC_{X_{\dot{v}}} & \bar{c}C_{X_{\dot{w}}} \\ \bar{c}C_{Y_{\dot{u}}} & bC_{Y_{\dot{v}}} & \bar{c}C_{Y_{\dot{w}}} \\ \bar{c}C_{Z_{\dot{u}}} & bC_{Z_{\dot{v}}} & \bar{c}C_{Z_{\dot{w}}} \end{bmatrix} \qquad \text{(B-15)}$$

$$\left[\frac{\partial \underline{F}_B}{\partial \dot{\underline{\omega}}_B^I}\right] = \frac{\rho_0}{8} S \begin{bmatrix} b^2C_{X_{\dot{p}}} & \bar{c}^2C_{X_{\dot{q}}} & b^2C_{X_{\dot{r}}} \\ b^2C_{Y_{\dot{p}}} & \bar{c}^2C_{Y_{\dot{q}}} & b^2C_{Y_{\dot{r}}} \\ b^2C_{Z_{\dot{p}}} & \bar{c}^2C_{Z_{\dot{q}}} & b^2C_{Y_{\dot{r}}} \end{bmatrix} \qquad \text{(B-16)}$$

$$\left[\frac{\partial \underline{M}_B}{\partial \underline{v}_B}\right] = \rho_0 S \begin{bmatrix} u_0 b C_{l_0} + \frac{1}{2} V_0 b C_{l_u} & v_0 b C_{l_0} + \frac{1}{2} V_0 b C_{l_v} & w_0 b C_{l_0} + \frac{1}{2} V_0 b C_{l_w} \\ u_0 \bar{c} C_{m_0} + \frac{1}{2} V_0 \bar{c} C_{m_u} & v_0 \bar{c} C_{m_0} + \frac{1}{2} V_0 \bar{c} C_{m_v} & w_0 \bar{c} C_{m_0} + \frac{1}{2} V_0 \bar{c} C_{m_w} \\ u_0 b C_{n_0} + \frac{1}{2} V_0 b C_{n_u} & v_0 b C_{n_0} + \frac{1}{2} V_0 b C_{n_v} & w_0 b C_{n_0} + \frac{1}{2} V_0 b C_{n_w} \end{bmatrix}$$

(B-17)

$$\left[\frac{\partial \underline{M}_B}{\partial \underline{\omega}_B^I}\right] = \frac{\rho_0}{4} V_0 S \begin{bmatrix} b^2 C_{l_p} & b\bar{c} C_{l_q} & b^2 C_{l_r} \\ b\bar{c} C_{m_p} & \bar{c}^2 C_{m_q} & b\bar{c} C_{m_r} \\ b^2 C_{n_p} & b\bar{c} C_{n_q} & b^2 C_{n_r} \end{bmatrix} \qquad \text{(B-18)}$$

$$\left[\frac{\delta \underline{M}_B}{\delta \underline{u}}\right] = q_{\infty_0} S \begin{bmatrix} b C_{l_{\delta T}} & b C_{l_{\delta h}} & b C_{l_{\delta a}} & b C_{l_{\delta r}} \\ \bar{c} C_{m_{\delta T}} & \bar{c} C_{m_{\delta h}} & \bar{c} C_{m_{\delta a}} & \bar{c} C_{m_{\delta r}} \\ b C_{n_{\delta T}} & b C_{n_{\delta h}} & b C_{n_{\delta a}} & b C_{n_{\delta r}} \end{bmatrix} \qquad \text{(B-19)}$$

$$\left[\frac{\partial \underline{M}_B}{\partial \dot{\underline{v}}_B}\right] = \frac{\rho_0}{4} S \begin{bmatrix} b\bar{c} C_{l_{\dot{u}}} & b^2 C_{l_{\dot{v}}} & b\bar{c} C_{l_{\dot{w}}} \\ \bar{c}^2 C_{m_{\dot{u}}} & b\bar{c} C_{m_{\dot{v}}} & \bar{c}^2 C_{m_{\dot{w}}} \\ b\bar{c} C_{n_{\dot{u}}} & b^2 C_{n_{\dot{v}}} & b\bar{c} C_{n_{\dot{w}}} \end{bmatrix} \qquad \text{(B-20)}$$

$$\left[\frac{\partial \underline{M}_B}{\partial \dot{\underline{\omega}}_B^I}\right] = \frac{\rho_0}{8} S \begin{bmatrix} b^3 C_{l_{\dot{p}}} & b\bar{c}^2 C_{l_{\dot{q}}} & b^3 C_{l_{\dot{r}}} \\ b^2 \bar{c} C_{m_{\dot{p}}} & \bar{c}^3 C_{m_{\dot{q}}} & b^2 \bar{c} C_{m_{\dot{r}}} \\ b^3 C_{n_{\dot{p}}} & b\bar{c}^2 C_{n_{\dot{q}}} & b^3 C_{n_{\dot{r}}} \end{bmatrix} \qquad \text{(B-21)}$$

These stability derivative matrices are used in Eqs. (A.3-13) to (A.3-16) to determine the perturbation forces and moments, which themselves determine the aerodynamic terms in the linear perturbation equations of motion.

REFERENCES

1. Lanchester, F.W., Aerodonetics, A. Constable, London, 1908.

2. Bairstow, L., Jones, B.M. and Thompson, B.A., "Investigation into the Stability of an Airplane," ARC R&M 77, London, 1913.

3. Phillips, W.H., "Effect of Steady Rolling on Longitudinal and Directional Stability," NACA TN 1627, Washington, June 1948.

4. Abzug, M.J., "Effects of Certain Steady Motions on Small-Disturbance Airplane Dynamics," Journal of the Aeronautical Sciences, Vol. 21, No. 11, November 1954, pp. 749-762.

5. Moul, M.T. and Paulson, J.W., "Dynamic Lateral Behavior of High Performance Aircraft," NASA RM L58E16, Washington, August 1958.

6. Porter, D.F. and Loomis, J.P., "Examination of an Aerodynamic Coupling Phenomenon," Journal of Aircraft, Vol. 2, No. 6, November-December 1965, pp.553-556.

7. Hamel, P., "A System Analysis View of Aerodynamic Coupling," Journal of Aircraft, Vol. 7, No. 6, November-December 1970, pp. 567-569.

8. McConnell, C.W., "Application of the Lateral and Longitudinal (Coupled) Equations of Motion to an Inertially-Slender Aircraft in Unsymmetric, Rectilinear Flight," M.S. Thesis, Air Force Institute of Technology, December 1973.

9. Johnston, D.E. and Hogge, J.R., "The Effect of Nonsymmetric Flight on Aircraft High Angle of Attack Handling Qualities and Departure Characteristics," AIAA Paper No. 74-792, New York, August 1974.

10. Stengel, R.F., "Effect of Combined Roll Rate and Sideslip Angle on Aircraft Flight Stability," Journal of Aircraft, Vol. 12, No. 8, August 1975, pp. 683-685.

REFERENCES (Continued)

11. Greer, H.D., "Summary of Directional Divergence Characteristics of Several High-Performance Aircraft Configurations," NASA TN D-6993, Washington, November 1972.

12. Weissman, R., "Preliminary Criteria for Predicting Departure Characteristics/Spin Susceptibility of Fighter-Type Aircraft," Journal of Aircraft, Vol. 10, No. 4, April 1973, pp. 214-218.

13. Pelikan, R.J., "Evaluation of Aircraft Departure Divergence Criteria with a Six-Degree-of-Freedom Digital Simulation Program," AIAA Paper No. 74-68, New York, January 1974.

14. Weissman, R., "Status of Design Criteria for Predicting Departure Characteristics and Spin Susceptibility," AIAA Paper No. 74-791, August 1974.

15. Ross, A.J., "Investigation of Nonlinear Motion Experienced on a Slender-Wing Research Aircraft," Journal of Aircraft, Vol. 9, No. 9, September 1972, pp. 625-631.

16. Haddad, E.K., "Study of Stability of Large Maneuvers of Airplanes," NASA CR-2447, Washington, August 1974.

17. Wykes, J.H., "An Analytical Study of the Dynamics of Spinning Aircraft," WADC TR 58-381, Part III, Wright-Patterson AFB, February 1960.

18. Scher, S.H., "Post-Stall Gyrations and Their Study on a Digital Computer," AGARD Report 359, Paris, April 1961.

19. Anglin, E.L. and Scher, S.H., "Analytical Study of Aircraft-Developed Spins and Determination of Moments Required for Satisfactory Spin Recovery," NASA TN D-2181, Washington, February 1964.

20. Grafton, S.B., "A Study to Determine Effects of Applying Thrust on Recovery from Incipient and Developed Spins for Four Airplane Configurations," NASA TN D-3416, Washington, June 1966.

21. Powers, B.G., "A Parametric Study of Factors Influencing the Deep-Stall Pitch-Up Characteristics of T-Tail Transport Aircraft," NASA TN D-3370, Washington, August 1966.

REFERENCES (Continued)

22. Bihrle,W., Jr., "Influence of the Static and Dynamic Aerodynamic Characteristics on the Spinning Motion of Aircraft," Journal of Aircraft, Vol. 8, No. 10, October 1971, pp. 764-768.

23. Moore, F.L., Anglin, E.L., Adams, M.S., Deal, P.O. and Person, L.H., Jr., "Utilization of a Fixed-Base Simulator to Study the Stall and Spin Characteristics of Fighter Airplanes," NASA TN D-6117, Washington, March 1971.

24. Champoux, R.L., "The Numerical Solution Analysis of Airplane Spin Equations Modeled in a Fixed Coordinate System," M.S. Thesis, Naval Postgraduate School, December 1972.

25. Bihrle, W., Jr., "Effects of Several Factors on Theoretical Predictions of Airplane Spin Characteristics, NASA CR-132521, Langley Research Center, August 1974.

26. Willen, T.B. and Johnson, K., "Anticipated Spin Susceptibility Characteristics of the A-10 Aircraft," AIAA Paper No. 75-33, New York, January 1975.

27. Eney, J.A. and Chambers, J.R., "Piloted Simulation of Spin," ASD Stall/Post-Stall/Spin Symposium, Wright-Patterson AFB, December 1971.

28. Bowman, J.S., Jr., "Airplane Spinning," Astronautics and Aeronautics, Vol. 4, No. 3, March 1966, pp. 64-67.

29. Adams, W.M., Jr., "Analytic Prediction of Airplane Equilibrium Spin Characteristics," NASA TN D-6926, Washington, November 1972.

30. Johnson, A.E., "A Literature Survey of the Problem of Aircraft Spins," M.S. Thesis, Naval Postgraduate School, September 1971.

31. McRuer, D.T., and Johnston, D.E., "Flight Control Systems Properties and Problems, Volume I," NASA CR-2500, Washington, February 1975.

32. Hawkins, M.L., "An Investigation of the Departure Modes of a F-4D Aircraft from a Steady Sideslip Flight Condition," M.S. Thesis, Air Force Institute of Technology, December 1974.

REFERENCES (Continued)

33. Rudolph, R.J., "Stability Analysis of an F-4C Aircraft in Steady Level Turning Flight," M.S. Thesis, Air Force Institute of Technology, December 1974.

34. Chambers, J.R. and Anglin, E.L., "Analysis of Lateral-Directional Stability Characteristics of a Twin-Jet Fighter Airplane at High Angles of Attack," NASA TN D-5361, Washington, August 1969.

35. Chambers, J.R., Anglin, E.L. and Bowman, J.S., Jr., "Effects of a Pointed Nose on Spin Characteristics of a Fighter Airplane Model Including Correlation with Theoretical Calculations," NASA TN D-5921, Washington, September 1970.

36. Chambers, J.R. and Bowman, J.S., Jr., "Recent Experience with Techniques for Prediction of Spin Characteristics of Fighter Aircraft," Journal of Aircraft, Vol. 8, No. 7, July 1971, pp. 548-553.

37. Coe, P.L., Jr., Chambers, J.R., and Letko, W., "Asymmetric Lateral-Directional Characteristics of Pointed Bodies of Revolution at High Angles of Attack," NASA TN D-7095, Washington, November 1972.

38. Ray, E.J., McKinney, L.W., and Carmichael, J.G., "Maneuver and Buffet Characteristics of Fighter Aircraft," NASA TN D-7131, Washington, July 1973.

39. Grafton, S.B., Chambers, J.R., and Coe, P.L., Jr., "Wind-Tunnel Free- Flight Investigation of a Model of a Spin-Resistant Fighter Configuration," NASA TN D-7716, Washington, June 1974.

40. Tobak, M. and Schiff, L.B., "Nonlinear Aerodynamics of Aircraft in High Angle-of-Attack Maneuvers," AIAA Paper No. 74-85, New York, January 1974.

41. Coe, P.L., Jr. and Newsom, W.A., Jr., "Wind-Tunnel Investigation to Determine the Low-Speed Yawing Stability Derivatives of a Twin-Jet Fighter Model at High Angles of Attack," NASA TN D-7721, Washington, August 1974.

42. Hwang, C. and Pi, W.S., "Transonic Buffet Behavior of Northrop F-5A Aircraft," AGARD Report 624, Neuilly-sur-Seine, September 1974.

REFERENCES (Continued)

43. Taylor, C.R., ed., "Aircraft Stalling and Buffeting," AGARD Lecture Series No. 74, Neuilly-sur-Seine, February 1975.

44. Kao, H.C., "Side Forces on Unyawed Slender Inclined Aerodynamic Bodies," Journal of Aircraft, Vol. 12, No. 3, March 1975, pp. 142-150.

45. Tobak, M. and Schiff, L.B., "Generalized Formulation of Nonlinear Pitch-Yaw-Roll Coupling: Part I-Non-axisymmetric Bodies and Part II-Nonlinear Coning-Rate Dependence," AIAA Journal, Vol. 13, No. 2, March 1975, pp. 323-332.

46. Nguyen, L.T., "Evaluation of Importance of Lateral Acceleration Derivatives in Extraction of Lateral-Directional Derivatives at High Angles of Attack," NASA TN D-7739, Washington, October 1974.

47. Neihouse, A.I., Klinar, W.J. and Scher, S.H., "Status of Spin Research for Recent Airplane Designs," NASA TR R-57, Washington, 1960.

48. Fuchs, R. and Schmidt, W., "The Dangerous Flat Spin and the Factors Affecting It," NACA TM 629, Washington, 1931.

49. Young, J.W., "Optimal and Suboptimal Control Technique for Aircraft Spin Recovery," NASA TN D-7714, Washington, October 1974.

50. Gilbert, W.P. and Libbey, C.E., "Investigation of an Automatic Spin-Preventing System for Fighter Airplanes," NASA TN D-6670, Washington, March 1972.

51. Chen, R.T., Newell, F.D., and Schelhorn, A.E., "Development and Evaluation of an Automatic Departure Prevention System and Stall Inhibitor for Fighter Aircraft," AFFDL TR-73-29, Wright-Patterson AFB, April 1973.

52. Anderson, C.A. and Walker, J.E., III, "A Stall Inhibitor for the F-111," NAECON'72 Record, May 1972.

53. Lamars, J.P., "Design for Departure Prevention in the YF-16," AIAA Paper No. 74-794, New York, August 1974.

REFERENCES (Continued)

54. McDonald, E.H., "F-15 Eagle Flight Control System" in Advances in Control Systems, AGARD CP-137, Neuilly-sur-Seine, May 1974.

55. Lindahl, J.H., "Application of the Automatic Rudder Interconnect (ARI) Function in the F-14 Aircraft," ONR Symposium on Optimal Control, Monterey, July 1975.

56. Nguyen, L.T., Anglin, E.L., and Gilbert, W.P., "Recent Research Related to Prediction of Stall/Spin Characteristics of Fighter Aircraft," Proceedings of the AIAA 3rd Atmospheric Flight Mechanics Conference, Arlington, Texas, June 1976, pp. 79-91.

57. Price, C.F. and Koenigsberg, W.D., "Adaptive Control and Guidance for Tactical Missiles," The Analytic Sciences Corp., TR-170-1, June 1970.

58. Stengel, R.F., Broussard, J.R. and Berry, P.W., "The Design of Digital-Adaptive Controllers for VTOL Aircraft," The Analytic Sciences Corp., TR-640-1, NASA CR-144912, March 1976.

59. Kaufman, H., Alag, G., Berry, P. and Kotob, S., "Digital Adaptive Flight Controller Development," NASA CR-2466, Washington, December 1974.

60. Kwakernaak, H. and Sivan, R., Linear Optimal Control Systems, Wiley-Interscience, New York, 1972.

61. Athans, M. and Falb, P.L., Optimal Control, McGraw-Hill, New York, 1966.

62. Bryson, A.E., Jr. and Ho, Y.C., Applied Optimal Control, Ginn-Blaisdell, Waltham, 1969.

63. Gelb, A. ed., Applied Optimal Estimation, M.I.T. Press, Cambridge, 1974.

64. Perkins, C.F. and Hage, R.E., Airplane Performance Stability and Control, J. Wiley and Sons, New York, 1949.

65. Etkin, B., Dynamics of Atmospheric Flight, J. Wiley and Sons, New York, 1972.

66. Seckel, E., Stability and Control of Airplanes and Helicopters, Academic Press, New York, 1964.

REFERENCES (Continued)

67. McRuer, D., Ashkenas, I. and Graham, D., Aircraft Dynamics and Automatic Control, Princeton University Press, Princeton, 1973.

68. Anglin, E.L., "Static Force Tests of a Model of a Twin-Jet Fighter Airplane for Angles of Attack from -10° to 110° and Sideslip Angles from -40° to 40°," NASA TN D-6425, Washington, August 1971,

69. Grafton, S.B. and Libbey, C.E., "Dynamic Stability Derivatives of a Twin-Jet Fighter Model for Angles of Attack from -10° to 110°," NASA TN D-6091, Washington, September 1970.

70. Jacob, H.G., "An Engineering Optimization Method with Application to STOL-Aircraft Approach and Landing Trajectories," NSAS TN D-6978, Washington, September 1972.

71. DeRusso, P.M., Roy, R.J. and Close, C.M., State Variables for Engineers, J. Wiley and Sons, New York, 1967.

72. Patel, R.V., "On the Computation of Numerators of Transfer Functions of Linear Systems," IEEE Transactions on Automatic Control, Vol. AC-18, No. 4, August 1973.

*U.S. GOVERNMENT PRINTING OFFICE: 1977 - 735-004/2